Dune Erosion on the Falsterbo Peninsula

Assessing the Dune System for Coastal Safety in Regions with Complex Interactions Between Waves and Water Levels.

E. Sukchaiwan

Delft University of Technology

TU Delft

SWECO

Dune Erosion on the Falsterbo Peninsula

Assessing the Dune System for Coastal Safety in Regions with Complex Interactions Between Waves and Water Levels.

by

E. Sukchaiwan

to obtain the degree of Master of Science
at the Delft University of Technology.

Thesis committee	Dr. ir. A. Antonini (chair)	Delft University of Technology
	Dr. E. Ragno	Delft University of Technology
	Dr. E.C. Hallin	Lund University
	Dr. B. Almström	Lund University
	Ir. G. Österlund	Sweco (Malmö, Sweden)

Cover Image: Aerial photo of the Falsterbo Peninsula by Lars Bygdemark.
An electronic version of this thesis is available at http://repository.tudelft.nl/.

TU Delft

SWECO

Abstract

The Falsterbo Peninsula is a low-lying area that provides a home to 7,000 residents, as well as various bird and vegetation species. To protect this densely populated area, the municipality was granted a permit to build flood protections. As part of the strategy, the dune system in the study area will be used as natural barriers against storm surges. Despite being part of the protection strategy, the strength of the dune system in safeguarding the hinterland has not been assessed. This had led to the objective of this thesis, which aims to evaluate the strength of the current dune system. To achieve this objective, the following research question were formulated:

To what extent does the dune system on the Falsterbo Peninsula contribute to safeguarding the hinterland against the impact of historical storm conditions?

To seek answers to this question, the research was divided into three parts. The first part of the methodology involves collecting the environmental data such as the wind, water level and wave data. Additionally, the data on the dune's morphology was collected during the field work. The second step of the methodology involves identification of extreme conditions within the time series spanning from 1959 to 2022. Considering the complex interaction between waves and water levels, the extreme conditions were identified based on the combined effect of the two variables, which was represented in the total water level (TWL). The sampling method was based on the peak over threshold method applied to the time series of TWL. The choice of the threshold value was based on the scenarios of potential coastal flooding in the study area. The largest storm surge, the 1872 storm, was included in the analysis to evaluate its impact on the present dune system.

The dune erosion due to the selected extreme conditions was determined in the last part of the methodology. Two morphological models, the XBeach model and the storm impact model were employe to estimated the dune erosion in four transects within the dune system.

The obtained dune erosion was expressed as a fraction of the available dune volume. The maximum dune erosion was found in the transect situated at the far-right end of the dune system when facing north. The maximum dune erosion under extreme conditions in the period 1959 to 2022, estimated by the XBeach and the storm impact model are 7.67% and 32.89%, respectively. Based these results, it can be concluded that the present dune system is strong enough to provide protection to the hinterland against the impact of extreme conditions.

For the 1872 storm, the XBeach model estimated erosion percentage of 67.89%, whereas the storm impact model estimated more than 100%. This indicates that in the event of recurrence of the 1872 storm, a dune breach could be expected. While the 1872 storm may not be the design storm condition for the dune system, the storm impact model result highlights the need of reevaluation of the formulation of potential plans to reinforce the dune system.

For future studies, it is strongly recommended to establish a long-term monitoring program for the dune system on the Falsterbo Peninsula. The obtained dune erosion data can be used to calibrate the morphological model to enhance its accuracy in the predictions. Additionally, dune recovery data can aid in the understanding of the dune system as a whole.

Preface

Dear reader,

This master's thesis is written to obtain the degree of Master of Science in Hydraulic Engineering, specializing in Coastal Engineering, of the Technological University of Delft. The research for this was carried out under collaborative supervision from Lund University, the Technological University of Delft, and Sweco (Malmö, Sweden).

The thesis represents the final chapter in my academic journey. It marks my time as a student in Delft, as well as a guest student in Lund. I would like to express my gratitude to all those who have been part of this process. First and foremost, I would like to especially thank my supervisor Dr. E. C. Hallin at Lund University, for providing me with the opportunity to undertake my internship and master's thesis in Sweden. I am grateful for your guidance throughout this thesis and, most importantly, for sharing your passion for coastal engineering. I also want to thank my supervisor Dr. B. Almström for your expertise and guidance, along with your feedback and insights on the topic. I express my appreciation to A. Adell, a doctoral student at Lund University, for your guidance in working with the SWAN model and for consistently displaying enthusiasm and supporting me throughout the entire process. Special thanks to Hugo Lindbäck for the help with field measurements on a cold and windy day. I extend my gratitude to everyone at the TVRL division at Lund University for their support during challenging times and the shared moments of laughter.

In addition, I would like to thank Sweco for the collaborative opportunity in this thesis. A special thank goes to my supervisor Ir. G. Österlund, for dedicating your time and and providing valuable guidance throughout the entire process. I would like to extend my appreciation to the 'Kust och vattendrag' group at the Malmö office for their warm welcome and enjoyable conversations during coffee breaks (*fika*) and after-work gatherings.

Moreover, I would like to thank my committee members Dr. Ir. A. Antonini (chairman) and Dr. E. Ragno at the Delft University of Technology for their valuable insights, remarks during progress meetings, and expert feedback. Their support has played a crucial role in shaping the direction and quality of this thesis project.

Last but certainly not least, I would like to express my gratitude to my friends in the Netherlands, as well as my new friends in Sweden for their moral support. Special thanks to my family for their encouragement and my partner, Oliver, for always being there when it mattered most. Thank every one of you for being part of this journey and for all of the support that played an important role in the successful completion of this master's thesis.

E. Sukchaiwan
Lund, December 2023

Contents

Acronym

BM	Block Maxima
DIA	Discrete Interaction Approximation
ECMWF	European Centre of Medium-Range Weather Forecasts
EMODnet	European Marine Observations and Data Network
EVA	Extreme Value Analysis
GLM	Generalized Lagrangian Mean
GPS	Global Positioning System
JEP	Joint Exceedance Probability
JONSWAP	The Joint North Sea WAve Project
LIDAR	Light Detection and Ranging
LTA	Lumped Triad Approximation
MSL	Mean Sea Level
MWL	Mean water Level
NAO	North Atlantic Oscillation
PM	Pierson-Moskowitz
POT	Peak Over Threshold
RH 2000	The Swedish National Height System 2000
RP	Return Period
RTK-GPS	Real-Time Kinematic Global Positioning System
SD	Surge Dominated
SGU	Geological Survey of Sweden
SLR	Sea Level Rise
SMHI	The Swedish Meteorological and Hydrological Institute
SR	Structural Response
SWAN	Simulating Waves Nearshore
SWL	Still Water Level
WAM	Wave Model
WD	Wave Dominated
WGS84	Global Geodetic Reference System

Symbols

Symbol	Description	Unit
H_s	significant wave height	m
T_p	peak period	s
θ	wave direction (Cartesian convention)	°
WL	water level (RH 2000)	m
D	storm duration	h
S	surge	m
H	wave height	m
a	wave amplitude	m
L	wave length	m
N	number of frequencies	–
ρ	water density	$\mathrm{kg\,m^{-3}}$
g	gravitational acceleration	$\mathrm{m\,s^{-2}}$
f_p	peak frequency	Hz
E	wave energy	$\mathrm{J\,m^{-1}}$
K_{sh}	shoaling factor	–
γ	breaker index	–
h_b	breaking depth	m
H_b	breaking wave height	m
H_0	deep water wave height	m
S_{wave}	wave setup	m
T_0	deep water wave period	s
$R_{2\%}$	wave runup by Hedges and Mase (2004)	m
H_{s0}	deep water significant wave height	m
ζ_0	foreshore slope	–
ξ	Iribarren number	–
L_{s0}	deep water wave length	m
C_{g0}	wave group velocity	$\mathrm{m\,s^{-1}}$
C_g	wave group velocity at breaking	$\mathrm{m\,s^{-1}}$
α_b	wave breaking angle	°
β_F	foreshore slope	–
c_m	phase speed	$\mathrm{m\,s^{-1}}$
c_{gm}	group speed	$\mathrm{m\,s^{-1}}$
H_m	wave height at an arbitrary depth	m
$U(y)$	shear flows	$\mathrm{m\,s^{-1}}$
k	wave number	–
d	water depth	m
k_p	peak wave number	–

Symbol	Description	Unit
H_{max}	maximum wave height	m
H_{rms}	root-mean-square wave height	m
u_L	Lagrangian velocity	$\mathrm{m\,s^{-1}}$
τ_{sx}	wind shear stress in x-direction	$\mathrm{N\,m^{-2}}$
τ_{sy}	wind shear stress in y-direction	$\mathrm{N\,m^{-2}}$
τ_{bx}	bed shear stress in x-direction	$\mathrm{N\,m^{-2}}$
τ_{by}	bed shear stress in y-direction	$\mathrm{N\,m^{-2}}$
F_x	wave-induced stress in x-direction	$\mathrm{N\,m^{-2}}$
F_y	wave-induced stress in y-direction	$\mathrm{N\,m^{-2}}$
ν_h	horizontal viscosity	$\mathrm{N\,m^{-2}}$
f	Coriolis coefficient	–
C	depth-averaged sediment concentration	$\mathrm{kg\,m^{-3}}$
D_H	sediment diffusion coefficient	–
T_s	Adaptation time	s
h	water depth	m
w_s	sediment fall velocity	$\mathrm{m\,s^{-1}}$
p	porosity	–
q_x	sediment transport in x-direction	$\mathrm{m^3\,s^{-1}}$
q_y	sediment transport in y-direction	$\mathrm{m^3\,s^{-1}}$
F	wave impact	N
ρ_s	sediment density	$\mathrm{kg\,m^{-3}}$
ΔW	weight of eroded sediment volume	kg
q_D	average dune erosion rate	$\mathrm{m^3\,s^{-1}}$
R	wave runup by Larson et al. (2004)	$\mathrm{m^3\,s^{-1}}$
D_F	dune foot elevation	m
C_s	empirical transport coefficient by Larson et al. (2004)	–
TWL	total water level	m
Z_s	water level in XBeach model	m
Z_s	bed level in XBeach model	m

List of Figures

List of Tables

1. Introduction

1.1. Background

Coastal zones are important areas as they serve as the habitat for a large part of the world's population. They have a significant role in socio-economic activities and host valuable ecosystems. According to Pörtner et al. (2022), these areas are facing an increasing risk of coastal flooding and erosion due to Sea Level Rise Sea Level Rise (SLR). Flooding can be caused by multiple factors such as storms, wave runup or tidal waves. The magnitude and frequency of these factors depend on the climate, the morphology of the region, and tidal forcing. Global climate change can alter the expected frequency and intensity of these factors (Wu et al., 2002; McCarthy et al., 2001; Mirza, 2003). Erosion, as defined by Skaggs and McDonald (1991), is the loss of beach, shoreline, or dune material due to coastal processes during extreme conditions or human-induced influences that can alternate the equilibrium of the sediment transport.

To protect the hinterland, infrastructure and ecosystems along the coast, coastal dunes can be used as natural barriers against extreme water levels and supply sand to the beach when it is eroding. Coastal dunes, hereinafter referred to as dunes in this report, have been implemented in the coastal defence strategy of the Netherlands, Denmark, Germany and the United Kingdom (Van Koningsveld et al., 2007; Kantamaneni et al., 2022; Kok et al., 2020). Moreover, the dunes contribute to the overall ecosystem of coastal environments. A significant erosion rate can cause the dune to lose its protective function, as it undermines its resilience. Consequently, dune erosion assessment is crucial to determine the level of safety that the dune system is providing. The assessment involves evaluating its response to a design storm condition. This design storm is derived from predicting the storm parameters (e.g. significant wave height (H_s), peak period (T_p), wave direction θ, surge (S), and event duration (D)) (Walker and Basco, 2011; Callaghan et al., 2008). The corresponding time series of the design storm is determined using a symmetric triangular storm shape (Duo et al., 2020). According to Sallenger Jr (2000), the impact depends not only on the storm-forced parameters but also on the dimension of the coastal region. Estimate dune erosion involves therefore the utilization of equilibrium or process-based models in the assessment (Roelvink et al., 2010; van Wiechen et al., 2023).

1.2. Study Area

The study area is the Falsterbo peninsula located in Vellinge Municipality, in Figure 1.2, Skåne County. This trumpet-shaped peninsula is a low-lying area that provides a home to various birds and vegetation and offers recreational opportunities. Additionally, with approximately 7,000 residents, the peninsula is a high-value area due to the presence of residential communities. The formation of the peninsula started some 6,000 years ago through sedimentation and the area is exposed to complex coastal processes such as nearshore circulation and large-scale currents (Blomgren and Hanson, 2000). From the final report by the Swedish Commission on Climate and Vulnerability (2007) and the study by Hanson and Larson (2008), the risk of floods, landslide and erosion are growing in magnitude and will affect the building construction and infrastructures in many areas along the coasts. The stress has been further increased by the growth of the population of the peninsula in the last decades.

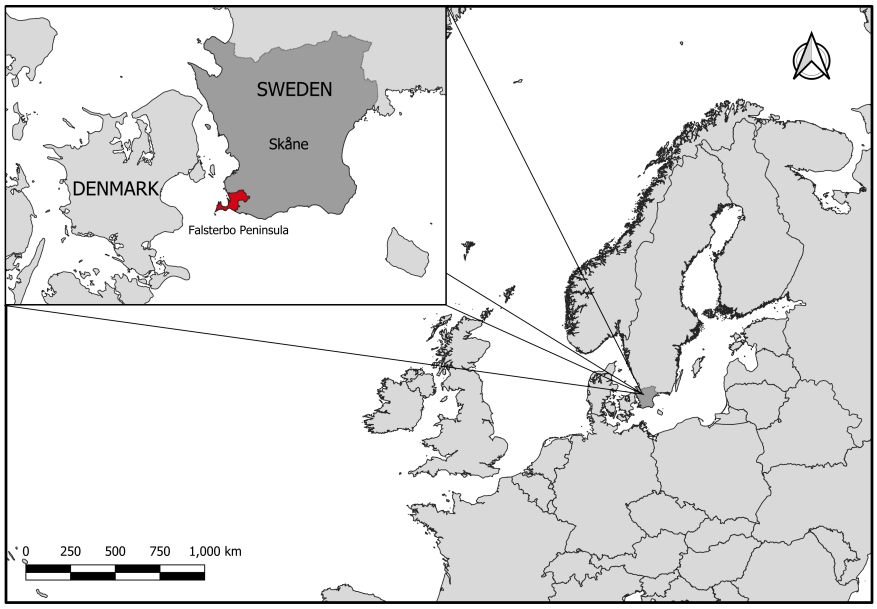

Figure 1.1: *Map of Sweden with Vellinge Municipally indicated in red.*

Responsibilities for coastal safety vary across different countries (Bontje et al., 2016). In the Netherlands, the responsibility lies with the initial and sub-national levels. In Denmark, coastal management is organised from the national level to the land-owners level. In the United Kingdom, depending on the county, the responsibility is at the country level or local level. In Sweden, coastal protections are organised by the municipality or the landowners. To protect the densely populated area in the Falsterbo Peninsula the municipality of Vellinge was granted a permit to build flood protections. As part of the strategy, a dike will be built at locations indicated in Figure 1.2 and the dunes will be used as natural barriers against storm surges.

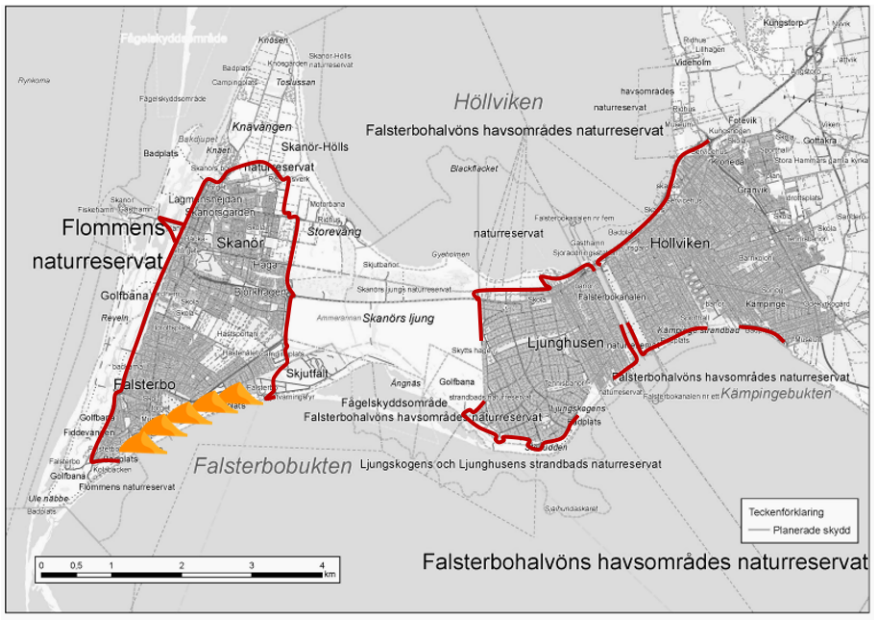

Figure 1.2: *Natural dunes (in orange) and to-be-constructed dikes (in red) as flood protection in the Falsterbo Peninsula. Figure from Municipality (2023)*

For the design of the dike, assessments had been conducted and both a storm surge with a 100-year return period Return Period (RP) and the most severe storm surge in 1872 had been

included. A crest height of +3.00 m above the Swedish National Height System 2000 (RH 2000) was derived and proposed, but this height is neither based on the 100-year surge level nor the 1872 storm surge level. Taking into account that the mean sea level Mean Sea Level (MSL) in Vellinge municipality from 1995 to 2014 was +0.15 meters in the reference system The Swedish National Height System 2000 (RH 2000) according to SMHI, which implies that the crest height would be +2.85 meters relative to MSL. According to Irminger-Street (2018), it is not clear what probability this crest level corresponds to. The dune system in the study area, despite being part of coastal protection against flooding, has not been assessed. Consequently, there is a need to evaluate the state of the current dune system to ensure coastal safety in the region.

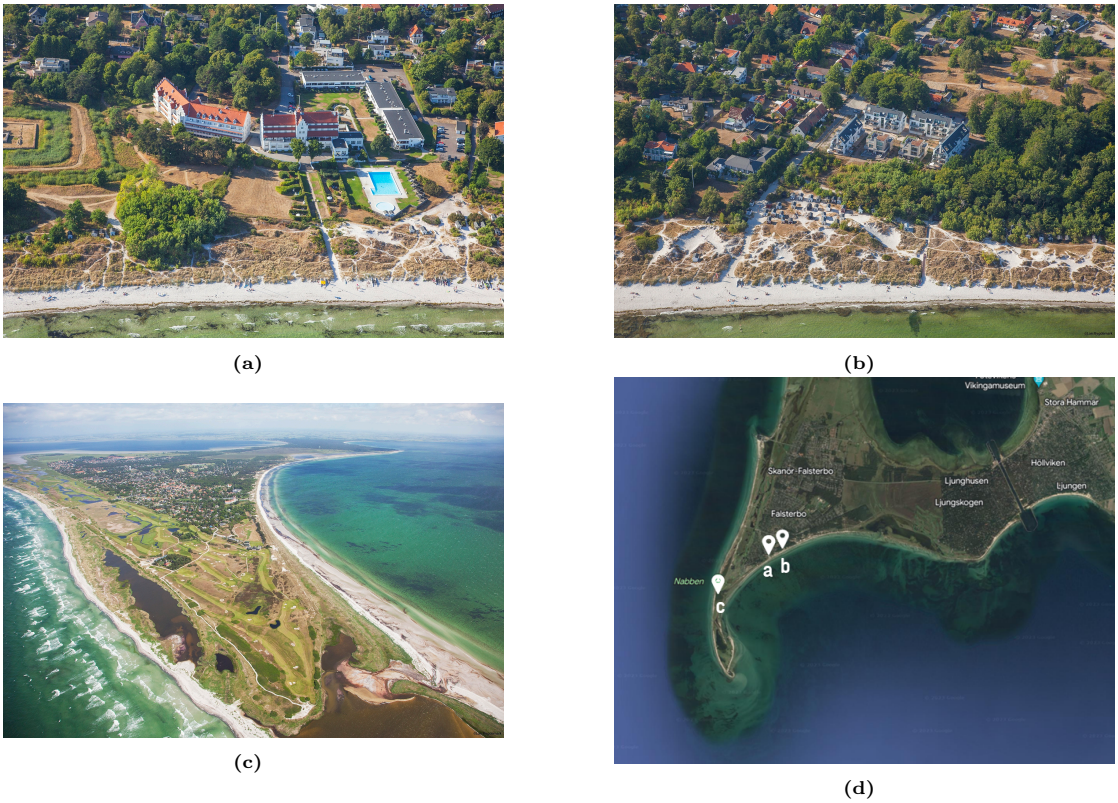

Figure 1.3: *Aerial photo of three different locations in the Falsterbo Peninsula, as indicated in figure* ***d****. Photos by Lars Bygdemark.*

The dune system is located on the left side of Figure 1.2, which is situated on the outermost tip of the peninsula. Behind the dune in Figure 1.3a and 1.3b, a densely populated area is directly situated. On the west side of the peninsula in Figure 1.3c, the area is separated from the water by wetlands and golf courts. The locations of where the pictures were taken are indicated in Figure 1.3d.

1.3. 1872 Storm

The 1872 storm in the Baltic Sea is considered the strongest storm surge on record up to today. Figure 1.4 shows the measured water level in Lübeck-Travemünde in Germany. The water level during the storm was over 3.3 m above MSL at this location (Rosenhagen and Bork, 2009) and in Falsterbo Peninsula the water level was estimated at about +2.4 m (+2.6 relative to RH 2000) (Fredriksson et al., 2016). The water level had not been recorded in this area so the water level had to be estimated based on flood marks and eyewitness stories. The extreme storm surge can be explained by an unusual interaction of atmospheric pressure systems. First, there were strong westerly winds which pushed the water into the Baltic Sea, causing the water level in the entire

basin to rise. Thereafter, easterly winds reached hurricane strength, pushing the water to the southwest Baltic Sea. Not only was there a high water level, but the strong winds also generated high waves that coincided with the storm surge peak. The rare combination of high water level and wave height makes the 1872 storm a unique event (Hallin et al., 2021).

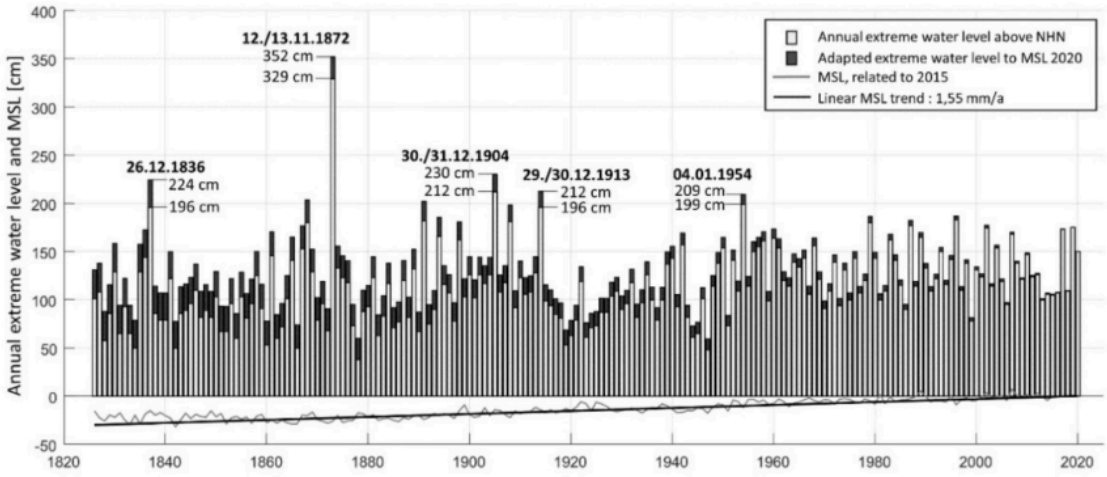

Figure 1.4: *Annual extreme water level and MSL at Lübeck-Travemünde gauge station for the period 1826 to 2020. Figure from Hallin et al. (2021).*

The consequences of the storm in Denmark and Germany were more severe than in Sweden, causing the storm to be more remembered by the Danish and German people. According to Hallin et al. (2021), the collective memory of the 1872 storm is related to the background knowledge about floods, the damage extent, and the response to the storm. The 1872 storm has been seen as a turning point for coastal flood defence in Germany. After the evaluation of the hydraulic load during the storm, the design criteria for coastal protection have been stipulated. In Denmark, existing dikes were reinforced and new dikes were constructed on Lolland and Falster. Since the collective memory in Sweden is smaller, fewer actions have been undertaken in terms of coastal flood defences.

The 1872 storm had little influence on the organisation of coastal management (Hallin et al., 2021). The storm is considered extreme but not a unique event (Hallin et al., 2019), indicating the possibility of its recurrence. For better preparedness, it is crucial to assess the potential impact on the current dune system in the event of a recurrence of the 1872 storm.

1.4. Problem Description

Storm surges in a semi-enclosed sea such as the Baltic Sea can be wind-driven, pressure-driven, or a combination of both (Wolski and Wiśniewski, 2021). Strong winds can produce large wave heights, depending on the wind direction, duration and fetch length, while differences in atmospheric pressure can increase the water level. In the Baltic Sea high wave heights are not necessarily correlated with high water levels (Hanson and Larson, 2008), unlike the open sea such as the North Sea. Due to the orientation of the coastline in the south of Sweden, wind-generated waves only come from directions between Southwest and Southeast. Higher wave heights can be expected as these directions have the longest fetch length.

According to Hünicke et al. (2015), strong winds from the West during storm conditions can push the water from the North Sea into the Baltic Sea, causing the water level to increase. Westerly

winds can also cause seiches in the Baltic Sea because of its semi-enclosed system, giving rise to the water level (Jensen and Müller-Navarra, 2008). Hanson and Larson (2008) found that winds from the North and Northeast are associated with high water levels as they can transport water from the North to the South part of the Baltic Sea.

Given the complex interaction between environmental factors (wave, wind, and water level), the prediction of extreme conditions requires an in-depth understanding of the interdependence between various storm parameters. A more detailed study is essential to obtain accurate predictions. Due to the involvement of multiple storm parameters, different scenarios of storm conditions can share the same level of occurrence. The study of Oo et al. (2022) shows that despite having the same return period, distinct scenarios of storm conditions can result in varying dune erosion. This study indicates that a range of scenarios could lead to an event with a certain return period but the impact on the dune will be different for each scenario. It is therefore essential to evaluate the dune's ability to withstand a range of possible scenarios within that return period.

To summarize, conducting dune erosion assessment in a semi-enclosed sea faces two significant challenges. Firstly, the complex interaction of environmental factors complicates the prediction of future storm conditions. Secondly, dune erosion can vary under different storm scenarios corresponding to the same probability of occurrence. Predicting the scenarios for dune erosion assessment should therefore be done with great care to avoid underestimation of dune erosion. Such underestimation could lead to inadequate preparedness and the implementation of insufficient protective measures.

An approach to enhance the prediction of storm conditions is the assessment of historical dune erosion with the storm conditions in the study area. Studying the dune erosion as a result of past storm conditions can aid in a comprehensive understanding of the interactions of waves and water levels with the dune system. However, challenges arise due to the absence of dune erosion data. In the context of coastal studies in Sweden, the research on dune systems is limited due to the scarcity of sandy beaches, which are predominantly concentrated in the southern regions (Hanson and Larson, 2008). Without the dune erosion data, there are no insights into the erosion patterns and the magnitude of dune erosion in remains unknown.

The dune system will be used as a first-line barrier against flooding on the Falsterbo Peninsula. However, the effectiveness of the dune system as coastal protection against storm impacts has not been comprehensively assessed. The unknown severity of erosion, resulting from the lack of historical dune erosion data, is a crucial problem in this context as it complicates the assessment of the safety level provided by the dune system. This safety level is important for the community in the study area as it ensures that the community is adequately protected during extreme weather conditions. Determining historical dune erosion using morphological models is essential to bridge this data gap in the study area.

1.5. Objective & Research Questions

This study aims to provide a numerical representation of the severity of dune erosion due to historical storm conditions spanning from the period 1959 to 2022. The 1872 storm is the largest storm surge in the study area, the storm is considered extreme but not a unique event. Suggesting its potential recurrence. To gain insight on the potential impact on the present dune system, this study incorporates the analysis of this storm. The analysis utilizes morphological models to simulate dune erosion. The insights derived from this study can aid in evaluating the extent to which the dune system contributes to the protection of the hinterland against storm conditions.

To achieve this objective, the following research questions were formulated:

To what extent does the dune system on the Falsterbo Peninsula contribute to safeguarding the hinterland against the impact of historical storm conditions?

In order to answer the main research question, several sub-questions have been formulated:

- **RQ1: How to extract scenarios of past storm conditions from historical time series data, considering the complex interactions between waves and water levels?**
- **RQ2: Which scenario of past storm conditions can potentially impact the dune system on the Falsterbo Peninsula?**
- **RQ3: What methods can be employed to estimate dune erosion volume resulting from the selected storm scenarios?**

1.6. Research Approach

The overall approach to collect the necessary data in this study is presented in Figure 1.5. This thesis methodology comprises three parts. The first part aims to collect the data of environmental factors (wind, water level, and waves) spanning the period from 1959 to 2022. The time series of wind and water levels is available in an hourly time resolution. The hourly wave data will be simulated in this study, using the SWAN model (Delft, 2022). The second part is dedicated to defining a storm condition in the 63-year time series and extracting the corresponding storm scenario. The last part involves estimating dune erosion using the storm impact model (Larson et al., 2004) and the XBeach model (Roelvink et al., 2010). More details about each part are described in Chapter 3.

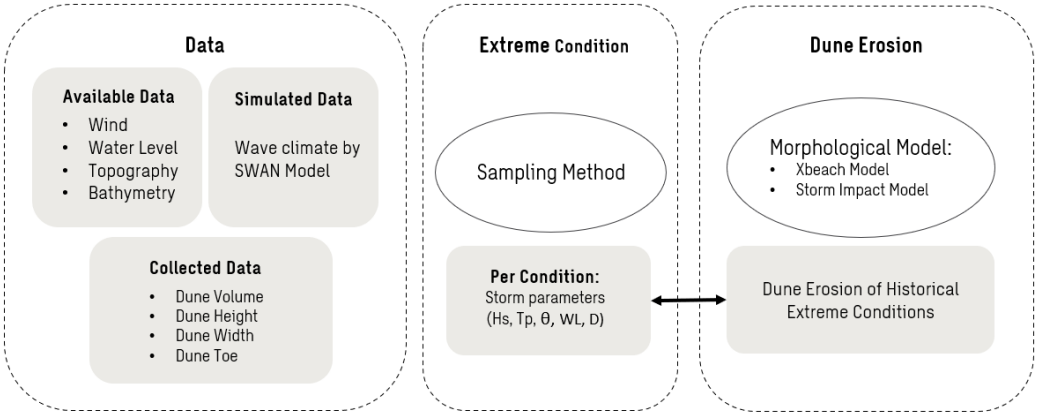

Figure 1.5: *Research overview to study the dune erosion due to historical storm conditions.*

1.7. Thesis Outline

The overview of this report is shown in Figure 1.6. Chapter 1 introduces the approach of dune erosion assessment and the implications of conducting such assessment in the study area. Chapter 2 provides the background on hydrodynamic and morphodynamic processes; and on numerical models that can be used to simulate coastal evolution. The research approach, including the data collection and processing methods in this study, is described in Chapter 3. Chapter 4 describes the collected data, including the dune morphology data obtained from the fieldwork. The SWAN

model results and description of the wave climate in the study area are presented in Chapter 5. How the storm conditions are extracted from the historical time series is described in Chapter 6. Chapter 7 represents the dune erosion, estimated by the XBeach and the storm impact model, corresponding to the storm conditions. Chapter 8 discusses the results and the methods used in this study. Finally, Chapter 9 provides the overall insight obtained in this thesis and offers recommendations for future research. The appendices include the supplementary formation that supports the main part of the thesis.

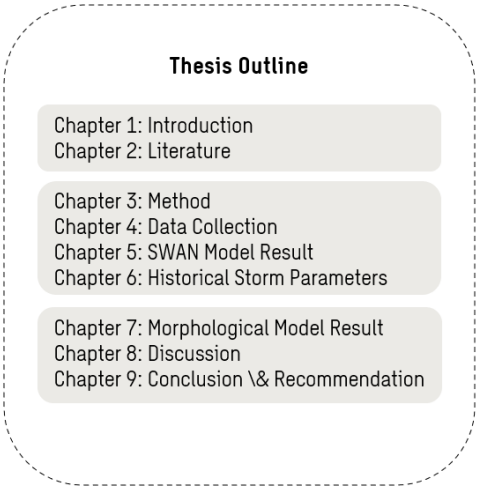

Figure 1.6: Thesis outline

2. Theoretical Background

This chapter establishes the foundational background for the thesis topic. The coastal terminology essential for this study is presented in Section 2.1 to provide readers an understanding about various coastal areas. Then a description is given regarding hydrodynamic processes and dune morphology in Section 2.2 and 2.3. Subsequently, the numerical models employed in this study is described in details in Section 2.4. Furthermore, the tools utilized in the field measurement (Section 2.5) and various methods that can be used to sample extreme events from the time series (2.6) are introduced. Finally, this chapter concludes with an explanation of coastal protection management in Sweden, providing the readers a contextual understanding of the strategies for coastal safety.

2.1. Coastal Terminology

When waves propagate from deep into intermediate and shallow water depths, the wave energy transforms due to processes such as refraction, shoaling, bottom friction and wave-breaking. The transformation, i.e. the change in wave height, wavelength and wave direction, continues until waves break and lose their energy. The definition of the processes together with terminologies in coastal zones and wave characteristics are given in Figure 2.1.

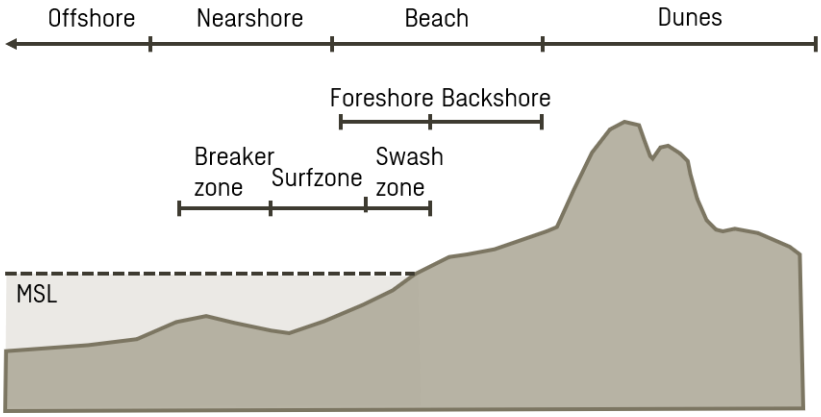

Figure 2.1: *Cross-section of nearshore areas, figure modified from USACE (2008).*

Offshore zone , also called deep water, refers to the area that is farther away from the coast where the water depth is less than half of the wavelength. In this area, the energy of the wave can be transformed by processes such as white-capping and current. White-capping is the process when the wave steepness becomes too large compared to the wavelength, this process can also be referred to as steepness-induced wave-breaking. In the presence of a current, energy transfer is possible between waves and currents.

Nearshore zone or littoral zone is the area where the energy balance can be transformed due to shoaling, refraction or bottom friction.

Breaker zone and **surf zone** can be found in the nearshore zone, where waves start to break when the wave height becomes larger than a certain fraction of the water depth. This process is

also called depth-induced breaking since the limiting wave height is governed by a water depth limitation. The main difference between the two zones is that the waves start to break in the breaker zone, while in the surf zone, the waves with reduced wave heights continue to break.

Swash zone can also be found in the nearshore zone, it forms the land-ocean boundary where wave bores runup the beach after the waves have broken and dissipate the last wave energy. This zone can be characterised by strong and unsteady flow, high turbulence levels and high sediment transport rates.

Beach area consist of **foreshore** and **backshore**. The foreshore is the area that is periodically wet and dry due to wave actions. The backshore is the area that is always above MSL in normal conditions. In extreme conditions such as storms, this area will be wet as well.

Dune is a hill of sand that is formed by wind, water flow or wave action. Coastal dunes are constructed of accumulated sand under the influence of waves and wind in coastal areas where the sediment supply is infinite. A more detailed description of the dune and its characteristics can be found in Section 2.3.

2.2. Hydrodynamic processes

Ocean waves are a collective term for several types of waves found in the ocean, such examples are wind waves, tides and tsunamis. A wave is best represented by a sine function, where the shape represents the variation of the water surface at a certain time. The wave characteristics are shown in Figure 2.2 and the definitions are given below.

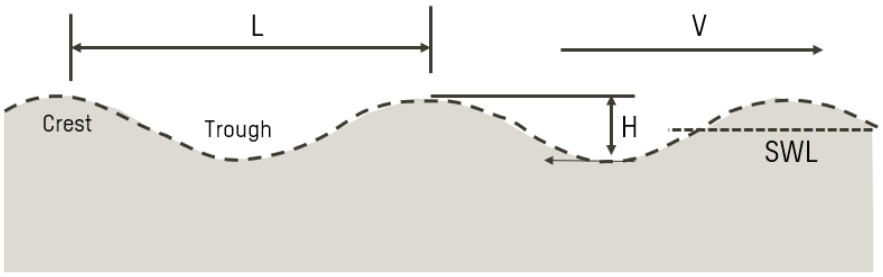

Figure 2.2: *Wave characteristic. Figure modified from Earle (2015).*

The wave height (H) is the vertical distance between the wave crest and wave trough. For a sinusoidal wave, the wave height is equal to twice the wave amplitude (a). The wave moves with the velocity (V) and the time needed to pass a location is called the wave period (T_p). The number of waves passing a fixed location is called the frequency, which is the inverse of the wave period. The wavelength (L) is the distance between two consecutive wave crests of wave troughs. It is the length that the wave will travel in the wave period (T_p). The typical unit of the wave period for wind waves is in seconds, for tides in hours and for tsunamis in minutes.

2.2.1. Wave Energy Density Spectrum

The variance density spectrum describes the surface elevation of ocean waves, where all statistical characteristics of the wave field can be modelled as a stochastic process. The surface elevation, described in Equation 2.1, is considered to be the sum of a large number of harmonic waves, each with an amplitude and a phase. This model is also called the random-phase/amplitude model. The number of frequencies is represented by N, and the amplitude $\underline{a}_i$ and the phase

$\underline{\alpha}_i$ are now random variables. The amplitude and the phase at each frequency follow Rayleigh and uniform distribution respectively. The realisation of a surface elevation is done by drawing a random amplitude and phase from the probability density functions. The expected value of the amplitude, defined as $\mathrm{E}(\underline{a}_i)$, along the frequency axis shapes the amplitude spectrum. Alternatively, the variance spectrum, defined as $E(\frac{1}{2}\underline{a}_i^2)$ in the second panel, can be considered instead of the amplitude spectrum.

$$\underline{\eta}(t) = \sum_{i=1}^{N} \underline{a}_i cos(2\pi f_i t + \underline{\alpha}_i) \tag{2.1}$$

As the frequency at sea is continuous rather than discrete, the variance spectrum needs to be modified by distributing the variance over the frequency interval. As a result, the continuous variance density spectrum ($E(f)$) fully describes the surface elevation of ocean waves and all statistical characteristics can be expressed in terms of this spectrum. When multiplying the variance spectrum by the gravitational force and water density ($g\ \rho$), the energy density spectrum follows according to Equation 2.2. The more narrow the energy density spectrum, the smaller the range of the frequencies and thus the more regular the waves.

$$E_{energy}(f) = \rho g E_{variance}(f) \tag{2.2}$$

In the JOint North Sea WAve Project JONSWAP by Hasselmann et al. (1973) wave spectra were measured in the North Sea by a number of scientists from England, Holland, the United States and Germany. The aim of this project is to obtain wave spectral data and density to construct the wave spectrum empirically.

The wave spectrum at fully developed conditions in deep water was described before by Pierson Jr and Moskowitz (1964). Here a smooth cut-off function was used at the low frequencies and the shape of high frequencies follows the shape suggested by Phillips (1958). The spectra observed during JONSWAP appear to have the same shape as the Pierson-Moskowitz Pierson-Moskowitz (PM) spectrum but with a sharper peak. To account for this observation, the JONSWAP spectrum follows the PM spectrum with a peak-enhancement function. The expression can be found in Figure 2.3.

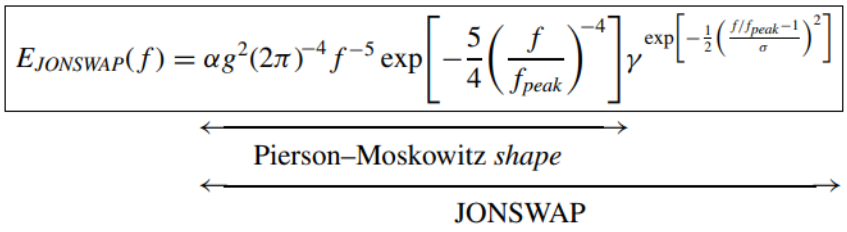

Figure 2.3: *Description of the JONSWAP spectrum, based on Pierson-Moskowitz shape and a peak-enhancement function. Figure from Holthuijsen (2010)*

2.2.2. Wave Energy

The energy conservation equation in Equation 2.3 is composed of the change of energy, the import of energy in the x-direction and y-direction, and the gain of energy. The first underlying assumption for this equation, by Bosboom and Stive (2021), is that the irregular wave field at one location can be represented by a single value. The second assumption is that the total energy is propagating with the wave group speed.

$$\frac{\partial E}{\partial t} + \frac{\partial (E c_g cos\theta)}{\partial x} + \frac{\partial (E c_g sin\theta)}{\partial y} = S - D \tag{2.3}$$

The input energy to the wave is indicated in the equation as S, which is the energy due to the wind. Dissipation of wave energy D modifies the wave's properties through transformation processes such as shoaling, refraction, bottom friction, and wave breaking. The definition of each term will be given below.

Wind-Generated Waves

Wind-generated waves are developed when the wind blows over the water surface in time and space, the energy is then transferred from the wind to the waves. The wave grows in the same direction as where the wind is blowing, meaning that the wave energy becomes concentrated in the direction of the wind. The growth follows the duration- and fetch-limited growth laws, according to Hwang (2006), they quantify the wave evolution under driving force. The duration-limited law can be explained with the uniform wind blowing over unlimited fetch far from the shore. The total energy E and peak frequency f_p depend on the duration of the wind, hence duration-limited. In the case of fetch-limited law, the wind has blown constantly long enough for wave heights at the end of the fetch to reach equilibrium. Here E and f_p only depend on the fetch length, which is the distance that the wind can travel in a constant direction over the water surface. The illustration of a wind-generated wave is given in Figure 2.4. The wind speed at 10 m elevation is chosen to be the reference wind speed in the study of wave growth, this is mainly due to practical considerations.

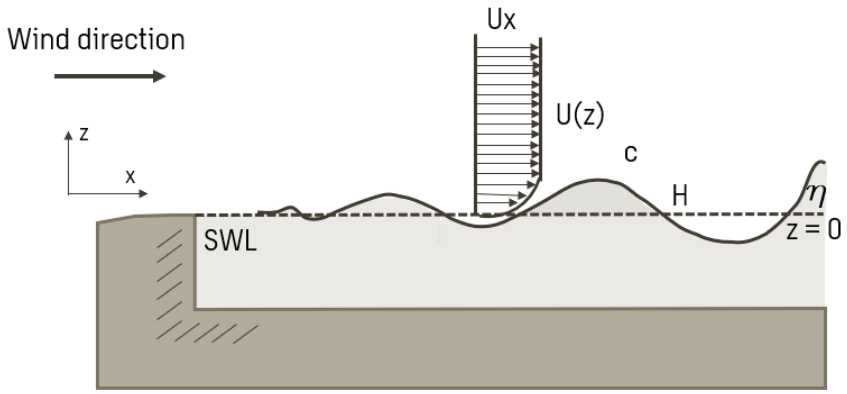

Figure 2.4: *Illustration of a wind-generated wave in a wind tunnel. Figure modified from Longo (2012).*

Shoaling

When waves travel into the intermediate water and parallel to the depth contours, the propagation speed decreases due to decreasing water depth. As the first wave in the wave train slows down, the waves behind are still travelling at a speed of slightly deeper water. At some point, these waves tend to catch up with the wave in the front, increasing the wave energy. The increase in wave energy results in higher wave height and wave steepness, this process is called shoaling. The change of the wave height compared to wave height at deep water can be expressed in the shoaling factor K_{sh}, see Equation 2.4. The magnitude decreases from 1.00 at deep water to a value of 0.91 and rises to infinity. In reality, the wave height does not grow to infinity but reaches the height at the wave wave-breaking limit.

$$\frac{H}{H_0} = \sqrt{\frac{1}{tanhkh}\frac{1}{2n}} = K_{sh} \tag{2.4}$$

Refraction

When waves approach at an angle, the part of the wave crest in deeper water travels faster than the part in shallower water. This bending effect causes the wave crest to turn and is referred to as refraction. According to Snell's law in Equation 2.5, the change in wave direction is proportional to the change in wave speed. When assuming the energy remains constant between two wave rays (normal to the wave crest) the wave rays refract in the same way due to the parallel depth contours. The refraction factor can be described as in Equation 2.6.

$$\frac{sin\phi_1}{c_1} = \frac{sin\phi_0}{c_0} = constant \tag{2.5}$$

$$K_r = \sqrt{\frac{cos\varphi_0}{cos\varphi}} \tag{2.6}$$

Bottom friction

The resistance experienced by flowing water as it interacts with the bed surface is called bottom friction. It is a frictional force that slows down the fluid's velocity where the reduction rate is based on the flow and seabed characteristics. This reduction in velocity plays a crucial role in dissipating wave and current energy and influencing sediment transport. The bottom friction decreases the fluid's velocity with depth, creating a velocity gradient which acts as a shear stress being transmitted from the fluid to the bed. This bed shear stress is expressed as a force per unit area (N/m^2). The influence of the bottom friction on the wave and current energy is a complex phenomenon, therefore several formulations have been developed to account for its impact. The simplest formulation is an empirical expression based on the JONSWAP experiment, Hasselmann et al. (1973). More complex formulations such as drag-law models and eddy viscosity models are developed by Hasselmann and Collins (1968), Collins (1972), Madsen et al. (1988) and Weber (1991). In the study on energy balance with bottom friction source term according to each formulation by Luo and Monbaliu (1994), it was found that the growth curves for the total energy for depth-limited wind-generated waves were quite different.

Wave-breaking

Wave breaking can occur due to two types of mechanisms. The first mechanism is based on the steepness of the wave and can also be referred to as steepness-induced wave-breaking or white-capping. The limit of wave steepness is defined by Miche (1944) based on the Stokes wave theory. The steepness is defined as the wave height divided by the wavelength. In deep water, $tanh(kh)$ can be assumed at 1.00 and Equation 2.38 reduces to a constant value. Due to this limit in the wave steepness, the wave height does not grow to infinity as expected due to shoaling.

$$\left[\frac{H}{L}\right]_{max} = 0.142tanh(kh) \tag{2.7}$$

$$\gamma = \left[\frac{H}{h}\right]_{max} = \frac{H_b}{h_b} \tag{2.8}$$

In shallow water Equation 2.38 reduces to Equation 2.8 with the breaker index defined as γ, the breaking wave height as H_b and water depth at the breaking point as h_b. When the solitary wave theory is used instead of the Stokes wave theory, the value of γ becomes 0.78. In the study

of Kamphuis (1991) where incipient wave breaking is studied from 225 model test results, it was found that the value γ of 0.62 can be used as a breaker index. The breaker index defines a threshold for the ratio between wave height and water depth. When this ratio exceeds the breaker index, the wave undergoes breaking. This is the second type of wave-breaking mechanism, also known as depth-induced wave-breaking.

2.2.3. Runup Height

The term runup (R) in the coastal engineering world can be described by Holman and Sallenger Jr (1985), as the time-varying location of the shoreline water level about still-water level. It is the highest level reached by water above the still water level Still Water Level (SWL), see Figure 2.5. The parameter is important when assessing coastal safety and the vulnerability of dunes. According to Holman and Sallenger Jr (1985), Hedges and Mase (2004), and Stockdon et al. (2006) the runup can be divided into two components: a superelevation of the mean water level also called the setup (S_{wave}), and fluctuations about the mean, called swash. Both components can be described as a function of deep-water wave height (H_0), deep-water wave period (T_0), and a representative slope as reported by Stockdon et al. (2006). The first component is important to the dynamics of near-shore currents and the process is driven by the cross-shore gradient in radiation stress that results from wave breaking, explained by Longuet-Higgins and Stewart (1964). The setup is the height of the mean water level Mean water Level (MWL) above SWL, indicated as S in Figure 2.5. The second component of the runup, the swash, is defined as the time-varying location of the intersection between the ocean and the beach.

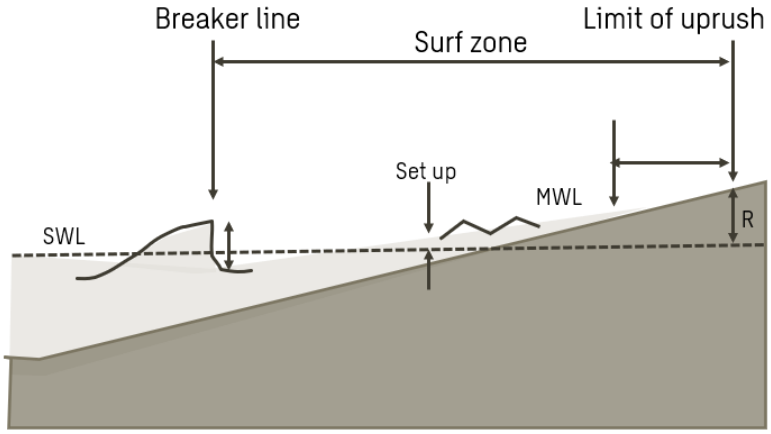

Figure 2.5: *Definition of runup and setup of regular waves. Figure modified from Hedges and Mase (2004).*

The runup height is an important parameter for coastal engineering in terms of designing coastal protections. It is a key factor in determining the potential for coastal flooding and erosion. Large efforts have been put into the development of equations to calculate the runup height. The most commonly used equations are empirical equations, which are based on observations. The equations can be used for a quick estimation of R when the data is not available. Each empirical equation is derived from specific hydraulic factors and beach characteristics, such as H_s, S and the beach slope. The use of each equation should be used in the appropriate circumstances. The equation by Hunt Jr (1959) can be used to compute R due to regular waves on structures. The equation is modified by Hedges and Mase (2004) for R due to irregular waves, it includes the swash and the wave setup. The runup height is defined as the height of the 2 % largest wave and can be calculated according to Equation 2.9. The equation is based on the equivalent deep

water significant wave height H_{s0} and the foreshore slope (β_F).

$$R_{2\%} = H_{s0}(0.34 + 1.49\zeta_0) \tag{2.9}$$

$$\zeta_0 = \frac{tan\beta_F}{\sqrt{H_{s0}/L_{s0}}} \tag{2.10}$$

ζ_0 was found by Holman and Sallenger Jr (1985) to be an appropriate value to calculate the surf similarity parameter, also called the Iribarren number (ξ). Laboratory evidence by Hunt Jr (1959) showed that the total runup is proportional to the Iribarren number and an empirical constant.

$$L_{s0} = \frac{g(1.15T_p)^2}{2\pi} \tag{2.11}$$

$$H_{s0} = \frac{H_{sby}}{K_s} \tag{2.12}$$

$$K_s = \sqrt{\frac{C_{g0}}{C_g}},\ C_{g0} = \frac{g(1.15T_p)}{4\pi},\ C_g = \sqrt{gd_b} \tag{2.13}$$

$$H_{sby} = H_{sb}\sqrt{cos\alpha_b} \tag{2.14}$$

The deep water wavelength (L_{s0}) is determined using the deep wave period which is defined as 1.15 times higher than the peak wave period (T_p). The significant wave height in deep water(H_{s0}) can be determined through a reversed shoaling of breaking wave height (H_b). The shoaling coefficient (K_{sh}) can be determined with the wave group velocity (C_{g0}) and the wave group velocity at breaking (C_g). The onshore component of the wave energy is obtained by multiplying H_b with the square root of the cosinus of the wave angle at breaking (α_b). H_b and α_b can be obtained by transforming the extracted waves from the SWAN model to the breaking depth using an explicit formula described by Larson et al. (2010):

$$H_b = \frac{\lambda C_m^2}{g} \tag{2.15}$$

$$\alpha = arcsin(sin(\alpha_m)\sqrt{\lambda}),\ \lambda = \delta\lambda_a \tag{2.16}$$

$$\lambda_a = (\frac{cos\alpha_m}{\theta})^{2/5},\ \theta = (\frac{C_m}{\sqrt{gH_m}})^4 \frac{C_m}{C_{gm}}\gamma_{b^2} \tag{2.17}$$

$$\delta = 1.0 + 0.1649\varepsilon + 0.5948\varepsilon^2 - 1.6787\varepsilon^3 + 2.8573\varepsilon^4,\ \varepsilon = sin(\alpha_m\lambda_a) \tag{2.18}$$

The explicit formula determines the wave properties at incipient breaking by solving the energy flux conservation equation and Snell's law, between an arbitrary water depth (denoted by subscript m) and breaking depth (denoted by subscript b). The formula makes use of the following parameters: phase speed (c_m), group speed (c_{gm}), gravitational acceleration (g), wave angle (α_b), wave height at an arbitrary depth H_m and breaking index (γ).

2.2.4. Wind-induced Setup

Wind blowing over the water's surface exerts a shear stress. The shear stress causes the upper parts of the water layer to move in the same direction as the wind direction. Figure 2.6 illustrates the onshore wind inducing a landward current in the upper part of the water. As a result, the water level rises near the coast to balance the wind-induced shear stresses, this mechanism is also known as the wind-induced setup.

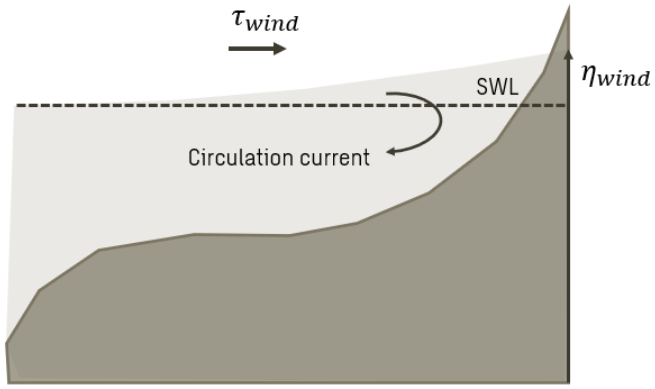

Figure 2.6: *Wind setup due to onshore wind on a shelf, figure by Bosboom and Stive (2021).*

In storm conditions, the water level can pile up to great height (storm surge) due to the combination of wind-induced setup and low atmospheric pressure. The severity depends on the duration of the storm system. The presence of waves can give rise to the water level that reaches the coastline due to wave setup and wave runup.

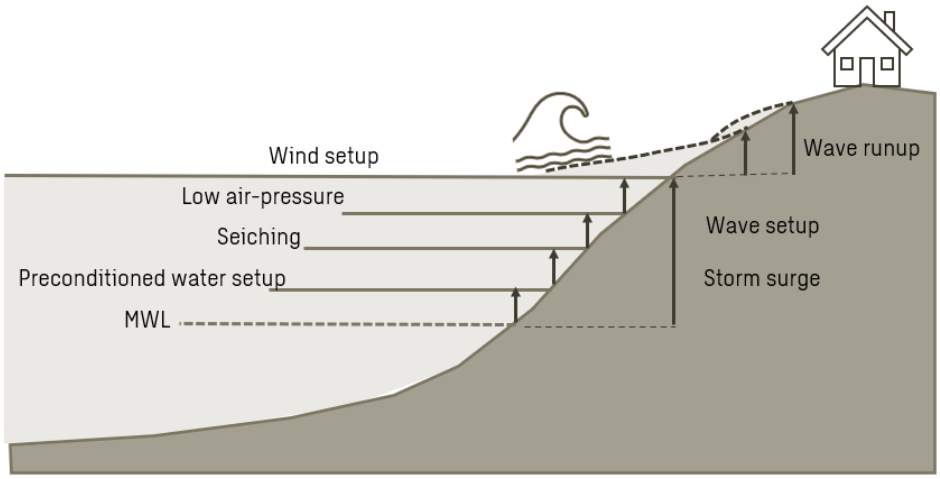

Figure 2.7: *Components contributing to coastal flooding. Figure modified from Hallin et al. (2022).*

2.3. Dune Morphology

Coastal dunes, also referred to as dunes, can be defined as a prominent landform that is shaped by various factors such as wave, current, wind (eolian transport), sediment availability and vegetation. Coastal dunes have multiple functions in the coastal ecosystem. The main function

of the dune in the coastal engineering field is that they act as a natural barrier, safeguarding the hinterland from coastal flooding. Beyond their protective role, dunes also maintain the sediment balance by serving as sediment reservoirs and sources. Additionally, dunes provide habitats for diverse plant and animal species, increasing the biodiversity in coastal areas. Moreover, recreational spaces can be added to the dune area for tourism potential and economic benefits to local communities.

2.3.1. Dune Erosion In Storm Conditions

Processes that can contribute to the dune development are mainly wind transport or eolian transport and sand trapping due to the vegetation. Dune erosion can be the result of the wave and current action if the sediment availability is inadequate. Most severe dune erosion occurs under storm conditions where the mean water level increases and the waves can reach the dune face, as illustrated in Figure 2.8. The eroded volume from the dune face is transported further seaward, creating a new beach profile that is more efficient in dissipating the wave energy. As the storm progresses, the dune erosion rate decreases due to the reduced impact of the wave.

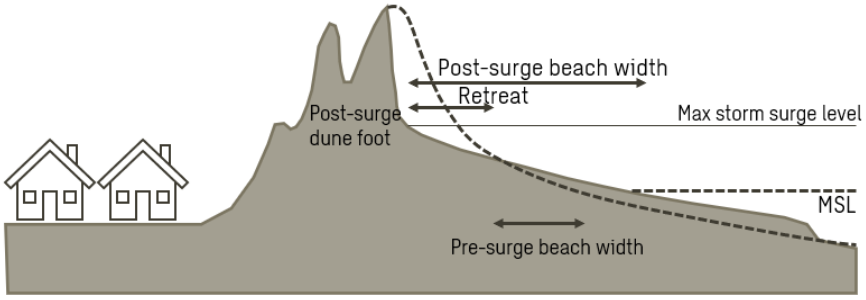

Figure 2.8: *Illustration of a storm surge dune erosion, modified from Bosboom and Stive (2021).*

The sediment transport from the dune can be distinguished in two stages by Van Gent et al. (2008). The first stage is drag-induce erosion where the sediment higher in the profile is brought into suspension by the wave action and transported to the lower profile. The process continues until the dune face is vertical and slumps of sediment slide down from the dune face. This is the second stage of sediment transport and can be referred to as avalanching.

2.3.2. Storm Regimes

The storm impact on the dunes is divided by Sallenger Jr (2000) in four different types of regimes, depending on the impact scale. Figure 2.9 by Hallin et al. (2019) illustrates the different regimes. The first regime is the swash regime, where the swash only reaches the foreshore and transports the sand offshore, leaving the dune intact. In the second regime, the collision regime, the wave runup collides with the base of the dune and erodes the sediment from the dune. The sediment either ends up at the beach or is transported offshore. Unlike the swash regime, the eroded sand does not typically return to re-establish the dune. The third regime is the overwash regime, where the wave overtops the dune and washes away the sand landwards. The eroded sand does not return seaward to the beach but contributes to the process where the dune is migrating landward. The last regime is the inundation regime, where the dune is completely submerged and the impact is due to surf-zone processes. The different impact scale can be used to categorise and forecast the wave impact, in case the storm forcing and the coastal geometry is known.

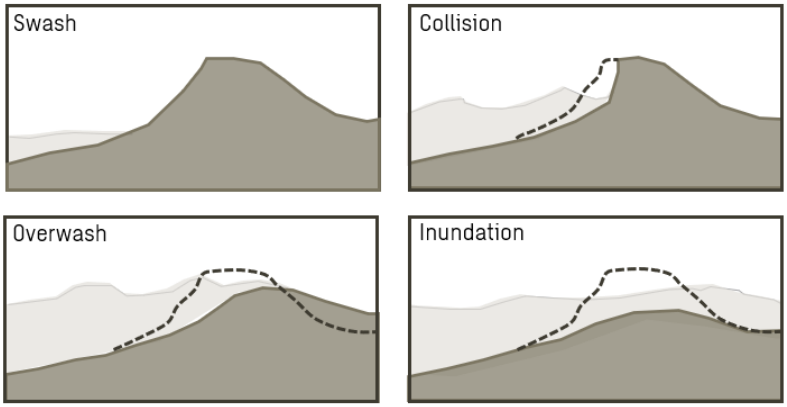

Figure 2.9: *Different types of regimes according to the storm impact scale by Sallenger Jr (2000). Figure modified from Hallin et al. (2019).*

2.4. Numerical Model For Coastal Evolution

The complex real-world phenomena can be represented through numerical modelling using mathematical equations to simulate the behaviour and numerical techniques to obtain approximate solutions. Numerical modelling is a tool that can be used to investigate various scenarios, predict behaviour under different conditions and describe the effects of the different input parameters on the output parameters. The main elements of numerical modelling in Figure 2.10 include formulation, evaluation and application. The processes that need to be simulated by the numerical model and the selection of mathematical equations and numerical techniques are specified in the first step. The evaluation is done in the second step where the results of the numerical model are verified, calibrated, and validated. The verification is assessing whether the model is able to accurately represent the intended process, by comparing the numerical results with analytical solutions or experimental data. In the case of a significant difference, the model's parameter can be adjusted to improve the agreement between the two data sets. This process is called model calibration, where the model simulates the defined process using the optimum parameter values. The model evaluation is done by comparing the results with the observed data that were not used during the model calibration process. This way it is possible to see whether the model is able to accurately reproduce the defined process and to determine its reliability for future predictions. Once the numerical model produces satisfactory results, it can be used for various applications such as to analyze complex real-world phenomena, predict future behaviour, and optimize designs.

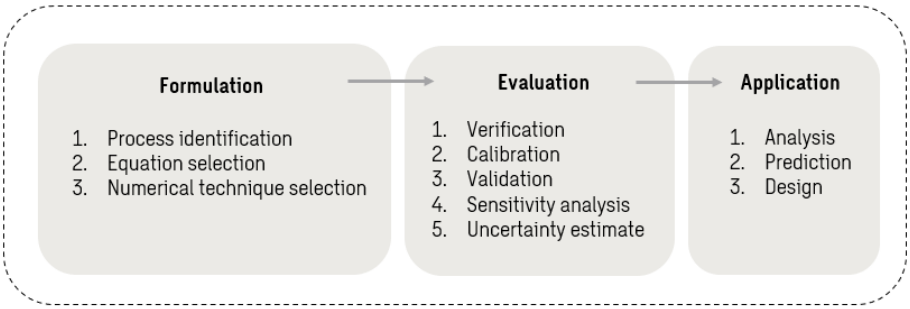

Figure 2.10: *Main elements in a numerical model. Figure modified from Larson (2005).*

Classification of numerical models of coastal systems is based on the time and space scales of the processes under study. According to Larson (2005), it is more common to develop a wide range of models that can simulate processes at different scales. This allows the model to include factors that are on the same scale as the process and neglect factors at other scales. An overview of the different types of numerical models for coastal areas is in Figure 2.11. As time and space scales decrease, the complexity of a model increases due to the computational challenges of the smaller time and space intervals.

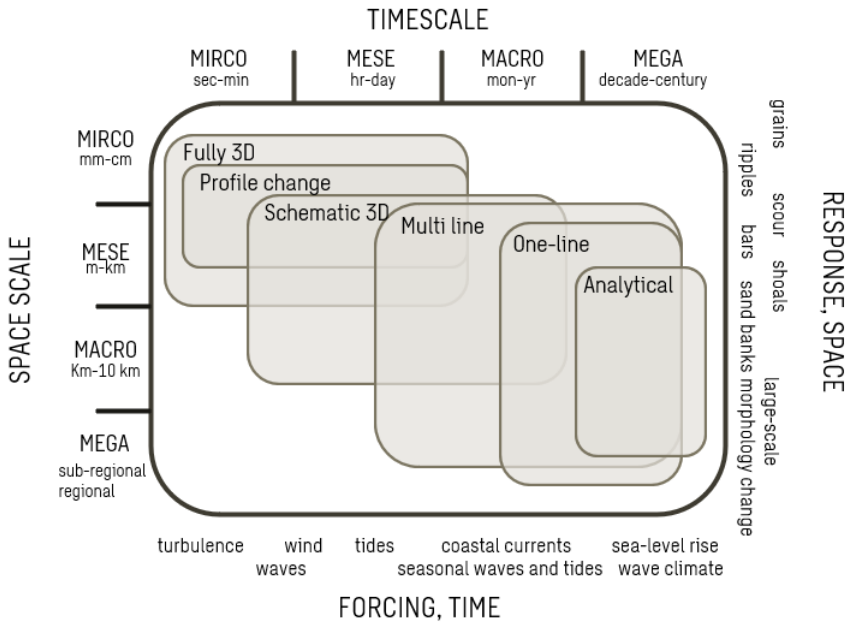

Figure 2.11: *Overview of coastal evolution models in terms of characteristic spatial and temporal scales. Figure modified from Larson (2005).*

The study will utilize three models, which are the SWAN, XBeach, and the storm impact model. The SWAN model will be used for wave simulations, and the XBeach and the storm impact model for dune erosion simulation. A description of each model is provided below.

2.4.1. SWAN Model Description

The Simulating Waves Nearshore SWAN model is a third-generation model for estimating wave characteristics and was developed at Delft University of Technology. The model can simulate wind-generated waves and swells in coastal areas, lakes and estuaries from input data such as wind, bottom and current conditions. The computations are based on the formulations of the Wave Model Wave Model (WAM) by Group (1988) for deep water and intermediate-depth water by adding formulations for depth-induced wave breaking and triad wave-wave interactions Booij et al. (1999).

The waves are simulated with numerical techniques that are suited for small-scale, shallow-water, and high-resolution computations. More information can be found in the SWAN manual Delft (2022). The wave spectrum is described by the spectral action balance equation, Hasselmann et al. (1973), where the terms on the left-hand side of the equation describe the kinematics and the terms on the right-hand side describe the source and the sick term.

$$\frac{\partial}{\partial t}N + \frac{\partial}{\partial x}c_x N + \frac{\partial}{\partial y}c_y N + \frac{\partial}{\partial \sigma}c_\sigma N + \frac{\partial}{\partial \theta}c_\theta N = \frac{S_{tot}}{\sigma} \tag{2.19}$$

- First term represents the local rate of change of action density in time.
- Second and third terms describe the propagation of action in geographical space.
- The Fourth term represents the shifting of frequency due to variations in depth and currents.
- The Fifth term represents depth-induced and current-induced refraction.
- The Sixth term is the source and sink term which represents the effect of generation, dissipation and nonlinear wave-wave interactions.

$$S_{tot} = S_{wind} + S_{wc} + S_{nl4} + S_{brk} + S_{bf} + S_{nl3} \tag{2.20}$$

The generation is due to the wind input S_{wind}, and dissipation is due to depth-induced wave breaking S_{brk}, bottom friction S_{bf} and white capping S_{wc}. The nonlinear terms are triad S_{nl3} and quadrupled S_{nl4} wave-wave interactions. The first three terms are deep water source terms, whereas the last three terms indicate shallow water source terms. How each of these terms is defined in the SWAN model, is explained below.

Wind Input

In SWAN, the transfer of wind energy to waves is described by two mechanisms according to Booij et al. (1999). The first mechanism is the resonance mechanism by Phillips (1957), where the birth of waves is due to the fluctuating pressure upon the water surface. If the frequencies in the pressure distribution coincide with the modes of free surface waves, then a type of resonance occurs and waves are generated at the surface. Surface waves can also be generated by shear flows $U(y)$, which is also known as the feedback mechanism by Miles (1957). The rate at which the energy is transferred to a wave of speed c_m turns out to be proportional to the profile of curvature at the elevation where $U{=}c$. The source terms of the two mechanisms are described as the sum of linear and exponential growth:

$$S_{in}(\sigma, \theta) = A + BE(\sigma, \theta) \tag{2.21}$$

The linear growth is expressed in term A according to Cavaleri and Rizzoli (1981) and the exponential growth in term B according to Komen et al. (1984). The formation of a wind-generated wave is illustrated by Longo (2012) in Figure 2.4.

Whitecapping

Whitecapping is controlled by the steepness of the waves and the formulation is based on a pulse-based model, according to Hasselmann (1974) formulation:

$$S_{ds,w}(\sigma, \theta) = -\Gamma \widetilde{\sigma} \frac{k}{\widetilde{k}} E(\sigma, \theta) \tag{2.22}$$

The wave number is indicated by k, mean frequency and mean wave number by $\widetilde{\sigma}$ and $\widetilde{k}$. The steepness-dependent coefficient Γ can be determined based on the following formulation:

$$\Gamma = C_{ds}(\frac{\widetilde{s}}{\widetilde{s}_{PM}})^p \tag{2.23}$$

The coefficients C_{ds} and p are tunable coefficients, $\widetilde{s}$ is the overall wave steepness and $\widetilde{s}_{PM}$ is the steepness of the Pierson-Moskowitz spectrum.

Quadruplet Wave-wave Interaction

In deep water, the quadruplet wave-wave interactions transfer wave energy from the spectral peak to lower frequencies and to higher frequencies. The interaction involves the exchange of energy

and momentum between four individual waves with different frequencies and directions. The wave energy can be transferred between the waves when the resonant condition is met, this process is also known as the wave-wave interaction. The calculation of interactions can be computed with the Discrete Interaction Approximation Discrete Interaction Approximation (DIA) according to Hasselmann et al. (1985), where two quadruplet wave number configurations for $\lambda = 0.25$ are considered.

$$\sigma_1 = \sigma_2 = \sigma, \sigma_3 = \sigma(1+\lambda) = \sigma^+, \sigma_4 = \sigma(1-\lambda) = \sigma^- \tag{2.24}$$

$$S_{nl4}(\sigma,\theta) = S^*_{nl4}(\sigma,\theta) + S^{**}_{nl4}(\sigma,\theta) \tag{2.25}$$

The source term for quadruplet wave-wave interaction S_{nl4} is the sum of the first quadruplet S^*_{nl4} and the second quadruplet S^{**}_{nl4}, where S^{**}_{nl4} is identical to S^*_{nl4} but mirrored. In shallow water, the interaction is obtained by multiplying the deep water nonlinear transfer rate by a scaling factor:

$$S^{finitedepth}_{nl4} = R(k_p d) S^{deepwater}_{nl4} \tag{2.26}$$

$$R(k_p d) = 1 + \frac{C_{sh1}}{k_p d}(1 - C_{sh2} k_p d) e^{C_{sh3} k_p d} \tag{2.27}$$

The depth is indicated by d, the peak wave number by k_p, and C_{sh1}, C_{sh2} and C_{sh3} are tunable coefficients.

Depth-induced Wave Breaking

The process of depth-induced wave breaking is poorly understood but the total dissipation due to this process can be well-modelled with the dissipation of a bore applied to breaking waves in a random field, described by Battjes and Janssen (1978). The mean rate of energy dissipation per unit horizontal area due to wave breaking D_{tot} is expressed as:

$$D_{tot} = -\alpha_{BJ} Q_b \widetilde{\sigma} \frac{H^2_{max}}{8\pi} \tag{2.28}$$

$$\frac{1 - Q_b}{ln Q_b} = -8 \frac{E_{tot}}{H^2_{max}} \tag{2.29}$$

In the SWAN model α_{BJ} is defined as 1, the fraction of breaking waves is indicated by Q_b and the total energy by E_{tot}. The maximum wave height H_{max} is determined by multiplying the breaker index γ by the total water depth d.

Bottom Friction

Bottom-induced dissipation is implemented in SWAN with the simplest friction models such as the empirical Joint North Sea Wave Project JONSWAP model of Hasselmann et al. (1973), the drag law model of Collins (1972) and the eddy-viscosity model of Madsen et al. (1988).

$$S_{ds,b} = -C_b \frac{\sigma^2}{g^2 sinh^2 kd} E(\sigma,\theta) \tag{2.30}$$

The bottom friction coefficient is indicated by C_b, for a C_b-value of $0.038 m^2 s^{-3}$ the coefficient is in agreement with the JONSWAP coefficient C_{JON} for swell dissipation.

Triad Wave-wave Interaction

Triad wave-wave interactions are the result of resonance between wave components in shallow water. The computation of the nonlinear interactions can be done with the Lumped Triad Approximation Lumped Triad Approximation (LTA) method, described by Eldeberky (1996). This method only consists of the increase of energy S^{+}_{nl3} due to transfer from low frequencies and the decrease of energy S^{-}_{nl3} as a result of energy transfer to higher frequencies.

$$S_{nl3}(f) = S^{+}_{nl3}(f) + S^{-}_{nl3}(f) \tag{2.31}$$

$$S^{+}_{nl3}(\sigma) = max[0, \alpha c_{\sigma} c_{g,\sigma} J^2 sin(-\beta) \left\{ E^2(\frac{\sigma}{2}) - 2E(\frac{\sigma}{2})E(\sigma) \right\}] \tag{2.32}$$

$$S^{-}_{nl3}(\sigma) = -2S^{+}_{nl3}(2\sigma) \tag{2.33}$$

A tunable scaling factor that controls the energy transfer is indicated by α, the phase and group velocity by c_{σ} and $c_{g,\sigma}$. The interaction coefficient J is based on the Boussineq theory described and is described based on the wave number k, water depth d, phase velocity c_{σ}, and the phase of self-self interaction σ.

$$J = \frac{k^2_{\sigma/2}(gd + 2c^2_{\sigma/2})}{k_{\sigma} d(gd + \frac{2}{15} gd^3 k^2_{\sigma}) - \frac{2}{5}\sigma^2 d^2} \tag{2.34}$$

2.4.2. XBeach Model Description

The XBeach model is developed to simulate hydrodynamic and morphodynamic processes and their impact on sand coasts. The model is an open-source, process-based numerical model which can be used as a standalone model or in combination with other models. The hydrodynamic processes taken into account by the model include short-wave transformation, long-wave transformation, wave-induced setup, unsteady currents, overwash and inundation. Whereas the morphological processes include bed load and suspended sediment transport, dune face avalanching and bed update. An overview of the modules in XBeach is given in Figure 2.12. More information on these processes can be found in the XBeach manual, Roelvink et al. (2010). The model resolves the surf beat mode, which is the long-wave motions created by the variation in wave height in time, allowing the model to simulate the development of the dune erosion profile.

Short Wave Action

Wave forcing in the shallow water momentum equation is based on the time-dependent version of the wave action balance equation. The wave-action balance is given in Equation 2.35 and the wave action (A) is described in Equation 2.36. The angle of incidence θ is defined with respect to the x-axis, S_w is the wave energy density in each bin, and σ is the intrinsic wave frequency which is obtained from the linear dispersion relation. The wave-action propagation speeds where the effect of bottom refraction and current refraction are included is defined in Equation 2.37. Dissipation processes such as wave breaking (D_w) and bottom friction (D_f) are taken into account by the XBeach model.

$$\frac{\partial A}{\partial t} + \frac{\partial c_x A}{\partial x} + \frac{\partial c_y A}{\partial y} + \frac{\partial c_{\theta} A}{\partial \theta} = -\frac{D_w + D_f}{\sigma} \tag{2.35}$$

$$A(x, y, t, \theta) = \frac{S_w(x, y, t, \theta)}{\sigma(x, y, t)}, \sigma = \sqrt{gktanhkh} \tag{2.36}$$

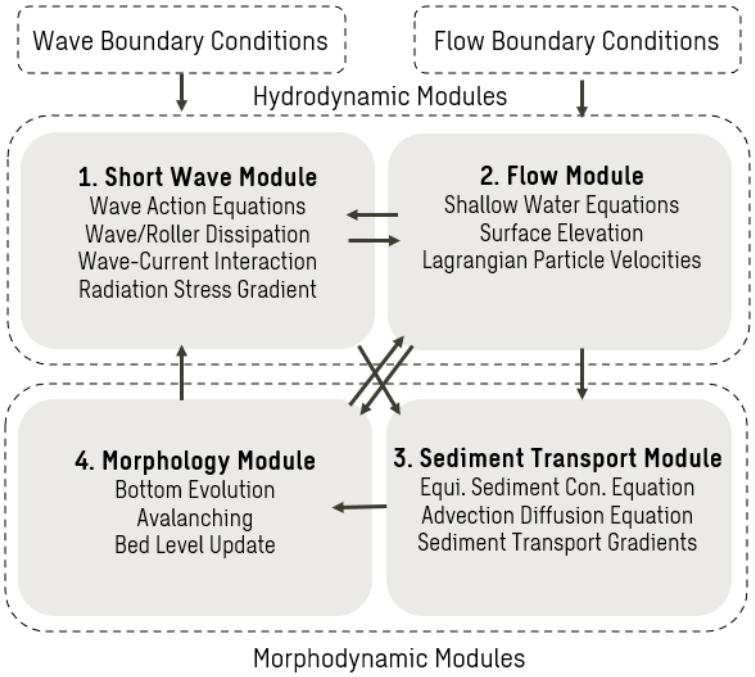

Figure 2.12: *Simulation modules within XBeach. The interaction between each module is indicated with errors, the results of each module are indicated by italic text. Figure modified from MacDonald (2019).*

$$c_\theta(x,y,t,\theta) = \frac{\sigma}{sinh(2kh)}\left(\frac{\partial h}{\partial x}sin\theta - \frac{\partial h}{\partial y}cos\theta\right) + cos\theta\left(\frac{\partial u}{\partial x}sin\theta - \frac{\partial u}{\partial y}cos\theta\right) + sin\theta\left(\frac{\partial v}{\partial x}sin\theta - \frac{\partial v}{\partial y}cos\theta\right) \tag{2.37}$$

The wave energy dissipation due to wave breaking in Equation 2.38 is defined according to Roelvink (1993). The dissipation with a fraction of breaking waves is defined as Q_b, wave dissipation coefficient as α, representative wave period as T_{rep} and the wave energy as E_w. The total wave energy in Equation 2.2 can be determined by taking the integration over all the wave directional bins.

$$D_w = 2\frac{\alpha}{T_{rep}}Q_b E_w \tag{2.38}$$

$$Q_b = 1 - exp(-(\frac{Hrms}{Hmax})^n), H = \sqrt{\frac{8E_w}{\rho g}}, H_{max} = \gamma(h + \delta H_{rms}) \tag{2.39}$$

$$E_w(x,y,t) = \int_0^{2\pi} S_w(x,y,t,\theta)d\theta \tag{2.40}$$

The bottom friction can be modelled according to Equation 2.41, using the Johnson friction factor f_w of the bed shear stress, water density ρ, the peak wave period T_p, the root-mean-square wave height H_{rms}, the wave number k and h as the local water depth.

$$D_f = \frac{2}{3\pi}\rho f_w(\frac{\pi H_{rms}}{T_{m01}sinhkh})^3 \tag{2.41}$$

Shallow Water Equation

For the calculation of the low-frequency and the mean flows the solves the shallow water equation based on the depth-average Generalized Lagrangian Mean Generalized Lagrangian Mean (GLM) formulation by Andrews and McIntyre (1978) and Walstra et al. (2001). The momentum equation and continuity equations are formulated in terms of the Lagrangian velocity, u_L. Here the velocity is defined as the distance that the water particles have travelled during one wavelength, divided by the wave period. The resulting GLM-momentum is given in Equation 2.42, 2.43 and 2.44. The wind shear stresses are defined as τ_{sx} and τ_{sy}, the bed shear stresses as τ_{bx} and τ_{by}, the wave-induced stresses as F_x and F_y, the horizontal viscosity as ν_h and f is the Coriolis coefficient.

$$\frac{\partial u^L}{\partial t} + u^L\frac{\partial u^L}{\partial x} + v^L\frac{\partial u^L}{\partial y} - fv^L - \nu_h(\frac{\partial^2 u^L}{\partial x^2} + \frac{\partial^2 u^L}{\partial y^2}) = \frac{\tau_{sx}}{\rho h} - \frac{\tau^E_{bx}}{\rho h} - g\frac{\partial \eta}{\partial x} + \frac{F_x}{\rho h} \tag{2.42}$$

$$\frac{\partial v^L}{\partial t} + u^L\frac{\partial v^L}{\partial x} + v^L\frac{\partial v^L}{\partial y} - fu^L - \nu_h(\frac{\partial^2 v^L}{\partial x^2} + \frac{\partial^2 v^L}{\partial y^2}) = \frac{\tau_{sy}}{\rho h} - \frac{\tau^E_{by}}{\rho h} - g\frac{\partial \eta}{\partial y} + \frac{F_y}{\rho h} \tag{2.43}$$

$$\frac{\partial \eta}{\partial t} + \frac{\partial hu^L}{\partial x} + \frac{\partial hv^L}{\partial y} = 0 \tag{2.44}$$

Sediment Transport

The sediment transport described in Equation 2.45 is based on the depth-averaged affection diffusion scheme by Galappatti (1983). The depth-averaged sediment concentration is defined as C, the sediment diffusion coefficient as D_H, the adaptation time as T_s, the local water depth as h and the sediment fall velocity as w_s.

$$\frac{\partial hC}{\partial t} + \frac{\partial hCu^E}{\partial x} + \frac{\partial hCv^E}{\partial y} + \frac{\partial \left[D_h h\frac{\partial C}{\partial x}\right]}{\partial x} + \frac{\partial \left[D_h h\frac{\partial C}{\partial y}\right]}{\partial y} = \frac{hC_{eq} - hC}{T_s} \tag{2.45}$$

The gradient of the sediment transport q_x and q_y are defined in Equation 2.46 and 2.47.

$$q_x(x,y,t) = \left[\frac{\partial hCu^E}{\partial x}\right] + \left[\frac{\partial}{\partial x}\left[D_h h\frac{\partial C}{\partial x}\right]\right] \tag{2.46}$$

$$q_y(x,y,t) = \left[\frac{\partial hCv^E}{\partial y}\right] + \left[\frac{\partial}{\partial y}\left[D_h h\frac{\partial C}{\partial y}\right]\right] \tag{2.47}$$

The sediment transport formulations in XBeach distinguish bed load and suspended load transport. The total equilibrium sediment concentration can be calculated according to Equation 2.48. The equilibrium concentration for bed load $C_{eq,b}$ and suspended load $C_{eq,s}$ can be calculated according to the sediment transport formulation by Soulsby (1997).

$$C_{eq} = max(min(C_{eq,b}, \frac{1}{2}C_{max} + min(C_{eq,s}, \frac{1}{2}C_max), 0) \tag{2.48}$$

Bottom Updating And Avalanching

The bed level changes are based on the gradients in the sediment transport, where the change can be calculated with Equation 2.49. The porosity is defined as p, the morphological acceleration factor as f_{mor}, and q_x and q_y represent the sediment transport in x- and y-direction.

$$\frac{\partial z_b}{\partial t} + \frac{f_{mor}}{(1-p)}(\frac{\partial q_x}{\partial x} + \frac{\partial q_y}{\partial y}) = 0 \tag{2.49}$$

To account for the slumping of sediment particles when the slope is too steep, the avalanching process is introduced in the model to update the bed evolution. The mechanism is taken into account through a critical bed slope in Equation 2.50.

$$\left|\frac{\partial z_b}{\partial x}\right| > m_{cr} \tag{2.50}$$

Boundary conditions
Wave conditions can be specified as a spectrum shape that describes the distribution of the wave energy across different frequencies. For the spectral type conditions, the wave spectra can be generated as JONSWAP spectra, Simulating Waves Nearshore (SWAN) spectra or variance density spectra at the offshore boundary. At the lateral boundaries, the alongshore or along-crest gradient is set to zero to avoid shadow zones that are found in many wave models, Roelvink et al. (2009). The flow boundary conditions are specified at all four boundaries in the model domain. Absorbing boundary conditions can be specified according to Van Dongeren and Svendsen (1996) at the offshore and landward boundaries. At the lateral boundaries, the so-called Neumann boundaries or no-flux boundaries can be specified.

2.4.3. Storm Impact Model Description

The storm impact model by Larson et al. (2004) is an analytical model that is developed to calculate recession distance and eroded volume for coastal dunes during severe storms. The model is based on wave impact theory and the sediment volume conservation equation, where swash waves hitting the dune face induce erosion. General solutions account for changes in the elevation of the dune foot during a retreat, while simplified solutions assume this elevation to be a constant. Validation was based on data sets from the laboratory and the field.

Wave Impact Theory Dune erosion can be determined based on the wave impact theory, where a linear relationship exists between the impact (F) and the weight (ΔW) of the sediment volume eroded from the dune. According to Fisher et al. (1987) and Overton et al. (1987), the relationship can be written as follows:

$$\Delta W = C_E F \tag{2.51}$$

C_E is an empirical coefficient and ΔW can be determined according to Equation 2.52 by the density of the sediment (ρ_s), the porosity (p), and the acceleration of gravity (g). The swash force (F) can be derived from the change in the momentum of the bore hitting the dune. Expressing the bore wavelength as the product of the bore speed (u_o)and the period (T), the total swash force can be written as Equation 2.53.

$$\Delta W = \Delta V \rho_s (1-p) g \tag{2.52}$$

$$F = \frac{1}{2}\rho \frac{u_o^4}{g C_u^2}\frac{\Delta t}{T} \tag{2.53}$$

The average rate of dune erosion (q_D) can be derived by combining Equation 2.51, 2.52 and 2.53. Equation 2.54 includes a minus sign to take into account that the dune volume must decrease with time. The simplified solution can be described according to Equation 2.56 based on the runup height (R), the still water level SWL, the dune food elevation (D_F) and the deep

water wave period (T_0). The empirical transport coefficient (C_s) is defined in 2.55. For practical application, it is recommended to use a range of C_s between $1.7 * 10^{-4}$ and $1.4 * 10^{-3}$ to include an uncertainty estimate of the results.

$$q_D = \frac{dV}{dt} = -\frac{1}{2}\frac{C_E}{C_u^2}\frac{\rho}{\rho_s}\frac{u_o^4}{g^2 T}\frac{1}{1-p} \tag{2.54}$$

$$C_s = \frac{1}{2}\frac{C_E}{C_u^2}\frac{\rho}{\rho_s}\frac{1}{1-p} \tag{2.55}$$

$$q_D = 4C_s\frac{(R + SWL - D_F)^2}{T_0} \tag{2.56}$$

For the model to give reliable estimates of dune erosion, R and C_s must be accurately predicted. Different runup height formulas were tested to predict R but the resulting optimum values on C_s displayed a large variation. Therefore, a Hunt-type formula was developed to predict R after which the optimum value of C_s was derived by least-square fitting the solutions to the calibration data, originating from the laboratory and the field. The derived runup height can be calculated based on the wave height (H_o) and the wavelength (L_o), both taken in deep water. For random waves, the root-mean-square (H_{rms}) in Equation 2.58 can be used.

$$R = 0.158\sqrt{H_{rms}L_o} \tag{2.57}$$

$$H_{rms} = H_{s0}/1.414 \tag{2.58}$$

$$L_o = \frac{g(T_0)^2}{2\pi} \tag{2.59}$$

2.5. Field Measurement of Dune Morphology

In the field of dune morphology, the traditional method for monitoring profiles that are perpendicular to the shoreline is by employing classical topographic techniques such as a total station, according to Sanjaume and Pardo (1991) and Andrews et al. (2002). An alternative approach involves the use of photogrammetry, which enables the measurement of the entire study area. However, both methods require a large amount of monitoring and according to Lerma (2002) the results have not always been of acceptable quality. A more precise method for measuring altitude is Light Detection and Ranging Light Detection and Ranging (LIDAR), in which lasers are used to measure altitude from a flying aeroplane at a low altitude. According to Woolard and Colby (2002), the altimetric accuracies are about 0.15 m and the planimetric are about 0.80 m. Despite the high accuracy, the use of the method for monitoring changes is restricted by the high cost of the technique. A cost-effective and accurate method for monitoring beach-dune systems in coastal areas is the Real-Time Kinematic Global Positioning System Real-Time Kinematic Global Positioning System (RTK-GPS) method. It is less expensive than the LIDAR method and is suitable for accurately tracking the evolution of beach-dune systems.

The RTK-GPS survey technique involves one stationary receiver and one or more moving Global Positioning System (GPS) receivers measuring simultaneously. To use this technique, it is necessary to know the coordinates of the stationary receiver. The code and carrier phase data of the stationary receiver are then sent to the moving receiver. By combining this data with that of the moving receiver, it is possible to calculate the coordinates of the moving receiver as described

by Leick et al. (2015). Note that the coordinates are referenced to a well-defined global geodetic reference system Global Geodetic Reference System (WGS84) and not a local system. Careful attention should be paid when analyzing the results.

2.6. Sampling Method Extreme Value

Extreme Value Analysis Extreme Value Analysis (EVA) is a tool that can be used to model and predict extreme or rare events, such as severe storms. The tool is a popular tool in coastal flood risk assessments because it can be used to understand the statistical behaviour of extreme values and quantify their likelihood. When the modelling of extreme values involves a single variable, this analysis is called the univariate extreme analysis. The primary goal is to estimate the distribution of the extreme values and quantify their likelihood. In contrast, applying EVA to two variables can be done through bivariate extreme analysis, where the focus lies on understanding the joint behaviour of extreme events from the two variables. Before fitting a statistical distribution to extreme values, extraction of these values from the time series has to be carried out first. Different sampling methods can be used to extract extreme values of the time series.

A popular sampling method used in univariate extreme analysis is the Peak Over Threshold POT method, where data points above the threshold are considered extreme. An example of the POT method used to define a storm is shown in Figure 2.13. The choice of the threshold value is based on the characteristics of the data, the value can be set as a fixed quantile (e.g. 95^{th}, 98^{th}, or 99^{th} percentile) of the data distribution. Another approach is the Block Maxima Block Maxima (BM) method, where the data set is divided into non-overlapping blocks and the maximum value within each block is considered an exceedance. Taking the annual maxima is a common practice approach in the BM method.

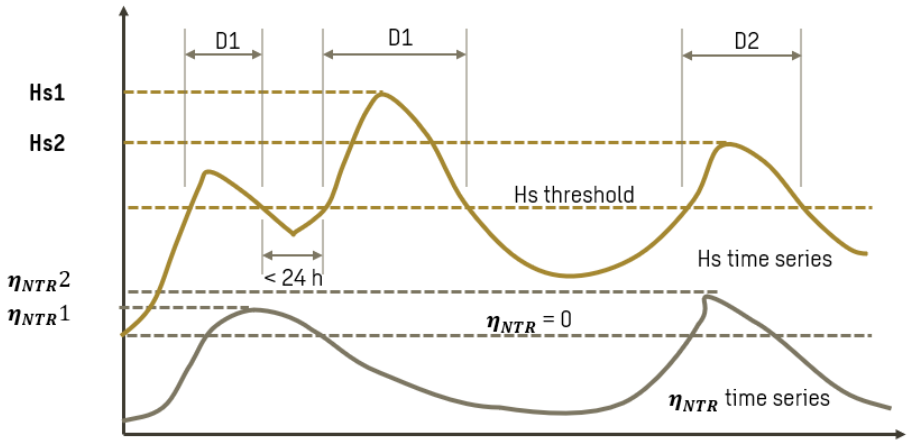

Figure 2.13: *Example of POT method used to define a storm event. A storm is defined when H_s is higher than the threshold. D indicates the storm duration and η_{NTR} the storm surge or nontidal residual. Figure modified from Wahl et al. (2016).*

Sampling of extreme values in bivariate extreme analysis can make use of the Joint Exceedance Probability Joint Exceedance Probability (JEP) method. The primary goal is to identify two variables having extreme values above their respective thresholds at the same time. The threshold value for each variable can be defined as a certain percentile of the corresponding data set. When the combination of the two variables is simultaneously above the two thresholds, the joint exceedance can be extracted from the time series. Other sampling methods described by

Chen et al. (2019) are the wave-dominated WD, surge-dominated SD and structural response SR sampling methods. In the WD method, the joint event of variables wave height and surge is selected based on the annual maximum wave height. While in the SD method, the joint event is based on the annual maximum surge. The last method also called the structural response SR method, is based on the annual maximum of the combined wave height and surge at the same time.

Table 2.1: *Overview of sampling method for univariate and bivariate analysis.*

Analysis	Sampling Method	Applicability
Univariate	POT	Estimation of the distribution of the upper tail of a dataset. Suitable for data that exhibits a Generalized Pareto Distribution (GPD).
	BM	Estimation of the distribution of the extreme values that occur within each block. Suitable for data where the maxima within each block follow the Generalized Extreme Event (GEV).
Bivariate	JEP	Tool to understand the likelihood of the joint occurrence of extreme values of multiple variables. Dependence between variables can be determined with copula models.
	WD	Applied to assess the impact of extreme wave conditions. Suitable for regions where the waves are the primary driver of coastal processes, such as open coastlines.
	SD	Applied to assess the impact of extreme water levels such as storm surges, tides and high water events. Suitable for regions where storm surges and water levels play a dominant role in influencing coastal processes, such as shallow coastal features.
	SR	Evaluate the response of a coastal structure under extreme conditions where extreme waves and surges are occurring simultaneously.

2.7. Coastal Protection Management

2.7.1. Protection Approach in Sweden

In Sweden, there are no official policies or national guidelines for how coastal protection should be organised, according to Bontje et al. (2016). Flooding and erosion risks have primarily been managed by landowners and the municipalities. According to Hallin et al. (2022), municipalities do not have a direct obligation to protect their residents against coastal flooding. In case the coastal protection is organised, it is done on the grounds to protect its infrastructure, beaches and larger built-up area. A permit is required from the County Administrative Board to construct a protection measure if the area is below 3000 m^2 and the impact on the environment is judged to be minor. For a larger project, the permission has to be granted by the Land and Environment Court. The design criteria for coastal protection are usually proposed by the applicant and assessed case by case.

Examples of projects in Scania with the corresponding design criteria are discussed by Hallin et al. (2022). In 2017, Lomma municipality built an embankment to protect a smaller residential area from flooding. The design was based on a storm surge with a 100-year return period in combination with the largest waves in the period of 1994-2011. In Ängelholm municipality, on the west coast of Scania, an embankment at Rönneå's outlet was constructed based on the design criteria of a storm surge with a 100-year return time in combination with a 100-year flow in the river. Another project is the construction of the dikes in Kristianstad (on the east coast of Scania) as protection against high flows in Helgeå. The design is based on the combination of high flow and a storm surge with a 100-year return period.

3. Methodology

The simulation of dune erosion during historical extreme events was done in three parts. The first part of the methodology, shown in Figure 3.1a, aimed to gather all necessary data for the analysis. The data collected from other sources are the wind, water level, topography and bathymetry data. A description of the data can be found in Section 4. In the study area, H_s were hindcast by Adell et al. (2023) with the SWAN model using three-hourly wind data acquired from the ERA5 reanalysis. However, when using three-hourly wind data for wave simulation, there is a possibility of missing peak values within a three-hour time interval, which can result in an underestimation of extreme wave values. Using the three-hourly wave data for extreme value analysis may result in inaccurate outcomes. Therefore, the time resolution of the wave data was increased from three-hourly to one-hourly resolution. The SWAN model setup for the simulation of the wave data in this study is given in Section 3.2.

The collected data is the dune morphology data. A fieldwork was conducted to measure the dune's profile in various transects in the study area. From the data, the dune volume was determined in each transect. How this was done is described in Section 3.1. The obtained results were combined with the topography and bathymetry data to determine the dune's dimensions, which are then used as input data in the morphological models to simulate dune erosion.

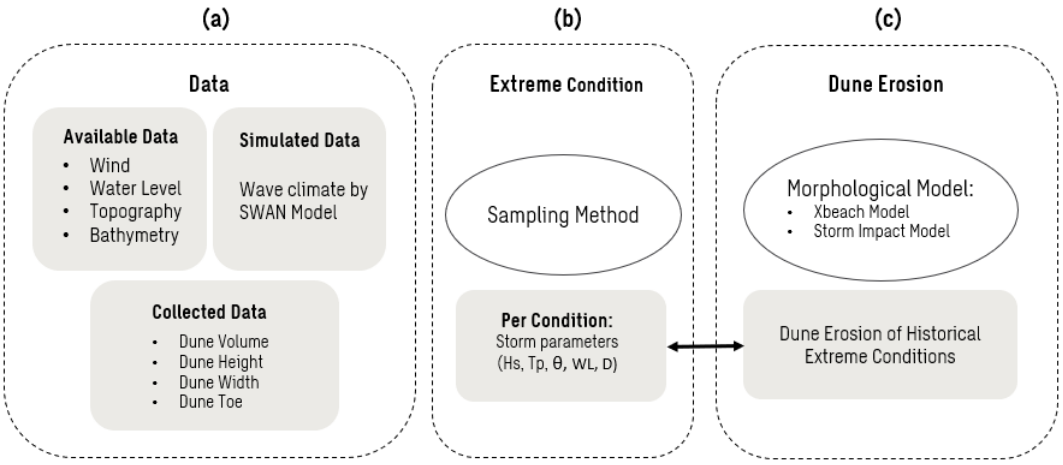

Figure 3.1: *Overview of the methodology.*

Figure 3.1b shows the overview of the second part of the methodology. In this part, extreme conditions were sampled from the time series in the period 1959-2021. The sampling approach is explained in Section 3.3. Note that the 1872 storm was included in the analysis to evaluate it impact on the present dune system. For every extreme condition, corresponding storm parameters (H_s, T_p, θ, WL, D) were extracted from the time series.

Dune erosion due to selected extreme conditions was determined in the last part of the methodology, see Figure 3.1c. The simulation of dune erosion was done utilizing two different morphological models, the process-based (the XBeach) and the analytical model (the storm impact model). A description of the models is given in Section 2.4.2 and 2.4.3. Both models require

storm parameters and dune morphology as input data. The model calibration from other studies was utilized due to the lack of observational dune erosion data in the study area. The XBeach model simulated dune erosion using two model setups which are the model calibration found by Geertsen et al. (2020) and the default model setting described by Roelvink et al. (2010). A sensitivity analysis was conducted to compare the results of these setups, the description can be found in Section 3.4. The storm impact model can be calibrated by adjusting the transport coefficient (C_s). The recommended range of C_s, given by Larson et al. (2004), is between $1.7 * 10^{-4}$ and $1.4 * 10^{-3}$. The best fitted C_s value to the wave condition of Birkemeier and Savage (1988) is $1.7 * 10^{-4}$ (Larson et al., 2004). The same value was used for the model calibration as the wave condition in this study is similar to the wave condition of Birkemeier and Savage (1988). The result of dune erosion determined by both the analytical and processed-based models was compared in Section 7.3. Finally, the dune erosion results are compared to the dune volume in each transect.

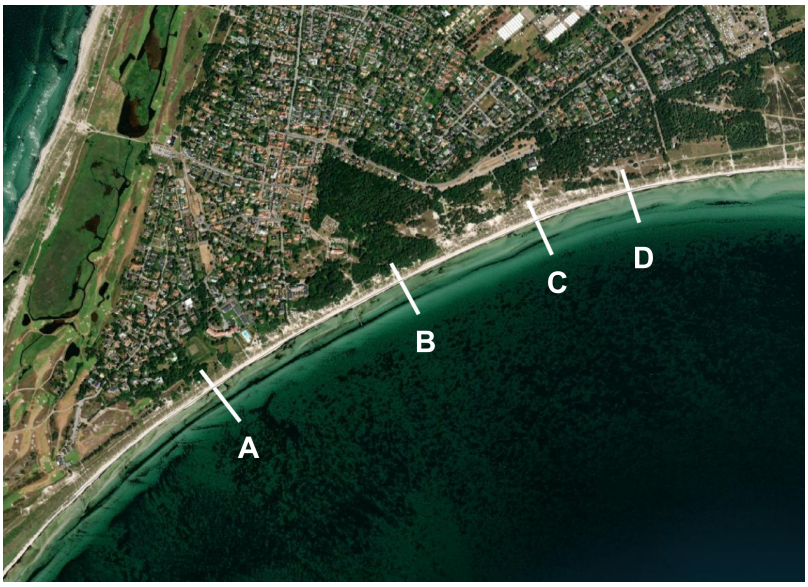

Figure 3.2: *Transects A, B, C and D in the dune in the Falsterbo Peninsula, where the profile was measured during the fieldwork.*

3.1. Fieldwork

3.1.1. Fieldwork Site

Field measurements took place on the 7^{th} of March 2023. To obtain a representation of the dune's morphology, four transects were defined in the dune system for the measurement. Figure 3.2, shows the different transects along the dune system. The southernmost transect indicated as Transect A in Figure 3.3a, differs from all the other transects due to the directly situated densely populated area behind the dune. In Transect B, the populated area is separated from the dune by an area filled with trees, see Figure 3.3b. In Transects C and D correspond to the widest section of the dune, see Figure 3.3c and 3.3d, the hinterland is located at a greater distance from the dune.

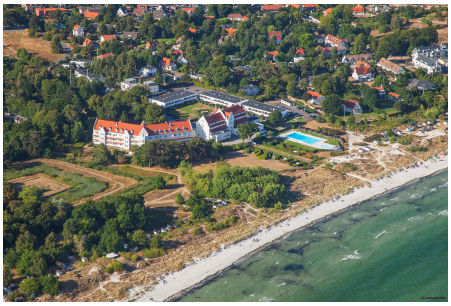

(a) *Transect A*

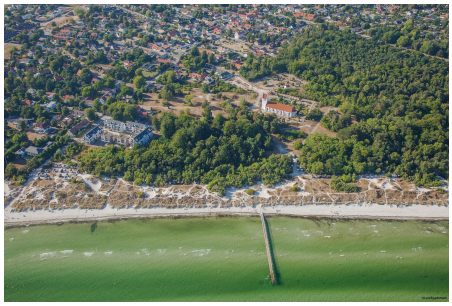

(b) *Transect B*

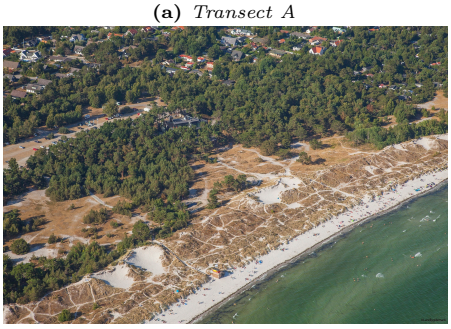

(c) *Transect C*

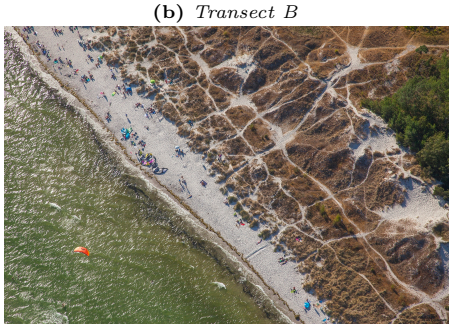

(d) *Transect D*

Figure 3.3: *Aerial photo of the different transects by Lars Bygdemark.*

3.1.2. Aim Fieldwork

The primary objective of the fieldwork was to determine the elevation of the dune toe. The dune toe is defined as the line separating the beach from the dune, and its position can vary on both temporal and spatial scales (Bochev-Van der Burgh et al., 2011; van IJzendoorn et al., 2021; Mehrtens et al., 2023). It is an important parameter as it plays a role in the vulnerability and stability of the dune system (Carter and Stone, 1989). Other studies have shown the potential use of dune toe as an indicator of coastal changes (Strypsteen et al., 2023; Bochev-Van der Burgh et al., 2011; Smith et al., 2020). Lower dune toe elevation means that the dune is more sceptical to wave impacts, whereas higher elevation indicates a greater buffer between the waterline and the base of the dune. To define the location and elevation of the dune toe, the dune's profile was measured in the cross-shore direction.

3.1.3. Fieldwork Approach

The measurement was done utilizing the RTK-GPS in the coordinate system SWEREF 99 TM. For the set-up of the GPS base station, it is important to do this in an area with a clear view of the sky to ensure good satellite signal reception. Once the set-up was done, the base station could be mounted on a pole to ensure the antenna was correctly positioned. The interface of the GPS could be used to navigate to measurement points and record measurements. Identification of the dune toe can be challenging as there is no generic definition. Methods that can be used to detect the dune toe elevation are based on an abrupt increase in beach slope or the edge of vegetation cover (Levin and Ben-Dor, 2004; Hesp and Smyth, 2016). In this study, the dune toe was defined as the location of the edge of vegetation cover.

From the analysis of the obtained location and elevation of the dune toe, the dune's characteristics such as crest height, width, volume, and slope of the foreshore were determined. The dune's volume was determined per-meter along-shore width (m^3/m) above the dune foot elevation. In the cross-shore direction, the volume was determined from the dune foot location to the inland boundary. The foreshore slope was determined by linearly fitting the bed profile 150 m in front

of the dune toe (van Wiechen et al., 2023).

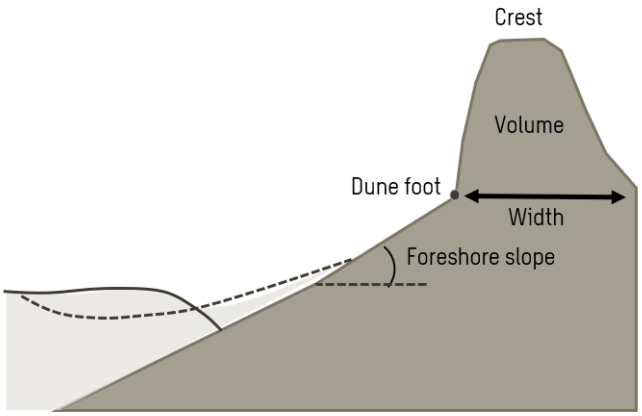

Figure 3.4: *Schematic of dune profile showing the dune crest, dune foot, dune volume, dune width and the foreshore slope. Figure modified from Sallenger Jr (2000).*

3.2. SWAN Model Setup

3.2.1. SWAN Domain

The computational grid was defined with the coordinates of the vertices and the numbering of triangles, created in OceanMesh2D which is a two-dimensional automated mesh generation toolbox intended for coastal ocean modelling. The same grid structure that was constructed in the study of Adell et al. (2023) was used in this study for computations of the wave heights. The grid domain in Figure 3.5 is between 54.0° and 60.5° north longitude and 9.3° and 29.8° east latitude.

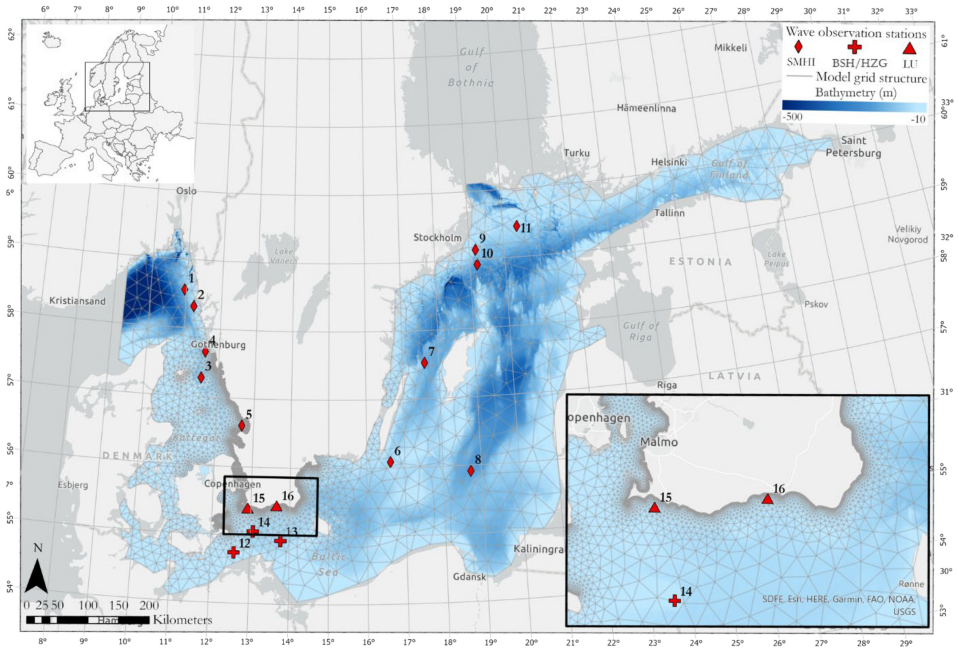

Figure 3.5: *The map of the SWAN model domain with a smaller grid size around Skåne and the locations of wave gauges operated by SMHI, BSH/HZG, and LU. Figure by Adell et al. (2023).*

The offshore bathymetry data was from the European Marine Observations and Data Network

European Marine Observations and Data Network (EMODnet) bathymetry portal and had a spatial resolution of 115 x 115 m. The resolution near the coastline in Skåne and Halland was increased to 2 x 2 m. The data was provided by the Geological Survey of Sweden Geological Survey of Sweden (SGU). The two data sets were integrated and the final resolution was resampled to 25 x 25 m nearshore.

3.2.2. SWAN Boundary

The frequency range and directional spreading resolution were defined in the model in the way that both swells and wind waves can be represented. Fixed boundary conditions were implied so that waves from outside the model domain would not be considered. The main forcing for the waves in this study is the wind forcing, hence only wind-generated waves will be simulated (Adell et al., 2023).

3.2.3. SWAN Model Setting

The SWAN model setup used in the study of Adell et al. (2023) was used to simulate the wave data in this study. The model validation can be found in Appendix C.2. In this model setup, the model was run with spherical coordinates where all geographic locations and orientations were defined in the longitude and the latitude in degrees (°). The wave data was computed based on input parameters such as depth, wind speed, and wind direction. The wind data was based on the ERA5 data set of averaged wind at 10 m height with a three-hourly time resolution. The SWAN model also takes into account processes such as depth-induced breaking, triad non-linear wave-wave interactions, dissipation by bottom friction and white-capping. The definition of these processes can be found in Chapter 2.4.1. The calibration parameters for physical processes are summarized in Table 3.1. For each year, the simulation time starts in a period of low wave activity, which is on the 20^{th} of June. For every simulation, a warm-up time was added to the simulation time to ensure that numeric errors due to uncertainties in the model's initial conditions were disregarded. The warming-up time was excluded from the results of each year, to obtain a continuous times series of the simulated wave data.

Simulating the wave climate for the 62-year period (1959-2021) with a model domain that covers the whole Baltic Sea can be time-consuming due to the high computational costs. To decrease the total running time, the simulations were done in the Lund University facilities for cluster processing called LUNARC. The centre provides computational resources for research within all aspects of computational science.

Table 3.1: *Overview of physical processes and calibrated model coefficients.*

Physical process	Formulation	Coefficient
Linear wind growth	Cavaleri and Rizzoli (1981)	Cdcap=2.5e-3
Exponential wind growth	Komen et al. (1984)	
Whitecapping	Hasselmann (1974)	Cds=1.1e-5
Depth-induced wave breaking	Battjes and Janssen (1978)	α=1 γ=0.73
Bottom friction	Hasselmann et al. (1973)	Cjon=0.038m2s-3
Triad wave-wave interactions	Eldeberky (1996) (LTA method)	a=0.95 b=0 lambda=0.25
Quadruplet wave-wave interactions	Hasselmann et al. (1985) (DIA method)	Cn/4=3e7 Csh1=5.5 Csh2=0.833333 Csh3=-1.25

3.2.4. SWAN Input and Output

The wind input data are based on the ERA5 reanalysis dataset, as described in Section 4.3. The obtained wind data comprises the u-component (eastward) and the v-component (northward) of the wind velocity at 10 m height above sea level. The spatial resolution is 0.5 x 0.5 m and the time resolution is one hour.

In the model, the output grids are independent of the input grid. When these grids are different, the information on the output grid is obtained from the computational grid by linear interpolation. In this study, the wind input grids were different from the output grids meaning that the wind had to be interpolated for the computation. The output file is in NetCDF file format, containing requested parameters such as the significant wave height Hs, peak period Tp and wave direction (θ). An example of the SWAN script and output file is shown in Appendix C.

3.3. Selection of Extreme Condition

The extraction of extreme conditions from the time series was achieved by suing a sampling method. The choice of methods depends on the type of analysis these extreme values are used for. This thesis aims to define extreme conditions in the time series that can potentially lead to severe dune erosion and coastal flooding in the study area. As H_s and S are the key drivers of coastal processes, these two variable are often the primary contributors to extreme water levels along the coastline during storm events. Selection of extreme conditions based on these two variables captures most conditions affecting the dune Oo et al. (2022). Four common different sampling methods are the JEP method, WD, SD and SRmethod. Section 2.6 describes the different sampling methods. An alternative method is the sampling method based on the time series of the Total Water Level (TWL), as it represents the combined effect of H_s and S. Each method is discussed below regarding its suitability for the analysis in this study.

The JEP method is used to determined the likelihood that two variables simultaneously exceed specified thresholds. Different combinations of waves and water levels can have the same likelihood but their impact on the dune may vary (Oo et al., 2022). As the focus lies on the selection of extreme conditions that can impact the dune system, choosing this method might not align with the objective. In regions where the waves are the primary driver of coastal processes, the

WD method is more suitable for sampling extreme conditions.

In the Baltic Sea, the interaction between waves and water levels is rather complex because these two parameters are influenced by various meteorological conditions (Hanson and Larson, 2008; Hallin et al., 2022; Jensen and Müller-Navarra, 2008). As the interaction between H_s and S is critical for dune erosion, using the WD method may not fully capture the complex interactions in the Baltic Sea. Surges occur primarily due to strong winds and low-pressure systems associated with severe storms. Extreme water levels in the Baltic Sea are not only influenced by surges but also depend on wind-driven water level changes, as explained in Section 1.4. Higher water levels in the south of the Baltic Sea are influenced by air pressure and wind patterns in the North Sea and the Baltic Sea. The water level can be higher locally due to the periodic oscillation of the water level within this semi-enclosed basin. Furthermore, northerly winds can push the water from the northern Baltic Sea to the southern regions. Therefore, using the SD method might lead to an incomplete assessment of the factors contributing to dune erosion.

The sampling method where the joint occurrence of H_s and S are taken into account is the SR method (Chen et al., 2019). The H_s and S samples were first extracted from the time series respectively, using the POT method. The simulated time series of H_s in this study and the time series of the observed water level (WL) from the SMHI station were used to determine the threshold value. The threshold values for H_s and WL are defined as the 99^{th} percentile of their respective time series. Combinations, where H_s and WL exceed their threshold simultaneously, with the same timestamp are then extracted from the time series. See Figure 3.6 for the example. In terms of its applicability, this method aligns with the research objective. However, as this method focuses only on the extreme conditions of the two parameters, certain combinations might be neglected when one of the two parameters falls under the threshold value defined in the first sampling stage.

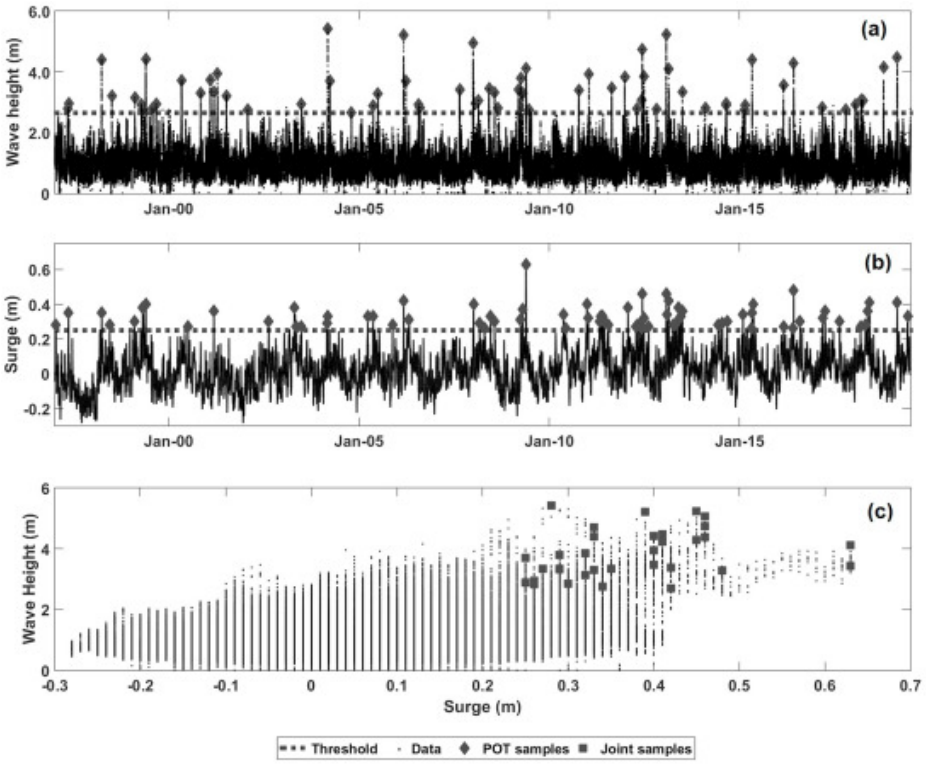

Figure 3.6: *Example of extreme condition sampling by the WD method (a), SD method (b) and SR method (c). The horizontal dashed line in (a) and (b) represents the threshold lines. The joint occurrence samples in the SR method are indicated by square dots in (c). Figure by Oo et al. (2022).*

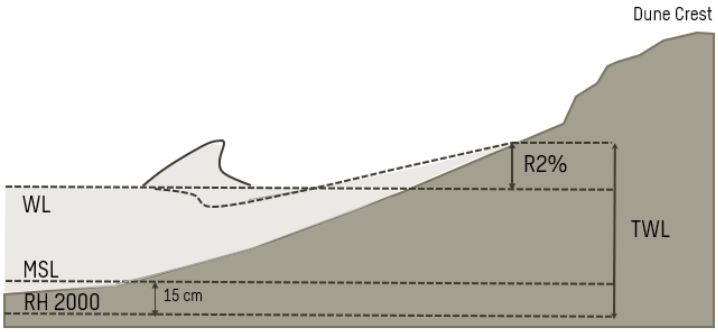

Figure 3.7: *Definition of Total Water Level (TWL), consisting of the observed water level (WL) and the wave runup ($R_{2\%}$). Figure modified from Serafin and Ruggiero (2014).*

Combinations of H_s and S can alternatively be selected based on their combined effect. According to Ruggiero et al. (2001), TWL can be defined as the elevation that comprises four components which are the mean sea level (MSL), astronomical tide (η_a), storm surge or non-tidal residual (η_{NTR}) and the wave runup (R). In this study, the observed water level (WL), which encompasses the components MSL, η_a, and η_{NTR}, were extracted from the SMHI station. The values are expressed in the reference system RH 2000. The effect of the waves was then included by adding WL to the wave runup ($R2\%$), calculated according to Equation 2.9. The time series of TWL was constructed using the simulated time series of the H_S to calculate $R2\%$, consequently adding to the time series of WL as defined in Equation 3.1.

$$TWL = WL + R_{2\%} \tag{3.1}$$

The extreme conditions were extracted from the TWL time series by using a POT method (Wahl et al., 2016). According to Serafin and Ruggiero (2014), dune erosion occurs when TWL is higher than the elevation of the dune toe and flooding occurs when this level exceeds the dune crest. An alternative scenario for flooding is when TWL exceeds the elevation of the inland boundary and all the sand in the dune has been eroded away. Possible scenarios for severe dune erosion are when the impact of a storm condition is severe or when the impact is mild but the storm duration is significant. Two sequences of mild storm conditions can also lead to flooding due to the limited recovery time of the dune. An overview of the scenarios is given in Figure 3.8.

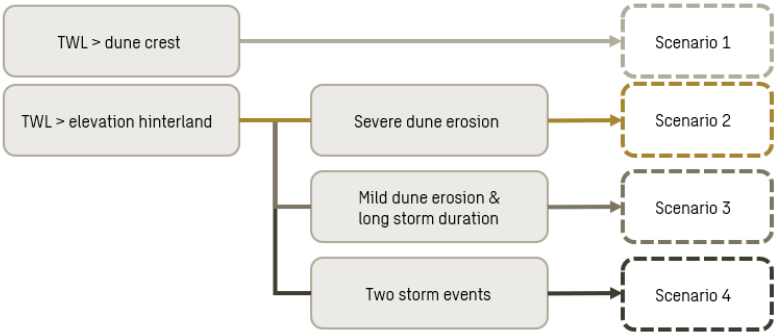

Figure 3.8: *Overview of the scenarios of coastal flooding in the study area.*

In this study, the objective is to evaluate whether the dune in the study area is strong enough to protect the hinterland from coastal flooding. Therefore, the threshold value for the TWL time

series will be set at the elevation of the inland boundary. The obtained scenarios will provide insights into the conditions that are representative of coastal flooding events. To choose the optimal method that extracts all critical combinations of H_s and WL for reliable analysis, the combinations selected by the SR method and the POT method in the time series of TWL were compared.

3.4. Xbeach Model Setup

3.4.1. XBeach Domain

Detailed topography and bathymetry data are provided by SWECO and SGU. To create a continuous profile, a field measurement was conducted to connect the two data sets. The provided bathymetry data has a depth down to -3.0 m and data at greater depths were taken from offshore bathymetry data used in the SWAN model. To account for the 115 x 115 m spatial resolution of the data, interpolation was necessary.

The coordinate system used in XBeach has the computational x-axis always oriented towards the coast and the y-axis alongshore. The coordinate system in Figure 3.9 is defined relative to world coordinates (x_w, y_w) through the origin (x_{ori}, y_{ori}) and the orientation alfa, which is defined counter-clockwise w.r.t the East.

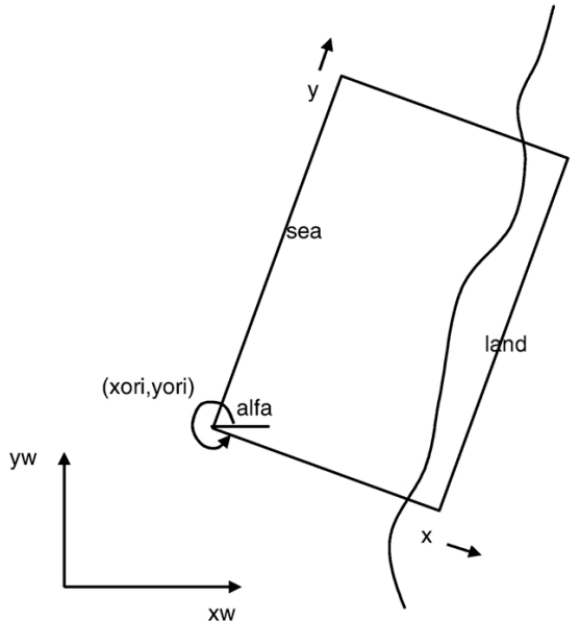

Figure 3.9: *Coordinate system in XBeach model. Figure from Roelvink et al. (2009).*

The grid is a rectilinear, non-equidistant, staggered grid. At the cell centres, parameters such as bed levels, water levels, water depth, wave energy balance, roller energy and radiation stress are defined. Parameters such as velocity, sediment transports, and radiation stress gradients are defined at the cell interfaces. The numerical discretization of the flow is based on an upwind explicit scheme, similar to Stelling and Duinmeijer (2003). The choice of upwind schematizations is made to avoid numerical oscillations which are prone to develop in shallow areas.

The one-dimensional grid used on the XBeach simulation consists of cross-shore (X) points and the corresponding elevation value (Z). As the simulation is one-dimensional, the alongshore (Y) points all contain zero values. The x-grid in Figure 3.9 in XBeach starts at zero at the offshore

boundary where the wave data were extracted, and increases in distance towards the coast. To optimize computational efficiency, the offshore grid has a coarser resolution compared to the grid near the beach.

3.4.2. XBeach Boundary

The XBeach model was forced by wave and water level boundary conditions. The wave boundary condition is set as a standard JONSWAP random wave spectrum. According to Blomgren et al. (2001), the JONSWAP spectrum is assumed applicable for the Baltic Sea. Constructing a JONSWAP wave spectrum requires wave parameters such as the significant wave height, peak period, wave direction, duration, peak enhancement factor, directional spreading coefficient and the highest frequency used to create the spectrum. The first four parameters were retrieved from the output of the SWAN model, whereas the last three parameters were set to the default values. Since the SWAN model provides the wave characteristic in an hour time resolution, the duration of each JONSWAP wave spectrum in this study was set to one hour. The number of JONSWAP spectra should match the computational time of the simulation.

Time-varying water levels at the boundary were imposed by providing the water level. The boundary conditions were specified at all boundaries of the model domain. Especially, at the offshore boundary, a weakly-reflective boundary in 1D was activated. This boundary allows the waves and currents generated in the model domain to pass through the offshore boundary to the deep sea with minimal reflection.

3.4.3. XBeach Model Setting

Conducting the XBeach model simulation was done by specifying all the necessary information for running the model into the file in Appendix D. In this study, two model settings are used to simulate the response of the dune. The first setting is the default setting, also known as Holland default, in the XBeach model. The second setting is the model calibration derived in the study of cliff retreats on sandy coasts in Denmark by Geertsen et al. (2020), defined as the Danish calibration. The calibrated model set-up was validated for the different coastal profiles covering most types of the Danish coastline. One of the coastlines was the coastline of Falster, which is exposed to the Baltic Sea. In Table 3.2, the calibration parameters are compared to the default parameters in the model.

Table 3.2: *XBeach model calibration compared to the default parameters.*

	Calibration	Default
Morphology parameters	morfac = 5.0 morstart = 100.0 s dryslp = 0.8	morfac = 1.0 morstart = 0.0 s dryslp = 1.0
Sediment transport parameters	facua = 0.3	facua = 0.1
Wave breaking parameters	gamma = 0.55	gamma = 0.55

The $morfac$ parameter serves to decouple the hydrodynamical and morphological time scales in the XBeach model. Acting as a morphological acceleration factor, it allows for increased erosion and deposition within a given time step. In a study conducted by Geertsen et al. (2020), it was observed that higher values of $morfac$ have a significant impact on cliff retreat and beach smoothing. By specifying the $morstart$ parameter, the initiation of morphological processes can be delayed compared to the hydrodynamic simulation. This option proves useful when a spin-up time is required for the hydrodynamics.

In contrast to the default value, the critical avalanching slope (*dryslp*) above water has a smaller magnitude. This means that the bed collapses and slides downward at a milder incline.

The $facua$ parameter is incorporated into the sediment transport equation to account for wave skewness and wave asymmetry. It adjusts the sediment advection velocity, which is responsible for stirring and transporting sediment toward the shore. The calculation of this velocity in Equation 3.2(denoted as U_a) involves the wave skewness parameter (S_k), wave asymmetry parameter (A_s), root mean square velocity (U_{rms}), and the $facua$ value. Shallow areas are expected to exhibit higher values of U_a as the difference between S_k and A_s increases. Consequently, greater onshore sediment transport occurs due to wave non-linearity. In this study, the calibration value for $facua$ exceeded the default value, indicating a higher sediment advection velocity and resulting in larger onshore sediment transport.

$$u_a = u_{rms}(S_k + A_s)facua \tag{3.2}$$

The wave-breaking parameters in the calibration of this study remained consistent with the default values, as specified by the Roelvink formulation.

A sensitivity analysis was performed in this study to comprehend the primary variations between the XBeach model outputs resulting from the Danish calibration and the Holland default settings. The aim of this analysis was to identify and quantify the impact of the different parameters on the model results, in order to identify the primary factor responsible for the observed difference. To effectively carry out the analysis, an event was simulated using various model setups outlined in Table 3.3. The first model setup is based on the Holland default setting, where the model simulates the output according to its predetermined parameters. In the second, third, and fourth simulations, only one parameter will be varied while keeping all other parameters at the default values. This approach will allow for a detailed study of the influence of each parameter on the results. The last simulation is based on a combination of the three parameters, which represents the Danish calibration setting.

Table 3.3: *Overview of the model setup in the sensitivity analysis.*

Factor	Setup 1	Setup 2	Setup3	Setup 4	Setup 5
drylp	1.0	0.8	1.0	1.0	0.8
morfac	1.0	1.0	5.0	1.0	1.0
facua	0.1	0.1	0.1	0.3	0.1

3.4.4. XBeach Input and Ouput

In addition to the topography and bathymetry data used for constructing the computational grid in XBeach, the wave and water level data were provided to the model to simulate the hydrodynamic and morphodynamic processes. Furthermore, the influence of wind was considered in the simulation.

XBeach model output has many output variables since the model is able to simulate hydrodynamic and morphodynamic processes. All variables are given for every grid point and at the specified time intervals. For this study, output variable wave height (H_s), water level (Z_s), and bed level (Z_s) were requested. The wave height given by the model is the short-wave height, any change in the magnitude can indicate where the waves are shoaling or potentially breaking. The water level, given in meters relative to the bed level. The bed level is the main variable to study dune erosion, as it demonstrates changes in the bed level over time.

4. Data Description

This chapter describes the data needed for this study. The topography and bathymetry data are described in Section 4.1. Section 4.2 covers the water level data, while Section 4.3 describes the wind data. The data available from the 1872 storm is presented in Section 4.4 and the collected data during the field measurement can be found in Section 4.5.

4.1. Topography & Bathymetry

The topography data was downloaded with the Terrain Model Download, grid 1+ from the official website of Lantmäteriet (2023). Lantmateriet is the cadastral and land registration authority that provides information about Sweden's geography and properties. The data was collected in 2019 using the LIDAR method with a resolution of 1.0 m. Bathymetry data can be obtained from SGU, which is the government authority responsible for bedrock, soil and groundwater-related issues in Sweden. The data was collected in 2014 and describes the procedure citepersson2014skaanes. Both the topography data and bathymetry data are in the SWEREF 99 TM coordinate system and the height is in the reference system RH 2000.

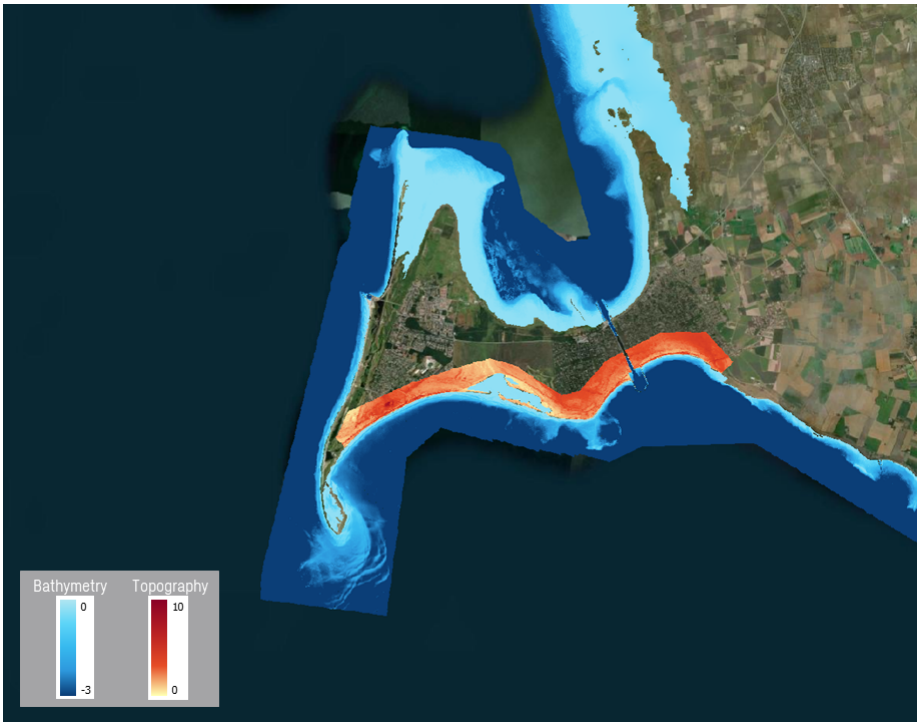

Figure 4.1: *Topography (in red) and Bathymetry (in blue) data in the study area.*

In Figure 4.1, the red colour represents the topography data while the blue colour represents the bathymetry data. As previously mentioned, the Falsterbo Peninsula is primarily a low-lying area. The highest elevation recorded in the topography data is 9.5 m. The deepest elevation recorded in the bathymetry data is -3.0 m. Additionally, the shallow area, indicated in light blue colour, around the spit is clearly visible in the bathymetry data.

4.2. Water Level Data

The hourly measured water levels in the study area were obtained from the SMHI station. Near the study area, there are two measuring stations in operation. The station in Skanör, in Figure 4.2, has been in operation since 1992 and is closer to the study site. The station in Klagshamn is located further away but has a longer operation time, from 1929 up until today. The measured water levels, in the reference system RH 2000, from both stations were compared for the same time interval from 1992 to 2021. The data is plotted with the identity line (y=x) in Figure 4.2. The maximum and minimum observed water level in Skanör is 1.69 m and -1.40 m, while in Klagshamn the levels are 1.58 m and -0.83 respectively. The correlation number between the two datasets is 0.96, meaning that the water levels in the two stations are highly correlated.

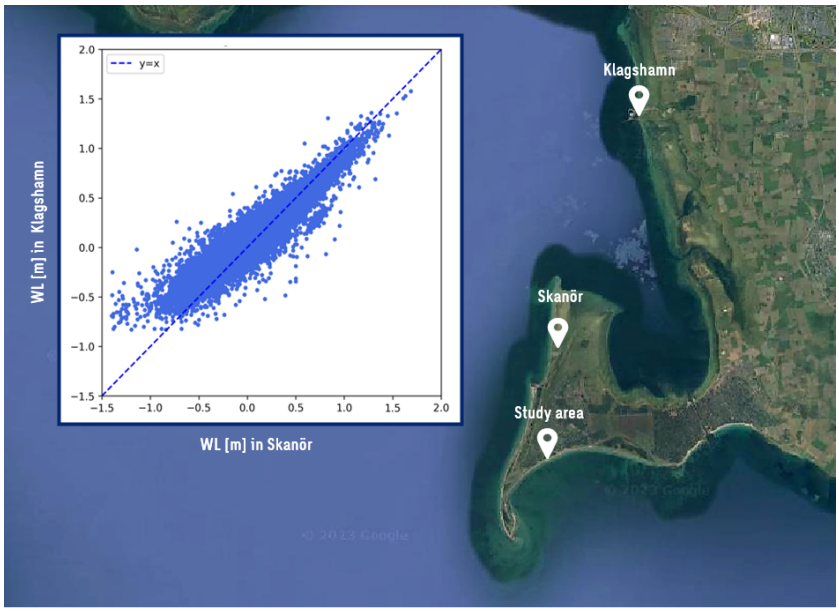

Figure 4.2: *Observed water level (WL) in the reference system RH 2000 from the stations in Klagshamn and Skanör.*

Since the observation at the station in Klagshamn is longer, the observed water levels from this station will be used for further analyses in this study. The dataset for the period between 1929 and 2021 was processed by removing the underlying trend from the water level data. The detrending process involves fitting a linear regression to the entire time series, which was then subtracted from the original data to obtain the detrended water levels in Figure 4.3. The maximum water level of 1.41 m was obtained.

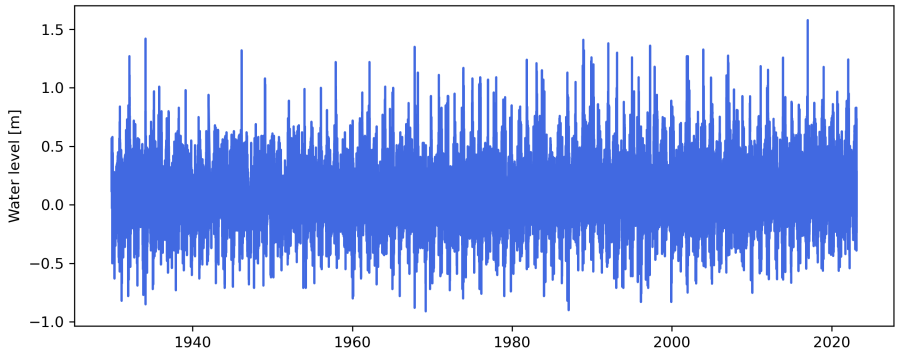

Figure 4.3: *Detrended hourly observed water levels in Klagshamn from 1929 till 2021 in the reference system RH 2000.*

4.3. Wind Data

The wind data is based on the ERA5 reanalysis dataset of averaged wind at 10 m height. The data provided by the European Centre of Medium-Range Weather Forecasts European Centre of Medium-Range Weather Forecasts (ECMWF) was downloaded by specifying the u- and v-component of the wind for the geographical area through the limit on latitude and longitude, for every hour from 1959 till 2021.

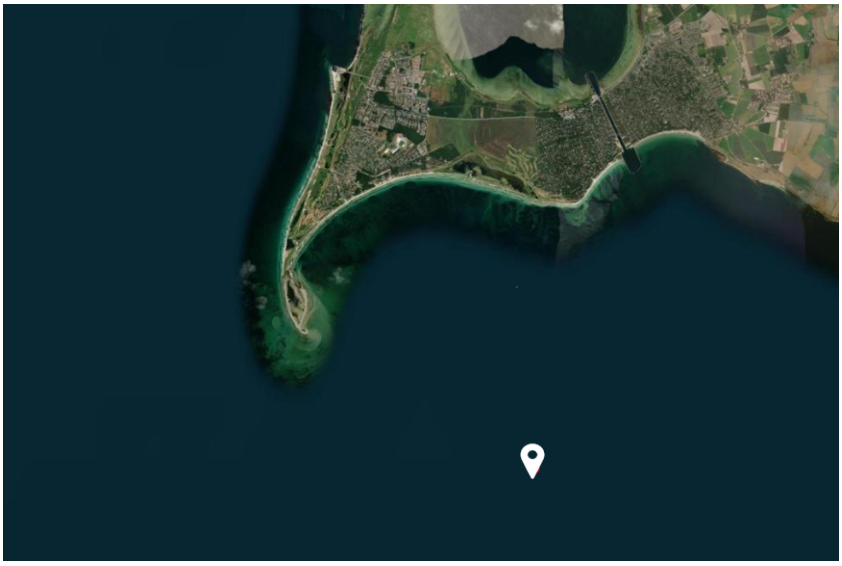

Figure 4.4: *Location of wind data extraction.*

The wind data was extracted at a location in front of the study area, shown in Figure 4.4. The prevailing wind directions are the west and the east, where the westerly winds are both stronger and more frequent. The time series of the 62-year wind data and the corresponding wave rose are shown in Figure 4.5. Westerly winds are indicated by the positive y-axis and easterly winds by the negative y-axis. The mean and maximum wind speeds for easterly winds are 5.75 m/s and 16.47 m/s. Conversely, for westerly winds, the speeds are 6.30 m/s and 23.77 m/s, respectively. While the mean wind speed for both prevailing wind directions is similar, the maximum wind speed is significantly higher for westerly winds.

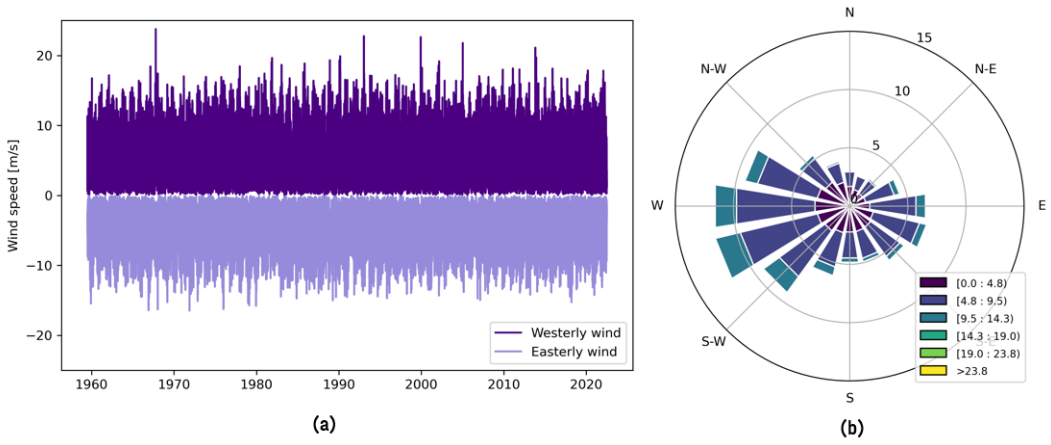

Figure 4.5: *Wind time series (a) and wind rose (b) of the ERA5 data in front of the study area spanning from 1959 to 2021.*

4.4. 1872 Storm Data

The wind, wave and water levels data during the 1872 storm were obtained either by the historical data or by numerical simulations using the historical data.

Reconstructed Wind

The weather during the storm of 1872 was reconstructed using historical data from studies such as Baensch (1875) and Colding (1881). A detailed description and evaluation of the reconstruction processes can be found in the study of Rosenhagen and Bork (2009). The wind field was reconstructed from manual air pressure analyses because the historical wind observations were insufficient to provide reliable wind data.

The reconstructed weather during the period of the 1^{st} till the 13^{th} of November 1872 is shown in Figure 4.6a. During the first nine days of November, the westerly winds push the water from the North Sea into the Baltic Sea through the narrow Danish straits. As mentioned earlier, the Baltic Sea can be considered a large basin. Therefore, the basin was being filled when westerly winds prevailed. After some time, on November 10, the weather changed. An extensive low-pressure system with two centres moved from the North Sea towards Central Europe. Since November 11, a high-pressure system was established over Scandinavia while a low-pressure system moved over Central Europe. The movement of the two pressure systems results in an extreme air pressure gradient over the southern Baltic Sea, leading to extreme wind speed. The wind data was extracted in the same location shown in Figure 4.4. Figure 4.6b shows the wind characteristics during the period of the 1^{st} till the 13^{th} of November in Falsterbo Peninsula. The maximum wind speed of 31.16 m/s is observed on the day of the storm, the 13^{th} of November.

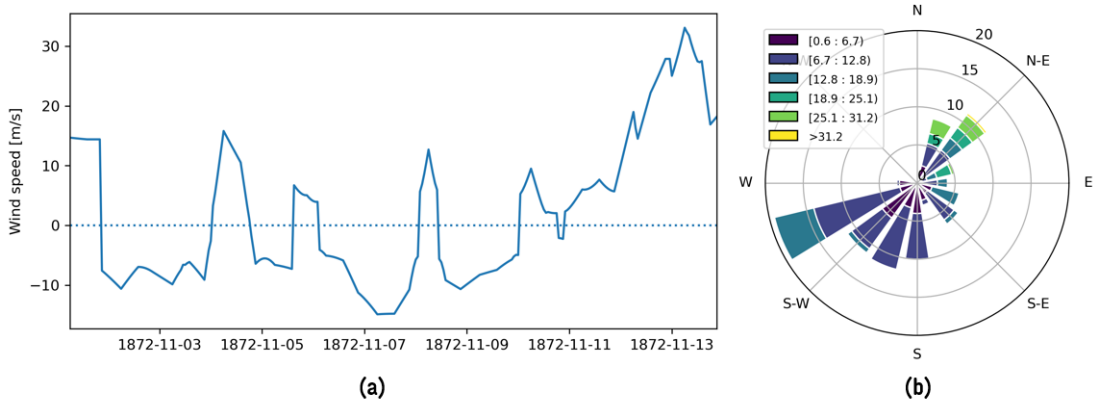

Figure 4.6: Wind time series (a) and wind rose (b) during the period of the 1^{st} till the 13^{th} of November in Falsterbo.

Water Level

The still water level during the 1872 storm reached up to 3.4 m above normal in Lübeck-Travemünde (Germany) according to Jensen and Müller-Navarra (2008) and 3.3 m above normal in Als and the south coast of Jutland (Denmark) according to Nielsen et al. (2015). In Sweden, there was no trustworthy observation of the still water level due to the lack of operating water gauges. From the historical data such as flood marks on a memorial stone and reports based on eyewitnesses, Fredriksson et al. (2016) estimated the water level in Skanör reached up to 2.4 m above mean sea level, which corresponds to 2.6 m (RH 2000). Figure 4.7 shows the water level during the storm. Note that the water level data is only available for the period of the 12^{th} till the 13^{th} of November.

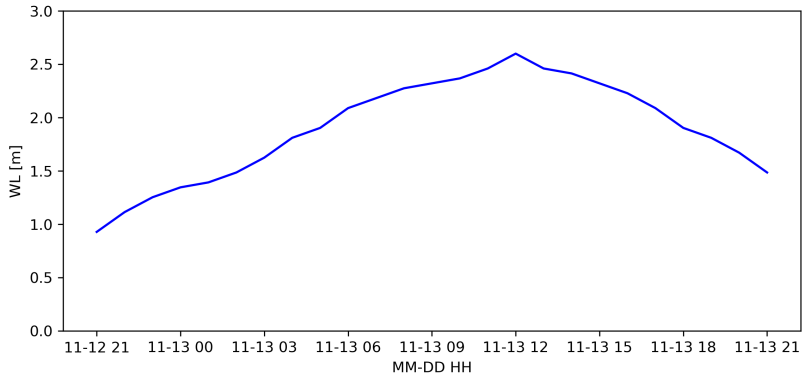

Figure 4.7: Water level in the reference system RH 2000 for the period of the 12^{th} till the 13^{th} of November.

Reconstructed Wave Climate

The reconstructed wind data during the 1872 storm by Rosenhagen and Bork (2009) was used to simulate the wave climate during the event. The simulation was done in the SWAN model, description of the simulation can be found in the study of E (2022). The significant wave height, the peak period and wave direction during the storm are shown in Figure 4.8. The data was extracted in the same location as where the wind data was extracted. see Figure 4.4.

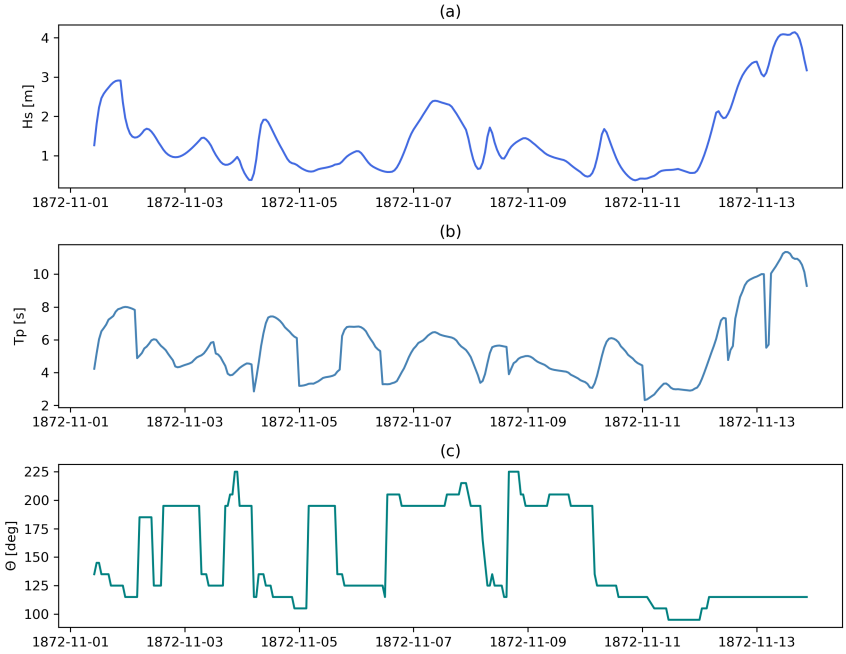

Figure 4.8: Wave characteristic the period of the 12^{th} till the 13^{th} of November in Falsterbo.

4.5. Dune Morphology

The cross-shore profile of a dune plays a crucial role in its vulnerability to hydrodynamic processes and it shapes the dynamic of coastal environments. The fieldwork was conducted in the study area to determine the dune toe elevation and to close the gap in the elevation between the topography and bathymetry data. Four transect profiles were determined during the fieldwork in various locations in the dune, as indicated in Figure 4.9b. The obtained elevation data is combined with the topography and bathymetry data to construct the full cross-shore profile of the dune. The profiles are shown in 4.10 and characteristics of the dune's profile in each transect are presented in Table 4.1. This information was used in morphological models to simulate the

bed levels and to determine dune erosion.

(a) *Dune location* **(b)** *Measurement transects*

Figure 4.9: *Location of the dune in the Falsterbo Peninsula and measurement transects in the dune.*

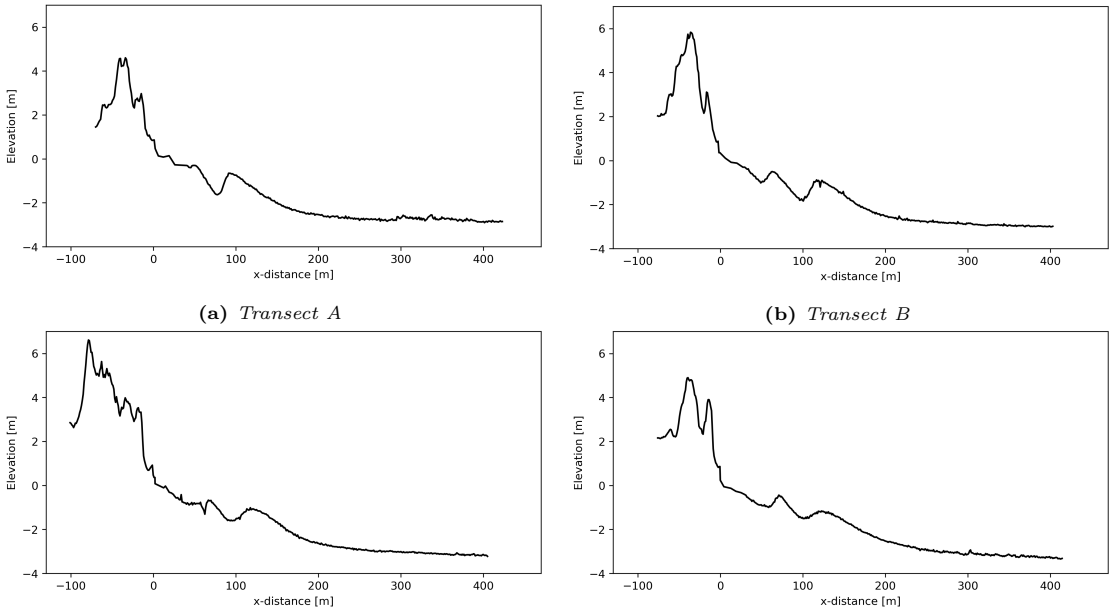

(a) *Transect A* **(b)** *Transect B*

(c) *Transect C* **(d)** *Transect D*

Figure 4.10: *Cross-shore dune profile at various transects in the dune in the Falsterbo Peninsula.*

Table 4.1: *Characteristic of dune profile in various transects.*

Transect	Crest $[m]$	Width $[m]$	Dune foot $[m]$	Volume $[m^3/m]$	Foreshore slope
A	5.280	65.887	1.128	119.804	0.005
B	5.769	87.582	0.894	102.661	0.008
C	6.019	163.972	0.726	157.398	0.009
D	4.702	90.533	0.815	57.494	0.007

5. SWAN Model Result

The time resolution of the wave data in the study area was increased from three hours to one hour. The difference between the two datasets is presented in Section 5.1. In Section 5.2 the wave climate around the Falsterbo Peninsula is described. The wave data that will be used for the analysis in this study is described in the last section of this chapter, Section 5.3.

5.1. Three-hourly vs One-hourly Wave Data

The hypothesis made earlier regarding using the three-hourly wave data for extreme analysis, would lead to inaccurate results as some peak values within a three-hour time interval would have been neglected. To demonstrate the validity of the hypothesis, a comparison was made between the three-hourly and one-hourly H_s data at the same location for the period 1959-2021. A direct hourly comparison was possible by interpolating the three-hourly dataset.

In Figure 5.1, one-hourly H_s is indicated by the x-axis and interpolated three-hourly H_s by the y-axis. The identity line is plotted in the figure to indicate the relationship between the two variables. Points that are located above the line indicate that three-hourly H_s is greater than one-hourly H_s. Conversely, points that are located below the identity line indicate higher one-hourly H_s. The 99^{th} percentile of one-hourly and three-hourly H_s is 1.49 and 1.47 m, respectively. Considering H_s above the 99^{th} percentile as extreme values. For three-hourly waves with H_s higher than the threshold, a greater number of waves are being underestimated than overestimated. Therefore, using the extreme values of the three-hourly dataset for dune erosion assessments would lead to the underestimation of the wave impact.

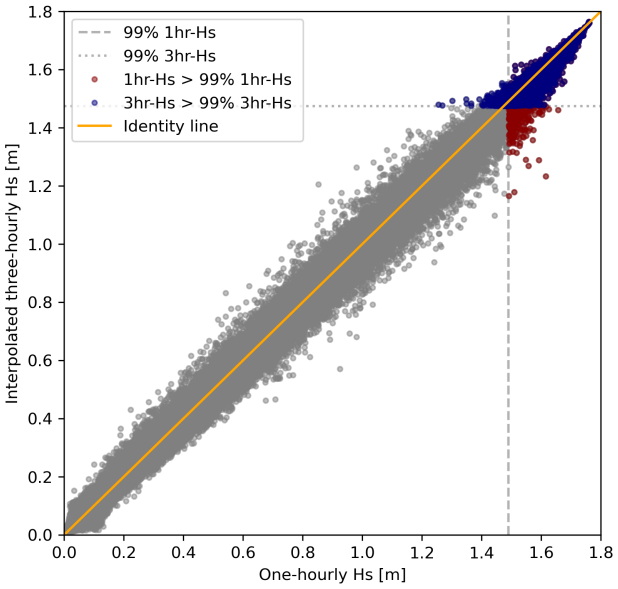

Figure 5.1: *Comparison one-hourly H_S with interpolated three-hourly H_S, simulated by the SWAN model for the period 1959-2021. The extreme values ($H_S > 99^{th}$ percentile H_S) are indicated by red scatters for the one-hourly dataset and blue scatters for the three-hourly dataset.*

To illustrate how the peak of H_s of the one-hourly data is not captured by the three-hourly data, the wind and wave characteristics are plotted in Figure 5.2. In the plot, the darker grey area indicates the period of the peak in wind data. This period exactly fits in three-hour time

intervals. To avoid neglecting these peaks in the wind data, it is important to use the one-hourly data of wave simulation.

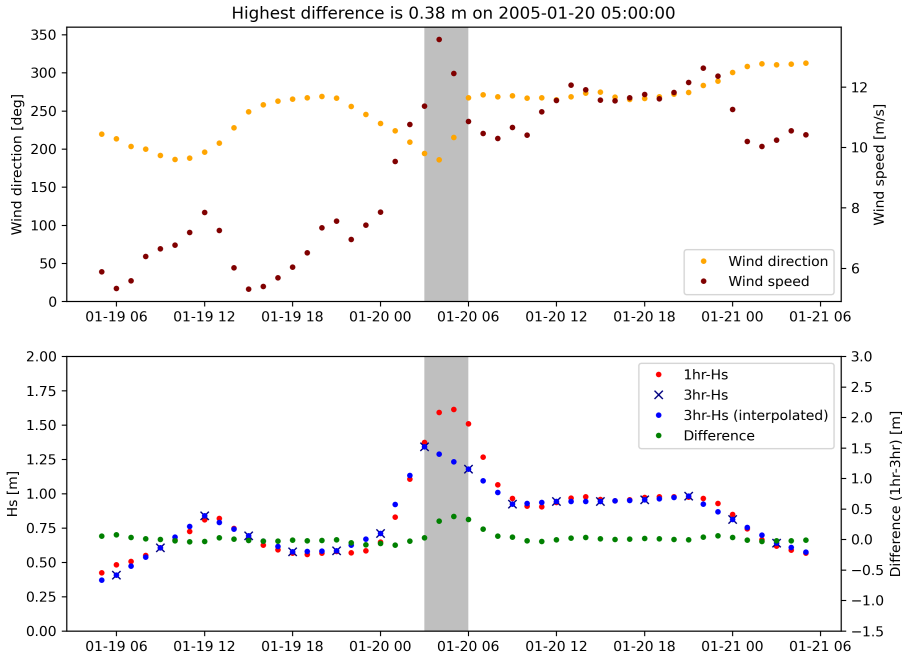

Figure 5.2: *Highest difference between the one-hourly H_s (red scatter) and three-hourly H_s (blue scatter). The grey area indicates the peak of the wind data within a three-hour time interval.*

5.2. Wave Climate Around The Falsterbo Peninsula

The wave climate in the Baltic Sea is influenced by factors such as wind pattern, ice cover, and coastal geography (Soomere, 2023). High variability and site-specific characteristics are present due to factors such as limited fetch length and the presence of islands. The wave climate along the south coast of Sweden is generated within the Arkona Basin in the southwest part of the Baltic Sea. Its characteristics can be described as short-period wind-generated waves, where the wave energy exposure gradually increases from west to east along the coast. Additionally, Adell et al. (2023) found that the interannual variability of wave energy and direction is correlated to the North Atlantic Oscillation North Atlantic Oscillation (NAO) index. The NAO index affects the wind patterns, resulting in alternating west-eastern dominance in the wave conditions. In conclusion, the wave climate in the Southern Baltic Sea is influenced by both local coastal features and large-scale atmospheric circulation patterns.

Wave data around the Falsterbo Peninsula were gathered to analyze the variability of wave climate across different locations. Understanding the prevailing wave pattern can be gained by analysing the wave rose, which illustrates the directional distribution of waves at a specific location over a given period. Wave roses, in Figure 5.3, quickly give a visual representation of the predominant wave directions and the magnitude of the wave height at a particular location.

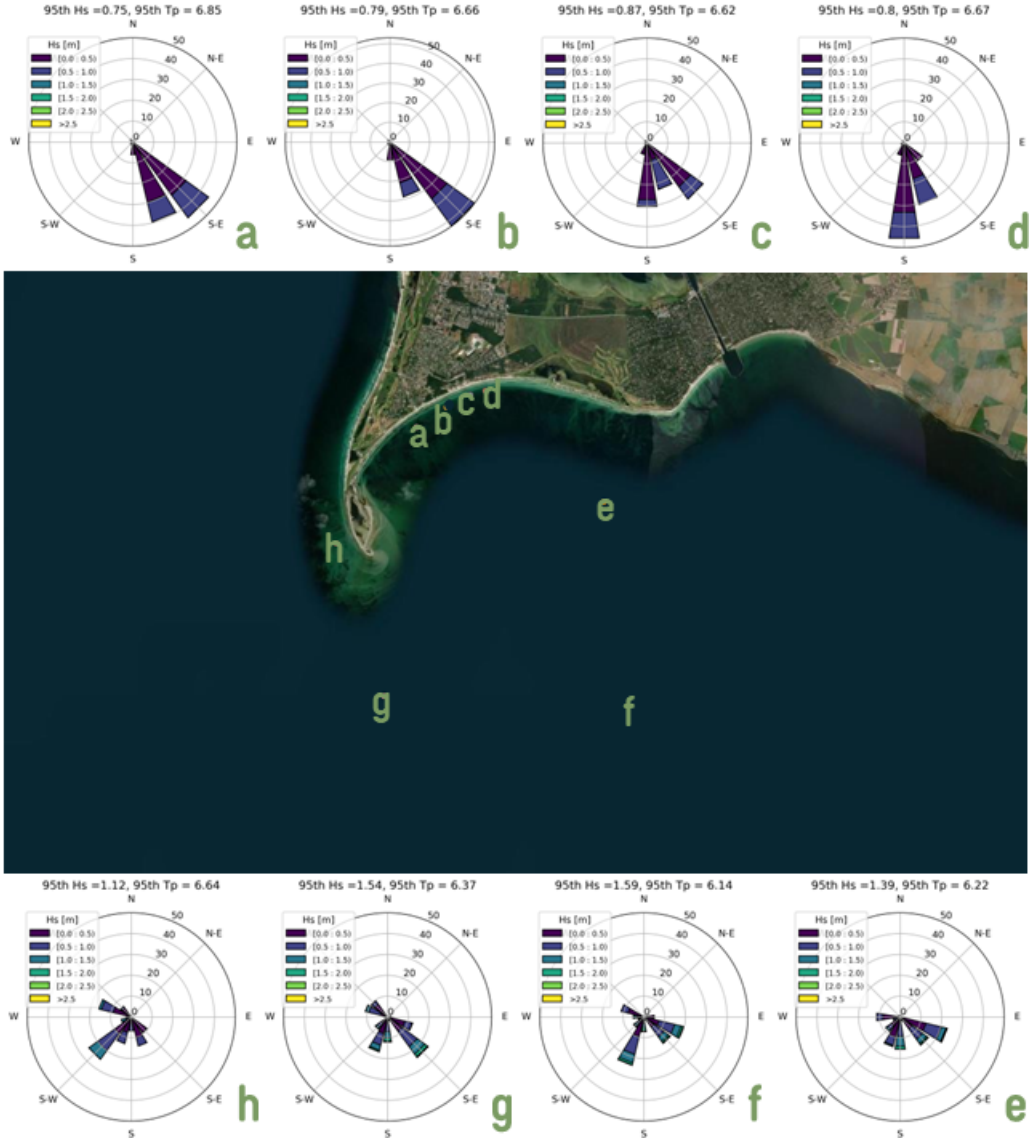

Figure 5.3: *Wave rose for the period 1959-2023, at various locations around the Falsterbo Peninsula.*

For the waves in front of the dune in locations a, b, and c, the wave rose reveals that the prevailing wave directions are from Southeast to South while for location d it is mainly from South-Southeast to South. No wave directions from the North or West are observed due to the orientation of the spit. Beyond the spit (locations e,f,g) at a deeper depth, waves are mostly arriving from East-Southeast to Northwest. Note that wave directions at these locations differ from wave directions observed in front of the dune. The difference in the observed wave directions at various locations can be explained by the phenomenon of refraction. As waves propagate from deep to shallow water, the change in seafloor depth causes the wavefront to bend. Next to the spit (location h), the main wave direction is from Southwest.

Table 5.1 displays statistical values of H_S and T_p at various locations in Figure 5.3. Note that H_s differs with the depth at various locations but T_p is comparable between all locations. As the wind is the primary driver of wave generation in the Baltic Sea, similar wind across the locations can result in similar wave characteristics. Additionally, the semi-enclose characteristic of the Baltic Sea ensures that the waves do not undergo significant changes, resulting in similar T_p at different locations.

Table 5.1: *Statistical significant wave height (Hs) and peak period (Tp) at various locations around the Falsterbo Peninsula.*

Location	Depth [m]	Mean Hs [m]	95th percentile Hs [m]	Max Hs [m]	Mean Tp [s]	95th percentile Tp [s]	Max Tp [s]
a	1.85	0.32	0.75	0.82	4.06	6.85	12.48
b	2.01	0.34	0.79	0.89	4.02	6.66	12.45
c	2.38	0.35	0.87	1.02	4.00	6.62	12.40
d	2.02	0.34	0.80	0.92	4.05	6.67	12.46
e	6.25	0.59	1.39	2.49	3.85	6.22	12.07
f	10.8 0	0.68	1.59	3.89	3.92	6.14	12.05
g	6.11	0.66	1.54	2.53	3.90	6.37	12.14
h	3.15	0.51	1.12	1.36	3.88	6.64	12.31

5.3. Simulated Wave Time Series

The wave data is obtained by extracting the simulated wave characteristic at a location in front of the dune, at a depth of 10.80 m, exceeding the depth of closure (Hallin et al., 2017). In this study the wave data is extracted in location f, see Figure 5.3. Figure 5.4 shows the time series of simulated H_s for the period 1959-2023. The highest recorded H_s is 3.90 m (RH 2000), while the arithmetic mean is 0.70 m. As shown in Figure 5.5a, a higher average of H_s is found during the period between October and March.

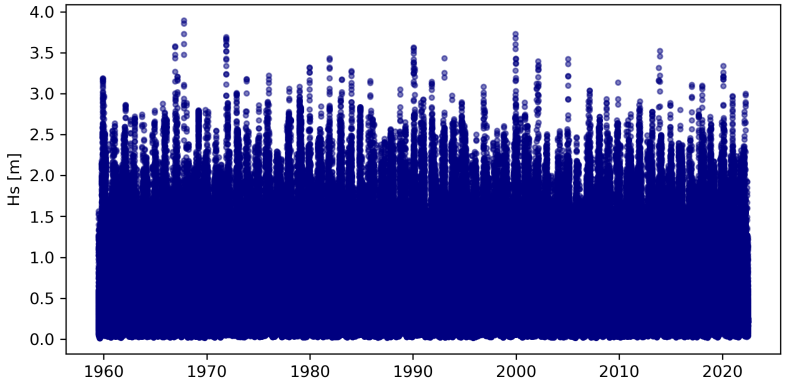

Figure 5.4: *Time-series of H_s for the period 1959-2023 at a depth of 10.80 m (RH 2000).*

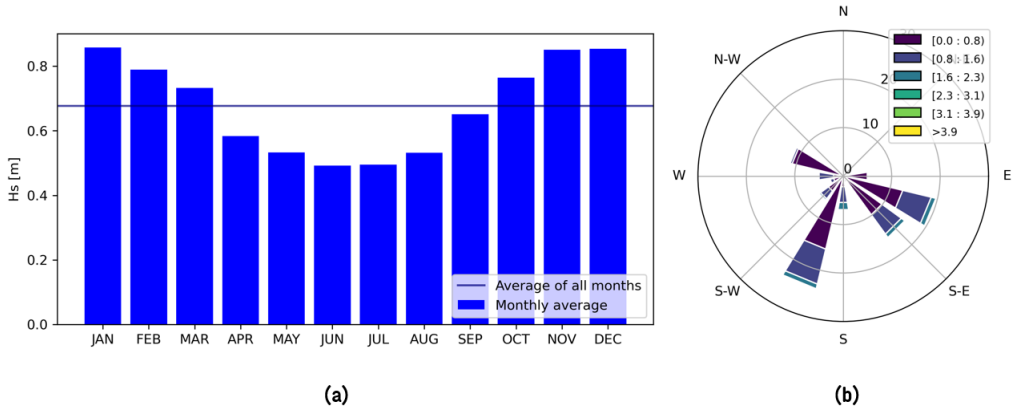

Figure 5.5: *Monthly average (a) and wave rose (b) of H_s for the period 1959-2022.*

The wave rose in Figure 5.5b shows that waves from the Southeasterly direction (90-180°) are most frequently observed, followed by waves from the Southwesterly direction (180-270°). The corresponding H_s and T_p of each dominant wave direction are shown in Figure 5.6. Individual waves are represented by each data point in the figure. The extreme H_s for both dominant wave directions are comparable. Notably, a large concentration of data points can be observed for

southeasterly waves with low H_s (below 1.00 m) and high T_p (exceeding 8.00 s). These waves can be associated with swell systems originating from distant weather systems or influenced by the fetch length.

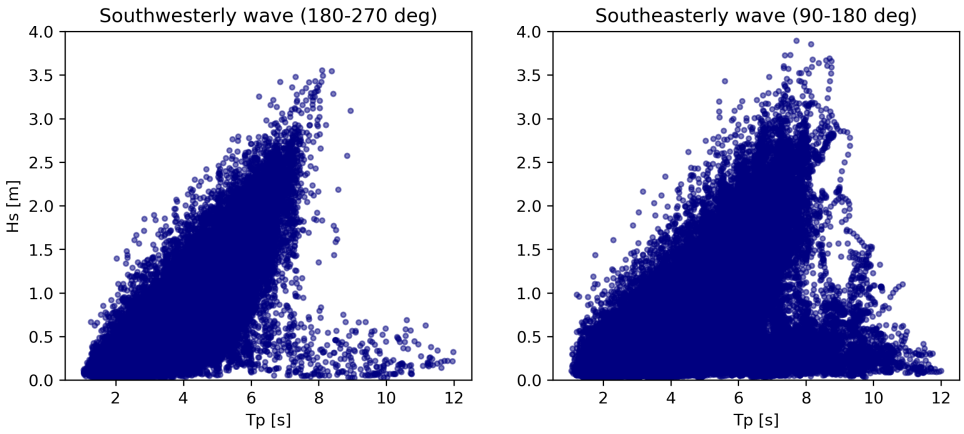

Figure 5.6: *Westerly and easterly wave characteristics.*

The fetch length is the distance over which the wind can blow uninterrupted across the water surface. Long fetch length allows the wave to grow and accumulate energy from the wind, resulting in higher waves. On the other hand, short fetch length leads to smaller and less energetic waves. The fetch length has an influence on the peak period, as it defines the time when the wind can transfer its energy to the water. The longer the fetch length, the longer the accumulation of wave energy, resulting in waves with longer peak periods. The fetch length, in Figure 5.7, is determined by measuring the distance from the study area across the water surface from various angles. Longer fetch lengths are found on the east side of the study area, explaining the longer peak period of Southeasterly waves.

Figure 5.7: *Fetch length to the study area, measured in various angles in Google Maps.*

6. Historical Storm Conditions

Extreme conditions were selected based on the method called the structural response (SR) method and the time series of TWL. The two methods are compared in Section 6.1. The corresponding storm parameters were extracted from the time series, the results are shown in Section 6.2. The obtained time series of each extreme condition were used as input data for the morphological models to determine dune erosion.

6.1. Extreme Condition Sampling

Selection based on the SR method relies on the combinations where WL and H_S are simultaneously higher than the defined threshold values, which are 0.59 m and 2.10 m respectively. In Figure 6.1, all combinations where H_s is higher than its threshold value are indicated by blue scatters and yellow scatters represent combinations where WL is higher than its threshold value. All combinations where both H_s and WL are simultaneously higher than the defined thresholds are indicated by green scatters, these combinations will be selected as extreme values according to the SR method. Note that Figure 6.1 shows that the earlier assumption made about the suitability of sampling methods WD and SD in this study area is valid. If the extreme conditions are to be selected based on either WD or SD method, a lot of combinations of H_s and WL will be neglected in the assessment.

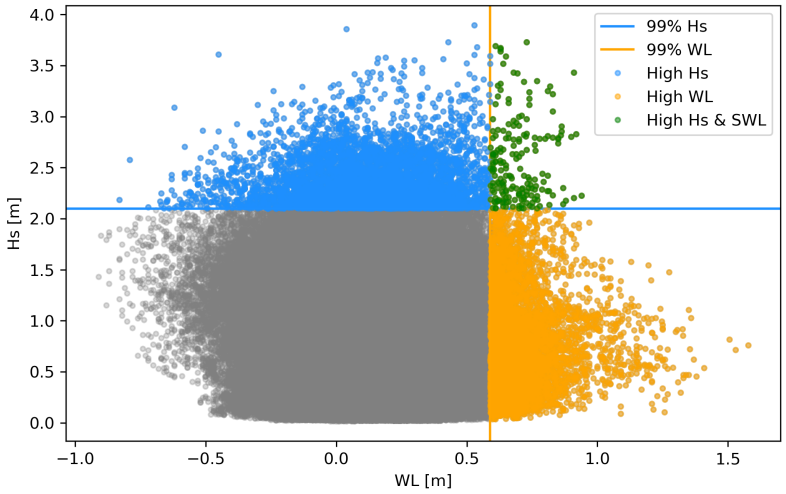

Figure 6.1: *Hourly H_s and WL (RH 2000) for the period 1959 till 2022. High H_S in blue and high WL in yellow. Combinations of high H_S and high WL simultaneously in green, are considered extreme values according to the SR method.*

Alternative method to select extreme values was based on the time series of TWL, which represents the combined effect of H_s and WL. The threshold value for TWL was set at the average elevation of the inland boundary in the study area. The cross-shore profiles in the dune are obtained from the topography data in Appendix A and the average value of the elevation is found to be 1.97 m. The threshold value for TWL was taken as 2.00 m to account for uncertainties in the measurement process. Combinations where H_W and WL lead to TWL above this threshold value are considered extreme.

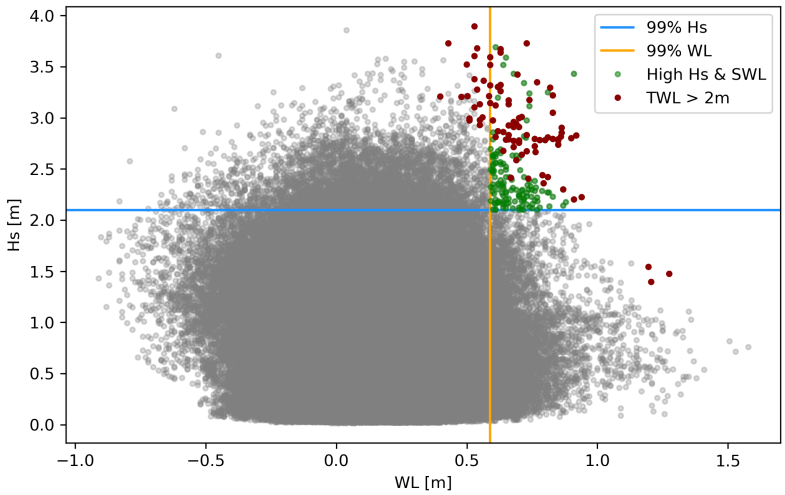

Figure 6.2: *Hourly of H_s and WL (RH 2000) for the period 1959 till 2022. Combinations of H_s and WL selected based on the SR method and the TWL method are indicated by green and red scatters respectively.*

Figure 6.2 shows the combination of H_S and WL according to the sampling method SR (in green) and based on the time series of TWL (in red). Notably, more combinations are selected in the SR method but the combinations based on the TWL time series are more interesting for the dune assessment. These combinations encompass a broader spectrum of the two variables. The results show the possible scenarios that can lead to TWL higher than 2.00 m. The first scenario is the common scenario where both H_s and WL exceed the 99^{th} percentile of their respective time series, denoted as high values. Other scenarios are high H_s in combination with moderate WL, with moderate values falling within the 75^{th} and 99^{th} of the time series. The last type of scenario can be characterised by high WL in combination with mild H_s. These scenarios would have been neglected when extreme values were sampled using the SR method. To ensure that the analysis includes all relevant combinations of the two parameters, extreme events will be selected based on the TWL time series. The selected scenarios are summarized in Table 6.1.

Table 6.1: *Scenarios of Hs and WL corresponding to TWL exceeding 2.00 m. High values are defined as exceeding the 99^{th} percentile of the time series, while moderate values fall within the 75^{th} and 99^{th} of the time series.*

Scenario 1	High Hs (Hs >2.10 m)	High WL (WL >0.59 m)
Scenario 2	High Hs (Hs >2.10 m)	Moderate WL (0.23 m <WL <0.59 m)
Scenario 3	Moderate Hs (0.95 <Hs <2.10 m)	High WL (WL >0.59 m)

Figure 6.3 shows the time series of TWL for the period 1959-2023 in each transect in the dune. The brown dashed line indicates the threshold value. In Appendix E, TWL time series are shown together with the time series of R and WL for each transect. According to the results from the fieldwork, see Section 4.5, the TWL varies with varying foreshore slope and shoreline orientation in each transect. The highest TWL occur in Transect C as this transect has the highest foreshore slope. A higher foreshore slope causes the wave to break and dissipate wave energy more rapidly. The concentrated wave energy results in a higher wave runup.

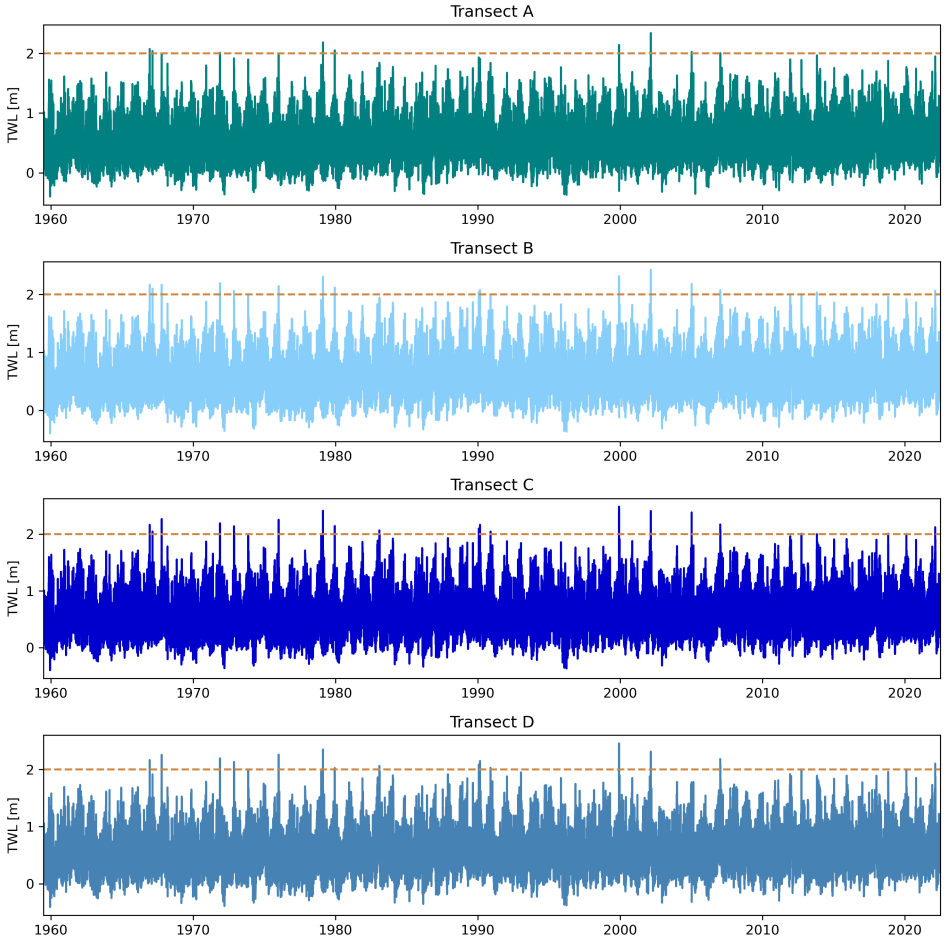

Figure 6.3: *Times series of TWL for the period 1959-2022 in various transects in the dune with a threshold line indicated by the brown dashed line.*

The total water level during the 1872 storm was determined using the historical water level data and the simulated significant wave height as described in Section 4.4. The results in Figure 6.4 show the total water level from November 12^{th} till November 13^{th}, where the total water level higher than the threshold is from 12^{th} at 14:00 h till November 13^{th} at 20:00 h. The maximum TWL during the peak of the storm on November 13^{th} at 12:00 h is 4.36 m in Transect C.

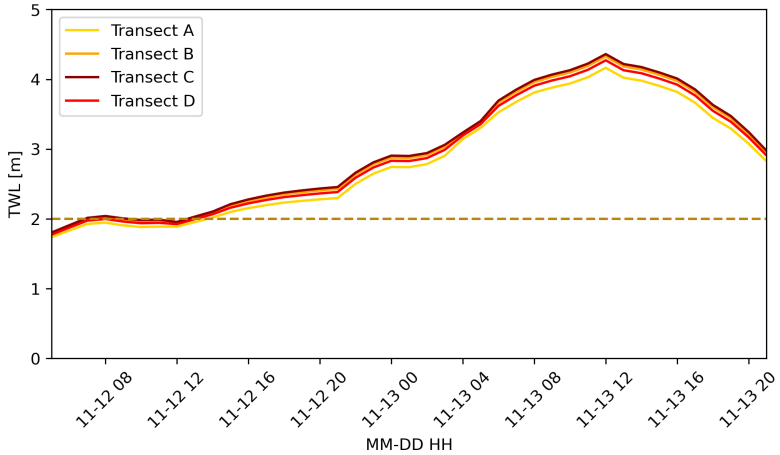

Figure 6.4: *Total water level (TWL) during the 1872 storm in various transects with the threshold line at 2.00 m.*

Selecting the corresponding wave, water level and wind characteristics to the extreme condition was by utilizing the date and time when the total water level exceeds the defined threshold. An example of the data selection process is shown in Figure 6.5. The duration of the extreme event is indicated by the grey area in the plot. Wave characteristics, water level and wind characteristics corresponding to the extreme event were obtained by extracting the data that fall within this grey area. These data was then used as input data for morphological models to simulate dune erosion.

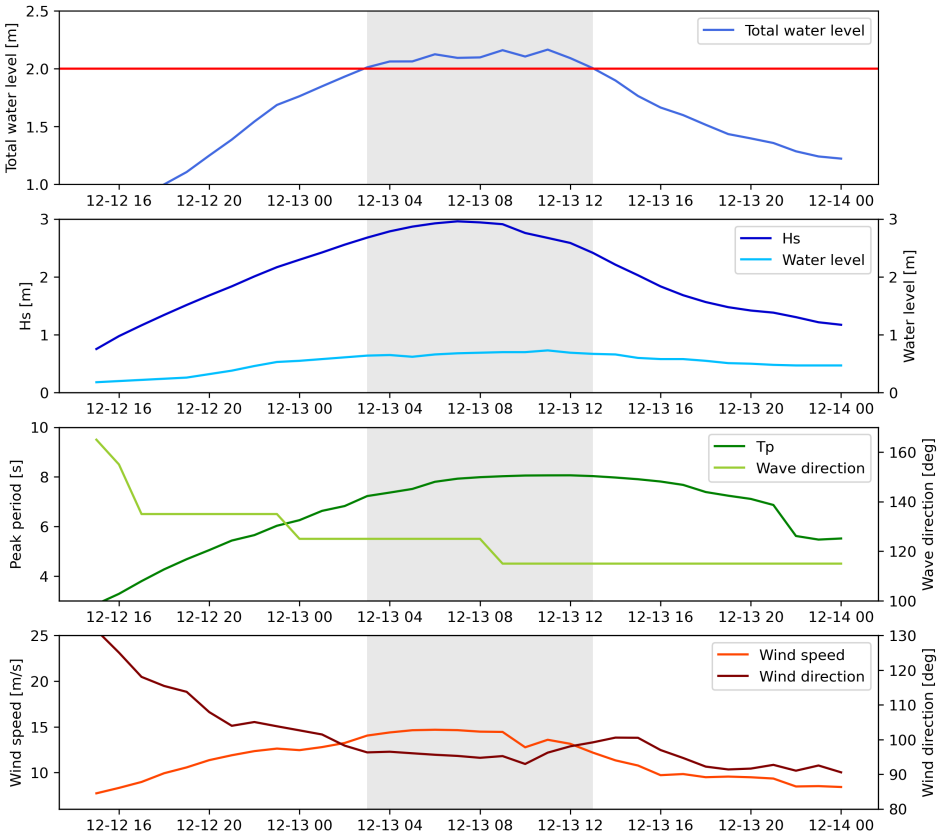

Figure 6.5: *Example of the selection of wave climate, water level (RH 2000), and wind data corresponding to an extreme event. The grey area indicates the duration of the extreme event. The red line in the top panel indicates the threshold value.*

6.2. Storm Parameters

Between the period 1959-2022, a number of extreme conditions were observed across various transects, with Transect C experiencing the most conditions. The 1872 storm was considered as one extreme condition in all transects. Figure 6.6 shows wave characteristics, water level, and duration during the peak TWL of each selected extreme condition in Transect C. Similar figures for other transects can be found in Appendix F. In the figure, extreme events identified in the period 1959-2022 are shown in blue, while the 1872 storm is indicated in red.

Figure 6.6a, shows the combination of H_s and WL and the threshold line for both datasets as the 99^{th} percentile. The combinations of H_s and WL were characterised according to Table 6.1. The 1872 storm is considered a unique event because during this storm high H_s occurred with significant WL. In Figure 6.6b, T_p is shown against H_s. In the selected extreme conditions in the period 1959-2022, the maximum and minimum T_p are 4.58 s and 9.85 s, respectively. However, during the 1872 storm, T_p reached a higher value of 11.35 s. Figure 6.6c, shows that wave characteristics corresponding to the extreme conditions are commonly Southerly or

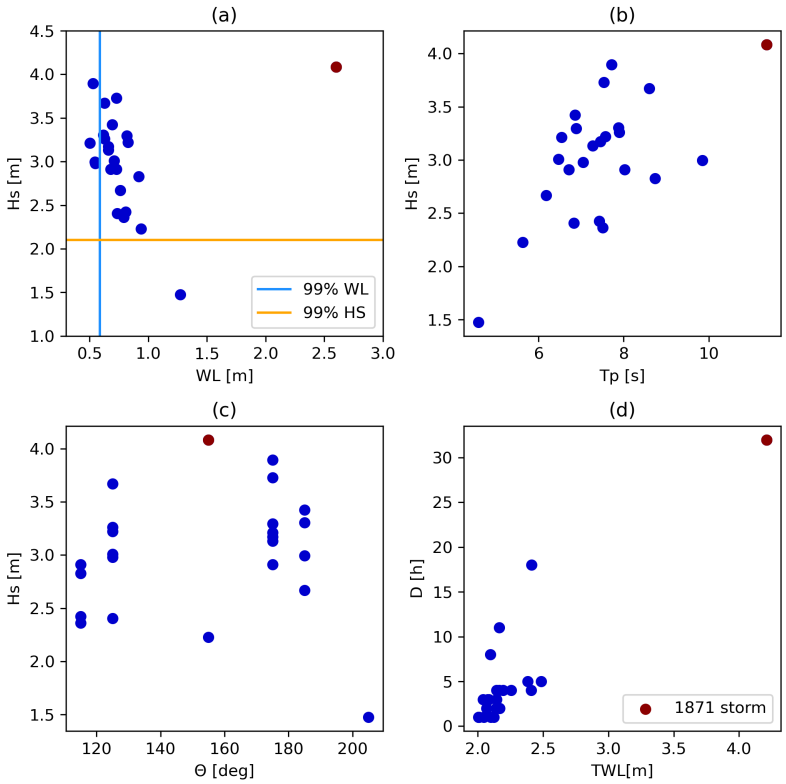

Figure 6.6: *Wave climate, water level (RH 2000) and wind characteristics at the timestamp coinciding with the peak of TWL in every selected extreme condition in Transect C. Each scatter represents the variable of that extreme condition.*

Southeasterly waves. Some Southwesterly waves are observed. The corresponding T_p of the Southerly and Southeasterly waves is higher than the T_p of Southwesterly waves. Lastly, Figure 6.6d shows the duration of the events along with the peak of TWL. Most of the events have a duration of less than 5 hours. However, it is clear that the 1872 storm was exceptionally extreme, with a much higher duration and TWL almost twice as high as the other events.

7. Morphological Model Result

This chapter represents the results of the simulated dune erosion using morphological models. Section 7.1 describes the XBeach model result, while Section 7.2 describes the storm impact model result. The correlation between dune erosion and the storm parameters is described in the last section of this chapter, Section 7.4. Finally, in Section 7.5, the maximum dune erosion is compared to the available volume within the dune system.

7.1. XBeach Model Result

7.1.1. Bed Level Change

The XBeach model uses wave, water level, and wind data from the selected extreme events as input to simulate the bed level change. An example of bed level change in one event is shown in Figure 7.2. The initial bed level is represented by the dashed grey line, while the red line represents the bed level after the simulation. The vertical grey line in Figure 7.2a and 7.2b represents the location of the dune toe. The area where there is an increase in volume after the simulation is indicated by accretion (green area), while the area with less volume is depicted by erosion (orange area).

Note that in the simulation with the Danish calibration in Figure 7.2a, large changes can be found at the lower part of the profile while minor changes are found in the simulation with the Holland default setting, in Figure 7.2b. The dune volume change was determined by comparing the dune volume before and after each simulation. Volume changes according to extreme events during the period 1959-2022, simulated by the Danish calibration and the Holland default setting are shown in Figure 7.3. The results of the Danish calibration indicated dune accretion for all four transects, in contrast to the default model's prediction of dune erosion.

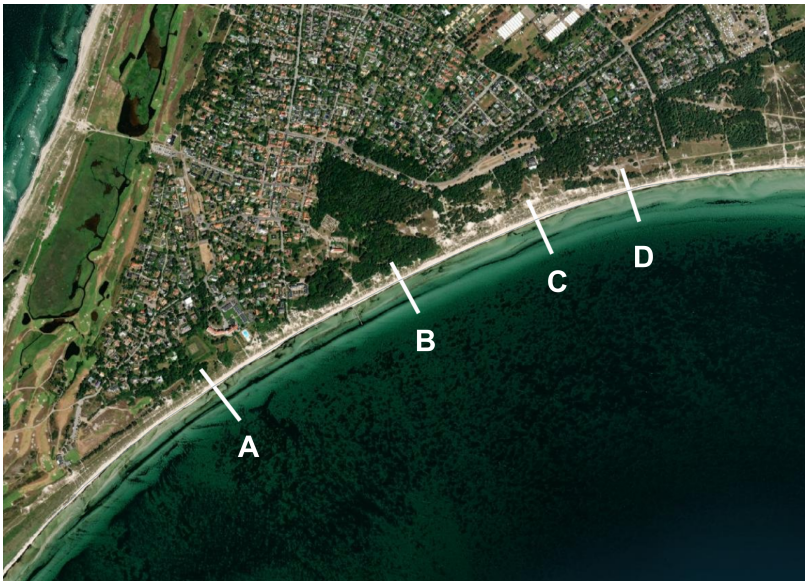

Figure 7.1: *Transect location in the dune.*

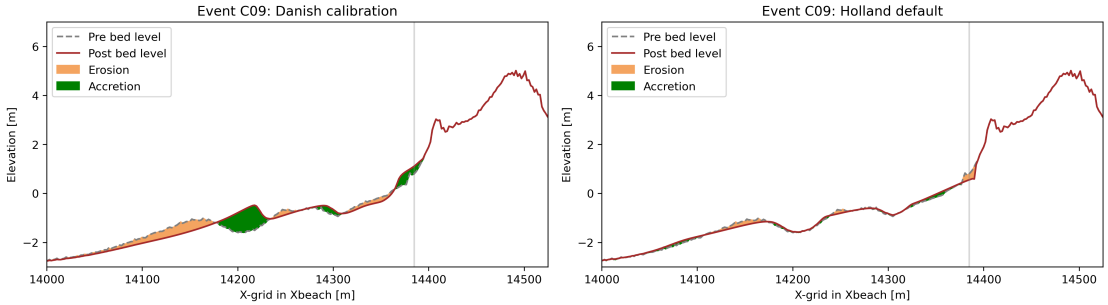

(a) *Danish calibration* **(b)** *Holland default*

Figure 7.2: *Example of simulated bed level change in Transect C using the Danish calibration and Holland default model settings in XBeach. The vertical grey line in both figures indicates the location of the dune toe.*

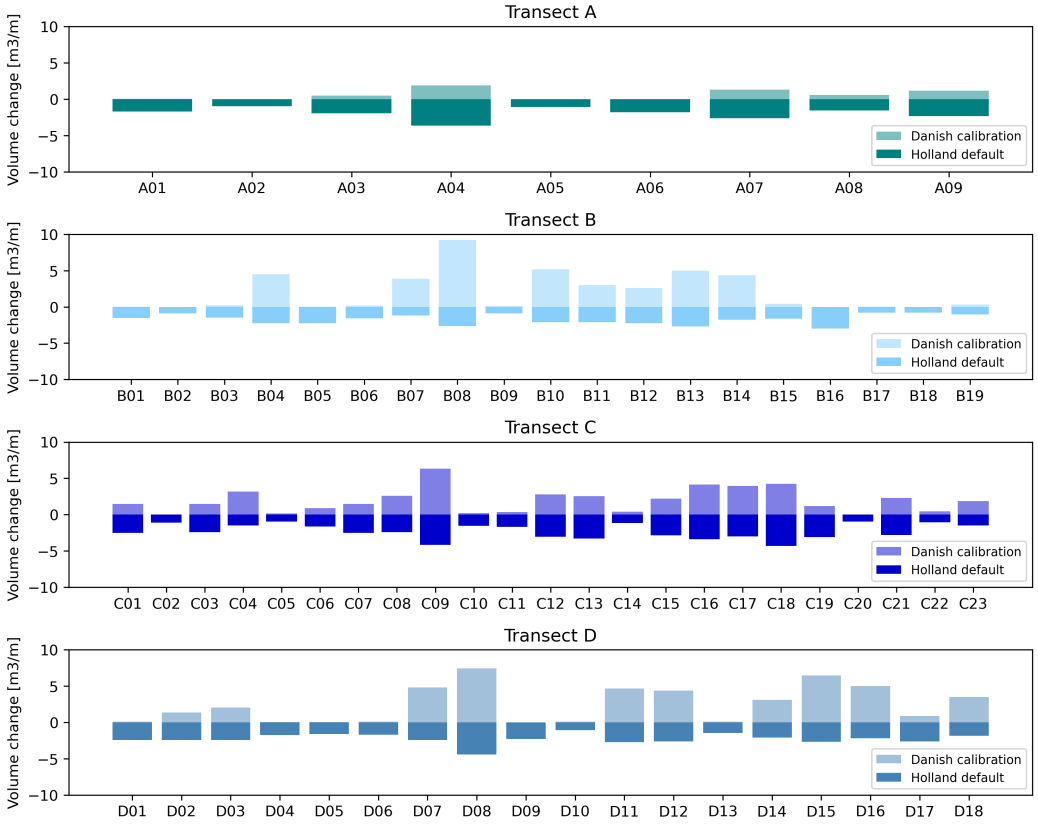

Figure 7.3: *Volume change simulated by XBeach using the Danish calibration and Holland default for the different transects in the dune.*

The bed level change due to the 1872 storm in Transect C is shown in Figure 7.4. Figures for other transects are available in Appendix G. The volume change in each transect was determined and the results are shown in 7.5. The model results with the Danish calibration showed accretion in Transects A and B, while erosion was observed in Transects C and D. With the default Holland simulations, dune erosion occurs in all transects. Additionally, the magnitude is significantly higher than the magnitude of the Danish calibration results. Moreover, these magnitudes are also significantly higher than the dune erosion found in the extreme events during the period 1959-2023.

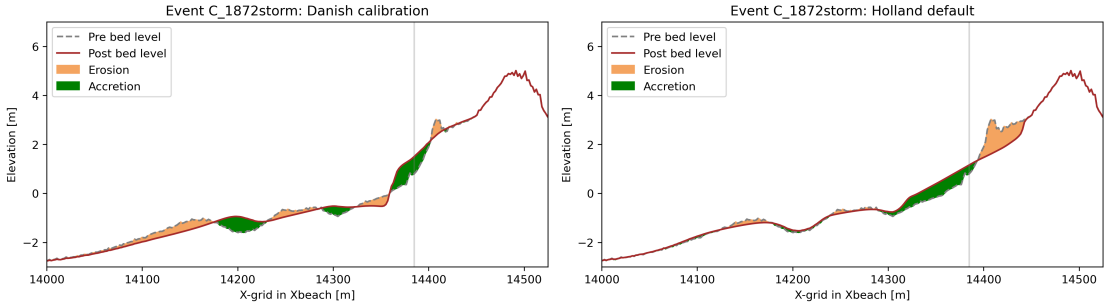

(a) *Danish calibration* **(b)** *Holland default*

Figure 7.4: *Example of simulated bed level change in Transect C due to the 1872 storm using the Danish calibration and Holland default model settings in XBeach. The vertical grey line in both figures indicates the location of the dune toe.*

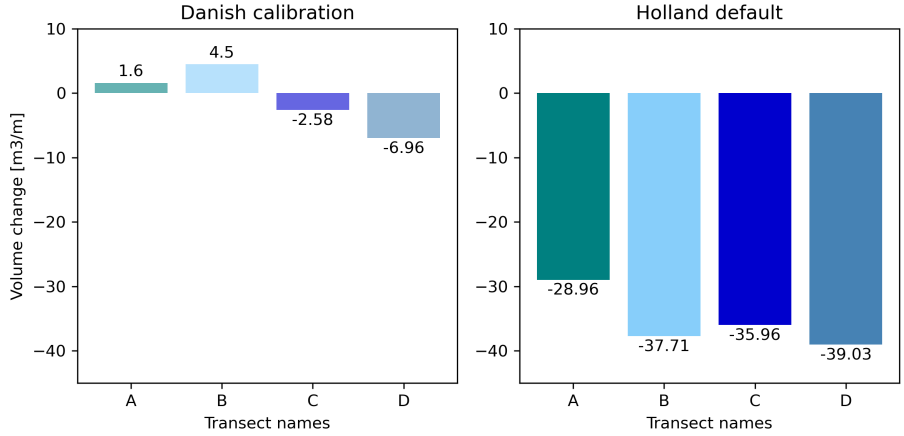

Figure 7.5: *Volume change after the 1872 storm in various transects in the dune, simulated in XBeach with Danish calibration and Holland default settings.*

The volume change under extreme conditions in different transects indicated significant differences between the XBeach model results for the Danish calibration and the Holland default settings. Insights into the parameters responsible for these differences are gained by analyzing the sensitivity analysis results.

7.1.2. XBeach Sensitivity Analysis Result

A sensitivity analysis was conducted to study the primary variations of the XBeach simulations resulting from the Danish calibration and the Holland default. Five simulations of the 1872 storm event were carried out in transect C in Figure 7.1, according to the model setup outlined in Table 3.3. The results of these simulations are shown in the top panel of Figure 7.6.

The lower panel of Figure 7.6 shows the difference in bed elevations resulting from the various model setups compared to the default setting, which is the first model setup. Minor differences were observed between the second and the third model setup with the default settings. The difference is indicated by the green and the yellow lines. In the second model setting the critical avalanching slope was reduced from 1.0 to 0.8, while in the third model setting the morphological acceleration factor was increased from 1.0 to 5.0. Although these parameter changes had some impact, the differences in the bed elevation were relatively small. However, significant deviations could be observed when comparing bed elevations due to the fourth model setup with the default setting, where the *facua* factor was increased from 0.1 to 0.3. Less erosion was observed at the upper part of the profile. Finally, the last model setup (indicated by the blue line), which

aligns with the Danish calibration, exhibited a large difference in bed elevation compared to the default setting but closely resembles the bed elevation simulated with the fourth model setup. These results showed that a large deviation in the model results was due to various model setups occurring when the *facua* parameter was increased. Additionally, the *facua* parameter caused a smoothed effect on the lower part of the bed profile.

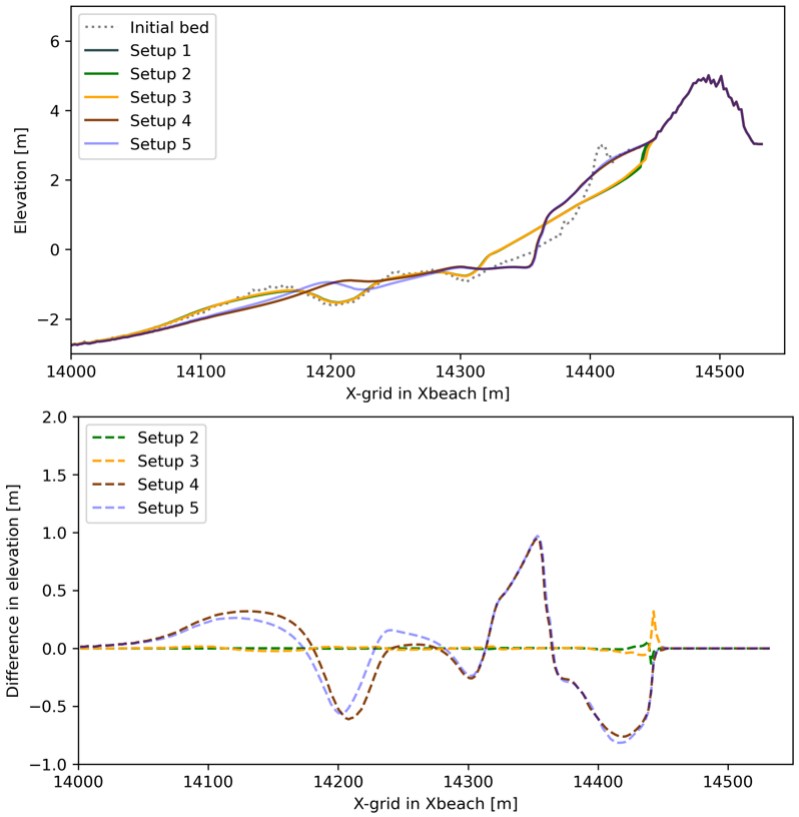

Figure 7.6: *Top panel: the bed elevation simulated with various model setups in Transect C. Bottom panel: the difference between the bed elevation simulated with the default setting and other model setups.*

Table 7.1: *Overview of the model setups of the XBeach model in the sensitivity analysis and the corresponding volume changes.*

	Parameter	Change factor of parameter	Volume change m^3/m	Change factor of volume
Setup 1 Holland default	dryslp = 1.0 morfac = 1.0 facua = 0.1	1 1 1	-35.96	1
Setup 2	dryslp = 0.8 morfac = 1.0 facua = 0.1	0.8 1 1	-38.84	0.92
Setup 3	dryslp = 1.0 morfac = 5.0 facua = 0.1	1 5 1	-38.83	0.92
Setup 4	dryslp = 1.0 morfac = 1.0 facua = 0.3	1 1 3	-3.91	9.12
Setup 5 Danish calibration	dryslp = 0.8 morfac = 5.0 facua = 0.3	0.8 5 3	-2.58	13.94

Investigation of different model settings in XBeach could also be accomplished by focusing on the change of the dune volume due to various model settings. The first model setup corresponds to the Holland default which contains all the default parameters in the XBeach model. The last model setup corresponds to the Danish calibration, where the main difference in the model setup lies in the critical avalanching factor, morphological acceleration factor, and the factor controlling the wave skewness and wave asymmetry. The first column of Table 7.1 shows the value of each factor corresponding to the different model setups. The volume of the original dune is compared to the volume after each simulation, and the difference is shown in the third column. The findings suggested that all the model configurations lead to dune erosion. The first three models demonstrate high erosion, while the last two exhibit minor erosion. Using the default settings, the eroded volume amounts to 35.96 m^3/m, which is 14 times greater than the eroded volume of 2.58 m^3/m obtained from the model setup in accordance with the Danish calibration. This implies that increasing the *facua* parameter in the model setup leads to a reduction in dune erosion in the model simulation.

7.2. Storm Impact Result

The storm impact model determined the erosion rate during the selected extreme events. To calculate the volume change per meter of the beach (m^3/m), the dune erosion rate per hour ($m^3/m/h$) was summed over the total duration of the event (in hours). Figure 7.7 shows the volume change calculated with C_s value of $1.7 * 10^{-4}$ for the different extreme events in various transects. The negative value of the volume change indicates dune erosion. The volume change during the 1872 storm for the different transects is shown in Figure 7.8. Note the significant difference between dune erosion due to extreme conditions during the period 1959-2022 and the dune erosion due to the 1872 storm.

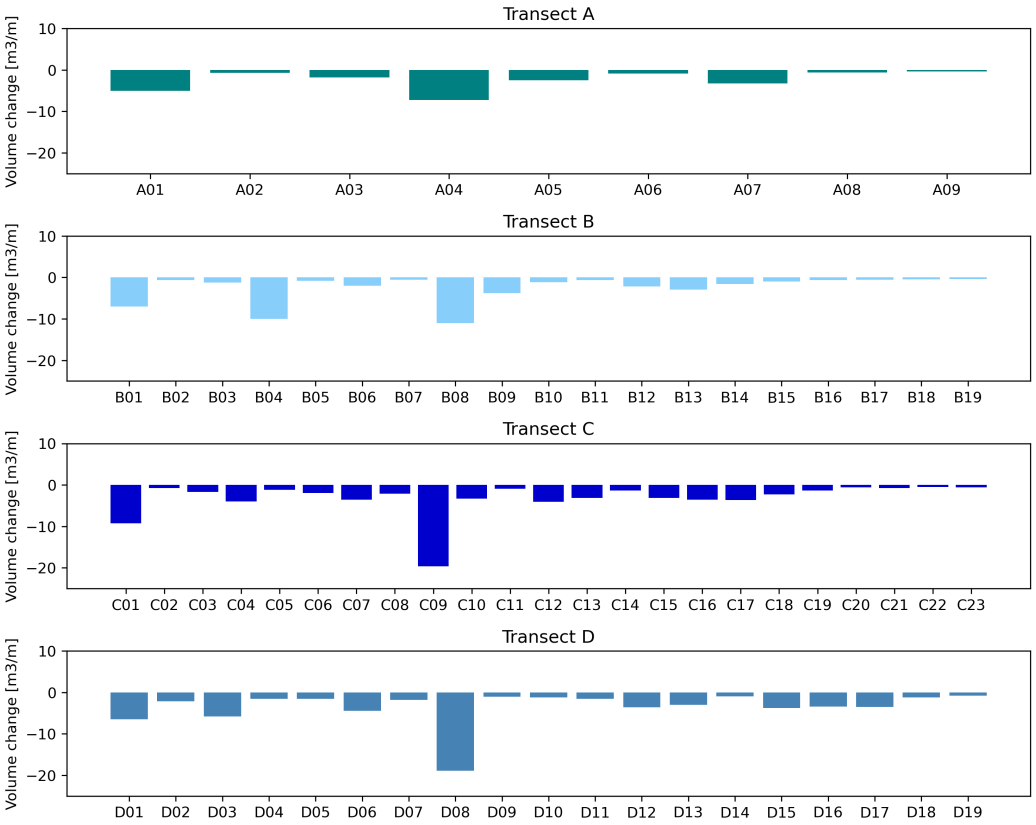

Figure 7.7: *Volume change per extreme event for the different transects in the dune, calculated by the storm impact model with C_s value of $1.7 * 10^{-4}$.*

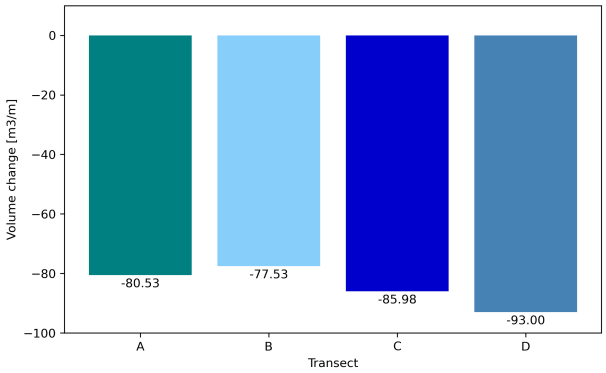

Figure 7.8: *Volume change due to the 1872 storm in various transects, calculated by the storm impact model with C_s value of $1.7 * 10^{-4}$.*

7.3. Comparison Simulated Dune Erosion

The dune erosion obtained using the XBeach and the storm impact model is compared in this section. Figure 7.9 shows the results of storm conditions in Transect C, during the period 1959-2022, corresponding to the XBeach model with the Danish calibration (blue) and Holland default (red) model settings, and the storm impact model (yellow). The comparison for other transects can be found in Appendix H. The XBeach model with the Danish calibration estimated a positive volume change, indicating an accretion in the dune after the simulation. The XBeach model with Holland default setting and the storm impact model determined similar dune erosion for most of the events.

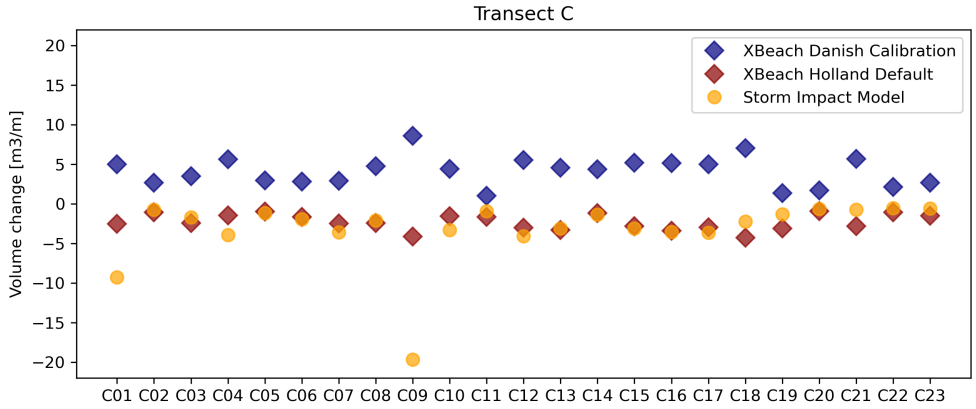

Figure 7.9: *Volume change in each extreme condition in transect C of the dune, determined with the XBeach and the storm impact models.*

The results of the 1872 storm are shown in Figure 7.10 for all transects. A comparison of the magnitude of the dune erosion due to the 1872 storm with the dune erosion due to extreme conditions between 1959 and 2022 shows a significant difference. According to the XBeach model with the Danish calibration, the estimation indicates dune erosion during the 1872 storm, whereas dune accretion was observed during the simulation of the selected extreme conditions. The XBeach model with Holland default estimated the dune erosion during the 1872 storm to be 8 to 13 times higher than the maximum dune erosion observed over the 62-year period. Similarly, the storm impact model estimated higher dune erosion with a factor ranging from 4 to 11, depending on the transect under consideration. The factors are summarized in Table 7.2. The significant difference found in the estimated dune erosion implies that the 1872 storm was indeed a severe event.

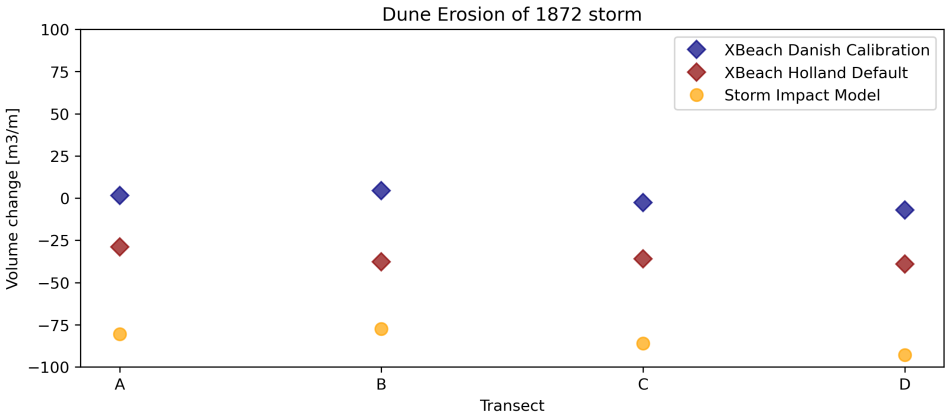

Figure 7.10: *Volume change during the 1872 storm for all transects in the dune, determined with the XBeach and the storm impact models.*

Table 7.2: *Comparison of the estimated dune erosion of selected extreme conditions between 1959 and 2022 with the 1872 storm, by the XBeach with Holland default and the storm impact model.*

Transect	Max erosion in 1959-2022 m^3/m	Erosion 1872 storm m^3/m	Change factor
XBeach Holland default			
A	3.66	28.96	8
B	3.01	37.71	13
C	4.29	35.96	8
D	4.41	39.03	9
Storm impact model			
A	7.26	80.53	11
B	7.02	77.53	11
C	19.65	85.98	4
D	18.91	93.00	4

The conditions where the results of the two models are significant are conditions C01, C09 in Figure 7.9 and the 1872 storm in Figure 7.10. An explanation for this difference was found by plotting the model results against the storm duration for each extreme condition. Figure 7.11 illustrates that for storm conditions with a duration of less than 10 hours, the results produced by both models are comparable. However, for longer storm duration, the storm impact model predicted larger dune erosion than the XBeach model with the Holland default. Note that the longer the storm duration, the higher the difference is between the model results.

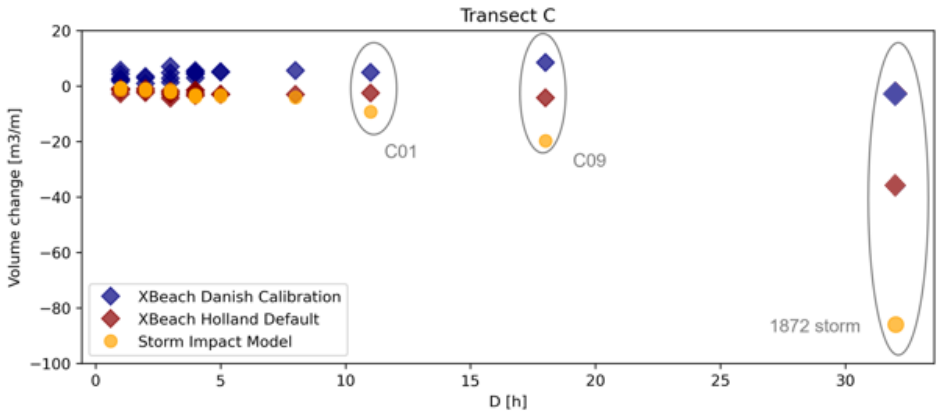

Figure 7.11: *Volume change of storm conditions including the 1872 storm against the storm duration, determined by the XBeach and the storm impact models.*

As the XBeach model with the Danish calibration predicts an outcome contrary to the hypothesis, dune accretion instead of dune erosion, these results were excluded from further analysis.

7.4. Dune Erosion & Storm parameters

The results of dune erosion as a consequence of the extreme conditions in Transect C and the storm parameters in each condition are presented in Figure 7.12 for the XBeach model and Figure 7.13 for the storm impact model. The erosion data are categorized into three levels in Table 7.3. Erosion volumes below 1.67 m^3/m are classified as low, within the range of 1.67 to 3.33 m^3/m as mild and exceeding 3.33 m^3/m as high. The classification was based on the maximum value of the estimated dune erosion in Transect C by the XBeach model. Figure 7.12a shows that high erosion was frequently observed in extreme conditions characterized by both high Hs ($>$ 2.10 m) and high WL ($>$ 0.59 m). Interestingly, condition numbers 18 and 19 also display high erosion despite not having this characteristic. This figure shows that high erosion can be the result of three types of scenarios as described in Section 6.1. The first scenario is when both parameters are high, the second scenario is when there is a high H_s in combination with moderate WL ($0.23 < WL < 0.59$ m), and the last scenario is with moderate H_s ($0.95 < H_S < 2.10$ m) in combination with high WL.

Table 7.3: Classification of dune erosion.

	Range erosion in m^3/m
Low	$<$ 1.67
Moderate	1.67 - 3.33
High	3.33 $<$

Figure 7.12b shows the wave angle relative to the shore normal at Transect C. Positive angles indicate waves arriving from the west, while negative angles represent the waves approaching from the east at Transect C. This figure clearly demonstrates that high erosion is commonly observed when the wave direction closely aligns with the shore-normal angle. In other words, the more wave angle approaches the shore-normal direction, the greater the erosion tends to be. When it comes to T_p, Figure 7.12b illustrates less relationship between high T_p and high dune erosion. The last plot in Figure 7.12 shows that the higher the TWL and D, the higher erosion can be observed. This suggests that there is a relationship between high dune erosion with high TWL and D, respectively.

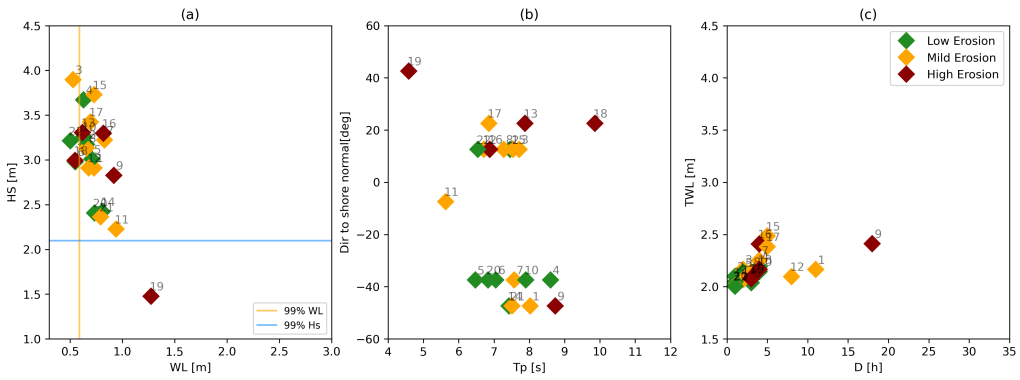

Figure 7.12: *Extreme conditions and the corresponding storm parameters and dune erosion determined by the XBeach model. The colours indicate the magnitude of dune erosion.*

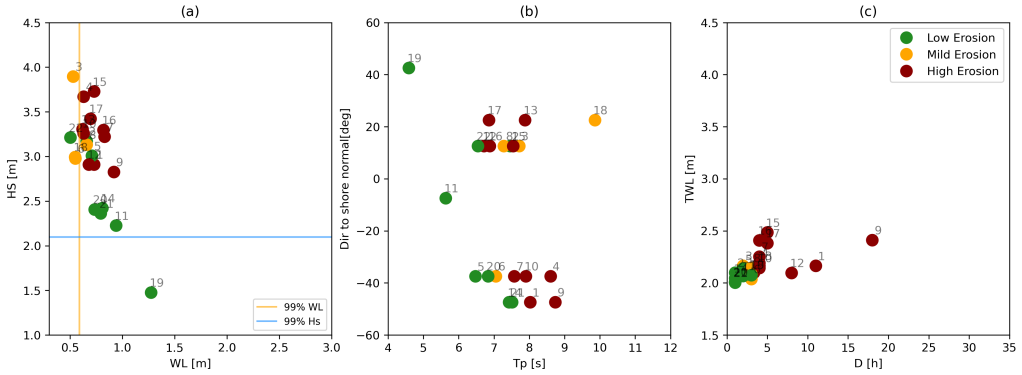

Figure 7.13: *Extreme conditions and the corresponding storm parameters and dune erosion determined by the storm impact model. The colours indicate the magnitude of dune erosion.*

Figure 7.13 presents a similar plot to Figure 7.12, but the results are obtained by the storm impact model. The dune erosion displayed in the figure is classified based on Table 7.3. In Figure 7.13a, high erosion can be observed for storm conditions characterized by high Hs and high WL. For conditions number 18 and 19, the XBeach model estimated high dune erosion, while the storm impact model estimated low and moderate erosion for these specific conditions. Figure 7.13b illustrates high dune erosion is less influenced by wave direction but exhibits a relationship with high T_p. The higher T_p, the higher the dune erosion. This is in contrast to the XBeach model, where such a relationship was absent. In Figure 7.13c, a clear relationship can be found between high dune erosion and high TWL and D. This finding aligns with the finding observed in the XBeach model.

In the previous section, it was found that the dune erosion magnitudes determined by the two models are comparable for most extreme conditions. However, when examining the corresponding storm parameters to individual storm conditions, differences can be extinguished. The storm impact model consistently predicts high erosion under conditions with high H_s and high WL. Conversely, the XBeach model also predicts high dune erosion for scenarios with high H_s and moderate WL, as well as those with high WL and moderate H_s. Regarding the wave direction, the XBeach results show that high erosion is associated with waves approaching from a more shore-normal direction. In contrast, the storm impact model exhibits less dependence on wave direction. In both model results, a clear relationship was found between high dune erosion and storm conditions with high TWL and D, respectively.

7.5. Dune Erosion along the Dune System

Dune resilience, according to Wernette et al. (2018), is the ability of coastal dunes to recover to a previous state after a storm event or to withstand its impact. The resilience is influenced by the dune's initial morphology, which comprises elements like the existing dune vegetation and the availability of the sediment. Additionally, it is affected by storm-related factors, such as frequency and intensity. As dune systems play a crucial role in coastal protection, it is therefore important to assess the strength of these natural barriers.

Evaluating the strength of the dune system was done by comparing the estimated dune erosion volume by the XBeach and storm impact model with the available volume in the dune system. The first column of Table 7.4 shows the available dune volume in each transect. The maximum estimated dune erosion for extreme conditions between 1959 and 2022 in each transect is shown in the second column. This erosion volume is expressed as a fraction of the available dune volume

Table 7.4: *Estimated dune erosion by the XBeach and storm impact model compared to the dune volume in various transects in the dune system on the Falsterbo Peninsula.*

Transect	Dune volume m^3/m	Max erosion in 1959-2022 m^3/m	Fraction	Erosion 1872 storm m^3/m	Fraction
XBeach Holland default					
A	119.80	3.66	3.06 %	28.96	24.17 %
B	102.66	3.01	2.93 %	37.71	36.73 %
C	157.40	4.29	2.73 %	35.96	22.84 %
D	57.49	4.41	7.67 %	39.03	67.89 %
Storm impact model					
A	119.80	7.26	6.06 %	80.53	67.22 %
B	102.66	7.02	6.84 %	77.53	75.52 %
C	157.40	19.56	12.43 %	85.98	54.62 %
D	57.49	18.91	32.89 %	93.00	>100 %

in the third column. Notably, the erosion volume estimated by the storm impact model is higher than the erosion volume found by the XBeach model in all four transects. The highest fraction was observed in Transect D, where the XBeach model estimated dune erosion to account for 7.67% of the available dune volume, whereas the storm impact model estimated a higher fraction of 32.89%. This difference between the two model results highlights the sensitivity in their estimations.

The 1872 storm was included in the analysis to evaluate the potential impact this storm would have on the current dune system. Considering the possibility of the storm event recurring, the interest lies in the strength of the current dune system to withstand its impact. The third column of Table 7.4, shows the erosion volume due to the 1872 storm estimated by the XBeach and storm impact model. The last column indicates the fraction of the available dune volume represented by this erosion volume. The highest fraction was found in Transect D. The XBeach model estimated the erosion to be 67.89% of the total volume, while the storm impact model estimated this fraction to exceed 100%. This suggests that all of the available dune volumes in Transect D would have been eroded away, indicating a potential dune breach in this transect.

8. Discussion

This section reviews the findings of this study and discusses the implications of the results. The sampling method used in this study will be discussed in Section 8.1. The results of the two morphological models will be discussed in Section 8.2. In the last section, the strength of the current dune system to withstand the storm impact in the study area will be discussed.

8.1. Extreme Condition Sampling

Two distinct extreme condition sampling methods were used in this study to extract extreme conditions from the time series spanning from 1959 to 2022. The first method is referred to as the Structural Response (SR) method. The sampling of this method relies on the combinations where H_s and WL are simultaneously higher than the defined threshold, which was set as the 99^{th} percentile of their respective time series. In addition to this simple method, a more advanced method was employed in this study. This method is based on the combined effect of H_s and WL, through the incorporation of the runup height $R2\%$ into the calculation of the total water level TWL. Extreme conditions were selected when TWL exceeded the defined threshold value of 2.00 m.

The selected storm conditions by the two methods were compared, and it was found that the TWL-based method captured a broader range of possible scenarios for extreme conditions. Three common scenarios were found in the selected extreme conditions, see Table 8.1. Additionally, the TWL-based method provides a more precise representation of the conditions within the study area as this is a site-specific approach. The TWL time series comprises $R_{2\%}$ which is calculated based on the foreshore slope of the dune transect.

Table 8.1: *Scenarios of Hs and WL corresponding to TWL exceeding 2.00 m. High values are defined as exceeding the 99^{th} percentile of the time series, while moderate values fall within the 75^{th} and 99^{th} of the time series.*

Scenario 1	High Hs (Hs >2.10 m)	High WL (WL >0.59 m)
Scenario 2	High Hs (Hs >2.10 m)	Moderate WL (0.23 m <WL <0.59 m)
Scenario 3	Moderate Hs (0.95 <Hs <2.10 m)	High WL (WL >0.59 m)

The choice of the threshold value for TWL depends on the objective of the analysis. In the study of Wahl et al. (2016) a threshold based on the 5^{th} percentile of the dune toe elevation was used, aligning with the objective of identifying extreme conditions that potentially induce morphological changes. Figure 8.1 shows the hourly H_s and WL in this study. The conditions that have the potential to influence the dune morphology are indicated in red, as well as combinations with high H_s and low WL in blue. The figure shows that conditions with high H_s do not necessarily lead to changes in dune morphology. Furthermore, the figure shows that when the threshold is defined as the dune toe elevation, it would lead to numerous extreme conditions. Since these conditions need to be simulated by the morphological models, significant computational time would be required. To reduce this time, the threshold value was based on the potential risk of coastal flooding in the study area, which is defined as TWL exceeding the elevation of the hinterland. This threshold resulted in a significant decrease in the number of extreme conditions.

The minimum duration that TWL must exceed the threshold, to be considered a storm, was

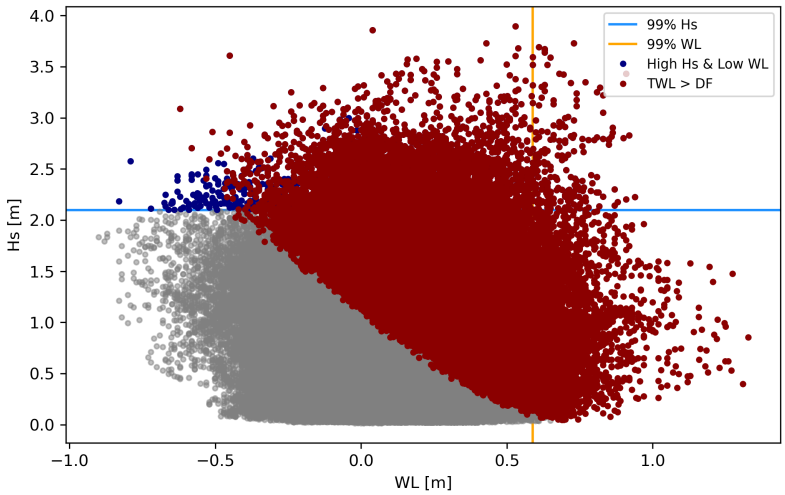

Figure 8.1: *Hourly of H_s and WL corresponding to high H_s and low WL (blue) and conditions where TWL is higher than the dune toe elevation (red).*

not defined. Because the aim was to include all possible extreme conditions in the analysis. The storm duration obtained in this analysis can provide valuable information about the typical storm duration in the study area.

8.2. Estimated Dune Erosion by Morphological Models

Two morphological models were used in this study to estimate the dune erosion due to the selected extreme conditions, including the 1872 storm. The storm impact model is the analytical model described by Larson et al. (2004) and the XBeach model is the process-based model described by Roelvink et al. (2010). The storm impact model was calibrated by setting the transport coefficient C_s to a value of $1.7 * 10^{-4}$, whereas the XBeach model was employed with the Danish calibration parameters and the Holland default parameters. The XBeach model with the Danish calibration estimated dune accretion, while both the storm impact model and the XBeach model with Holland default estimated dune erosion.

The variation between the XBeach model result derived by the Danish calibration and the Holland default was studied through a sensitivity analysis. The analysis revealed that the large deviation in the model results is primarily originating from the variation in the *facua* parameter. The parameter was incorporated into the sediment transport process to account for wave skewness and wave asymmetry. In the Danish calibration, this parameter was increased by factor three, leading to a higher sediment advection velocity. This higher velocity increased the sediment transport, resulting in more sediment being transported to the shore. Hence, the observed dune accretion in the XBeach simulation. The calibration was found in the study of a cliff retreat by Geertsen et al. (2020) for a Danish coastline that is also exposed to the Baltic Sea. Here a clear dune erosion was observed. The dune accretion observed in this study showed that the Danish calibration does not estimate reliable results, therefore these results were excluded from further analysis.

A comparative analysis between the estimated dune erosion by the XBeach model with the Holland default and the storm impact model was conducted. A large deviation was found between the two results in extreme conditions with long storm duration. The longer the duration, the higher the dune erosion estimated by the storm impact model. The longest storm duration corresponds to the 1872 storm, the dune erosion determined with the storm impact model is

approximately twice as high as the dune erosion estimated by the XBeach model. This difference can be explained by the incorporation of the negative feedback mechanism in the XBeach model. During the sediment transportation from the dune by the wave action, the waves gradually lose their energy. As the energy drops, sediment begins to accumulate in front of the dune. This accumulating sediment will further dissipate the wave energy. Hence the negative feedback mechanism. While the general solution of the storm impact model accounts for changes in dune foot elevation during retreat, the simplified solution employed in this study assumes the elevation to be constant. The inclusion of the changing dune foot elevation implies that the negative feedback mechanism can be incorporated into the model. While the integration of this mechanism can increase the model accuracy, it also requires a detailed study to improve the model performance.

In the study of van Wiechen et al. (2023), both morphological models were to predict the post-storm profile of a flume test after 8 h and after 18 h. The results showed that the models are capable of predicting the profile reasonably well. The storm impact model slightly underpredicts the dune erosion, while the XBeach model gives a slight overprediction, for both 8-hour and 18-hour tests. This suggests that when both models are calibrated, these models can provide reliable predictions under various conditions. However, a large difference between the two model results found in this study highlights the importance of validation data. Future studies focusing on the validation processes of these models are therefore needed to improve the model's accuracy and enhance their applicability in the field of coastal management.

8.3. Storm parameter in the Southern Baltic Sea

The highest H_s within the study area typically occurs between October and March. When analysing the dates of the identified extreme conditions, it can be concluded that all events fall within this period. Two extreme conditions within a single year were found but the two conditions were separated by a low H_s-period. There was no evidence found on a consecutive occurrence of extreme conditions, indicating that the likelihood of experiencing two extreme conditions in the same high H_s-period is relatively low. The absence of evidence in the 62-year time series does not provide a guarantee that consecutive events will not occur in the future. Future conditions may differ from historical patterns, due to the changing climate, which can shift the weather patterns and increase the frequency and intensity of extreme conditions (Rutgersson et al., 2022).

The analysis of storm parameters (H_s, T_s, θ, WL, and D) and dune erosion corresponding to the selected extreme conditions, revealed the importance of each storm parameter in dune erosion predicted by the different morphological models. The results of the XBeach model showed that the waves and water levels both can influence dune erosion. High dune erosion was predicted for conditions with high H_s in combination with high WL, high H_s with moderate WL and high WL with moderate H_s. In contrast, the storm impact model predicts high dune erosion only for conditions where the two parameters are high in magnitude simultaneously.

The XBeach model results showed a strong connection between the more shore-normal wave direction and high dune erosion. In contrast, the storm impact model results revealed a weaker connection between these two variables. The connection obtained in the XBeach results aligns with the finding in the study of Oo et al. (2022), which indicated that shore-normal waves produced the highest beach erosion. Regarding T_p, a strong connection between high T_p and high dune erosion was found in the results of the storm impact model. Conversely, the connection is less evident in the results of the XBeach model. The connection obtained from the storm

model results is more consistent with the outcomes of large-scale dune erosion tests conducted by Van Gent et al. (2008). The results from the tests revealed that a longer T_p was associated with a larger dune erosion volume. In both model results, a relationship was found between dune erosion, TWL and storm duration. Storm conditions with higher TWL and storm duration caused larger dune erosion.

The obtained connected between high dune erosion and high TWL in both morphological models is inline with previous studies (Sallenger Jr, 2000; Splinter et al., 2018). This implies that selecting the extreme conditions based on the time series of TWL is an effective approach. The parameter represents the combined influence of waves and water levels, allowing the method to capture different scenarios of extreme condition. Additionally, the parameter incorporates site-specific characteristic through the inclusion of the foreshore slope, which makes the method more applicable to local conditions. The approach provide a more accurate representation of the conditions contributing to dune erosion.

8.4. Dune System as Coastal Protection Measure

The strength of the current dune system in the study area was evaluated by comparing the maximum dune erosion estimated by the morphological models and the available dune volume in all four transects. The fraction, in percentage, of the available dune volume represented by the estimated erosion was determined in each transects. For extreme conditions between the period 1959 and 2022, the maximum dune erosion was found in Transect D. The estimated dune erosion by the XBeach and storm impact model was 7.67% and 32.89%, respectively. The relative low percentage suggests that the dune system is strong enough to withstand the impact of these extreme conditions.

However, this conclusion does not hold when considering the estimated dune erosion resulting from the 1872 storm. The XBeach model estimated fraction of 67.89%, while the storm impact model predicts a fraction exceeding 100% in Transect D. The obtained results implies that in the event of a recurrence of the 1872 storm, a potential dune breach could be expected in this specific transect of the dune system. While the 1872 storm may not be the design storm condition for the current dune system, the results of the storm impact model highlights the need of reevaluation and the formulation of potential plans to reinforce the dune system. This is essential to guarantee the safety of the hinterland against unforeseen extreme events.

9. Conclusion & Recommendation

This thesis aims to assess the historical dune erosion caused by extreme conditions during the period from 1959 to 2022, including the 1872 storm. The goal is to gain insight into the extent to which the current dune system contributes to safeguarding the hinterland against extreme conditions. To achieve this goal, the research was conducted in three parts. The initial step involved defining extreme conditions within the time series. Subsequently, the corresponding dune erosion was determined by two morphological models, the XBeach and the storm impact model. Finally, the estimated dune erosion was analysed together with the available volume in the dune system. The objective of this thesis was accomplished by answering the research questions, in Section 9.1. The recommendations regarding future studies are given in Section 9.2.

9.1. Conclusion

The conclusion of this study can be found by answering the research questions.

RQ1: How to extract scenarios of past storm conditions from historical time series data, considering the complex interactions between waves and water levels?

Given the complex interaction between environmental factors in the study area. There was not a strong dependence between waves and water levels, because the two parameters were not driven by the same meteorological conditions. To address this complexity, the combined effect of waves and water levels was considered in the analysis instead. The combined effect was represented by the parameter total water level (TWL), which was calculated by adding the runup height to the observed water level. To identify extreme conditions within the TWL-time series, the peak over threshold method was applied. The threshold was set at the same height as the elevation of the hinterland, to identify conditions that could potentially cause coastal flooding in the study area.

This method has proven to be highly effective in capturing a comprehensive range of scenarios of extreme condition. In addition, the method is site-specific as the calculation of TWL utilizes the foreshore slope of the dune transect.

RQ2: Which scenario of past storm conditions can potentially impact the dune system on the Falsterbo Peninsula?

Conditions that can potentially induce morphological changes in the dune system are conditions with TWL exceeding the dune toe. Various scenarios were identified when the threshold value was set at the elevation of the dune toe. The analysis showed that scenarios with high H_s (higher than 2.10 m) in combination with low WL (lower than 0.00 m), do not necessarily cause an impact on the dune system.

In the case of extreme conditions, where the threshold was established at the elevation of the hinterland, three different scenarios were identified. The first scenario is characterized by high H_s (higher than 2.10m) and high WL (higher than 0.59 m). The second scenario is when there

is a high H_s and moderate WL (between 0.23 and 0.59 m). And the last scenario involves the combination of moderate H_s (between 0.95 and 2.10 m) and high WL. These scenarios show that extreme conditions can be represented by different combinations of waves and water levels. Therefore, it is crucial to account for their combined effect when studying their impact on the dune system.

RQ3: What methods can be employed to estimate dune erosion volume resulting from the selected storm scenarios?

The dune erosion under selected extreme conditions were estimated by two different morphological models. The XBeach model is the process-based model, which determines the bed level change after each simulation. The dune erosion was determined by comparing the dune volume of pre- and post-simulation. The storm impact model is an analytical model, which calculates the dune erosion rate in m^3/m per hour. The total dune erosion was obtained by aggregating the erosion rate over the total duration of the storm.

The results showed that both models estimated comparable dune erosion for extreme conditions with a short duration. However, for conditions with long storm duration, the storm impact model estimated a higher magnitude of dune erosion. Specifically, for the 1872 storm with the longest storm duration, the storm impact model estimated dune erosion to be approximately twice as high as the XBeach model result.

The analysis of the storm parameters in each conditions and the obtained dune erosion revealed the performance of each morphological model. The XBeach model estimated high dune erosion for difference scenarios of waves and water levels. In contrast, the storm impact model only estimated high dune erosion for conditions when both parameters are simultaneously high in magnitude. Furthermore, a strong connection was found between the more shore-normal wave direction and high dune erosion in the XBeach model results. While in the storm impact model results, a strong connection was obtained between high T_p and high dune erosion. This highlights the different sensitivities of each model to specific storm parameter. Finally, in both model results, a relationship was found between high dune erosion and high TWL, as well as long storm duration.

To what extent does the dune system on the Falsterbo Peninsula contribute to safeguarding the hinterland against the impact of historical storm conditions?

The dune erosion under historical storm conditions spanning from the period 1959 to 2022, including the 1872 storm was estimated by two morphological models. Both models estimated the maximum dune erosion in transect D withing the dune system. For extreme conditions in the period of 1959 and 2022, the XBeach model estimated dune erosion at 7.67% of the total available dune volume, while the storm impact model found a higher percentage of 32.89%. In the study area, high H_s-period typically occurs between October and March. In the analysis, two extreme conditions were identified withing a single year but these conditions were separated by a low H_s-period. This indicates that the probability of experiencing high dune erosion withing the same year is relatively low. Considering the erosion percentage derived from the storm impact model result, it can be concluded that the present dune system has enough buffer of sand volume

to withstand the impact of storm conditions.

However, the results the storm impact model showed that the present dune system is not strong enough to withstand the impact of the 1872 storm. The estimated dune erosion was found more than 100% of the available dune volume in Transect D. This indicated that in the event of recurrence of the 1872 storm, a dune breach could be expected in this specific transect in the dune system. It is noteworthy that the XBeach model estimated a lower dune erosion under the 1872 storm, only 67.89% of erosion was found. In contrast to the storm impact model result, the XBeach model result suggests that there would be no dune breach under the impact of the 1872 storm.

9.2. Recommendation

Total Water Level

Sampling extreme conditions based on the time series of TWL for dune erosion assessment was a value method as this approach considers the cumulative effect of wave and water level, as they can simultaneously influence dune erosion. By representing combining the effect of H_s and WL, the dynamic interactions between the two parameters could be assessed.

According to Sallenger Jr (2000), the potential impact of a storm on a dune is based on whether the height of TWL exceeds the elevation of the dune toe (collision regime) or dune crest (overtopping regime). The study of Splinter et al. (2018) further supports this notion, by showing the area where TWL exceeds the dune toe elevation is linked to the area with dune erosion. Additionally, Sallenger Jr (2000) suggested that the wave runup is an appropriate parameter for dune impact assessment. Therefore, this parameter is widely used to determine TWL, with a common formulation being described by Stockdon et al. (2006). However, in this study, the formulation described by Hedges and Mase (2004) was utilized to calculate TWL. In this formulation $R_{2\%}$ is defined as the runup height of the 2% largest waves. Not to be mistaken by $R_{2\%}$ described by Stockdon et al. (2006), which is defined as a level that is exceeded by only 2% of the runup levels. Despite having the same expression, the values of $R_{2\%}$ can deviate.

The difference between the two $R_{2\%}$ was not explored in this study. The time series of TWL based on $R_{2\%}$ according to Hedges and Mase (2004) may deviate significantly from the one based on $R_{2\%}$ according to Stockdon et al. (2006). For a reliable assessment of the extreme conditions, is advisable to generate a time series of TWL for both runup heights, exploring the potential variations between the two results.

Design Dune Volume

The design dune volume is defined as the volume that should be present in the dune system to provide adequate protection against severe erosion, storm surges and wave impact. In the context of the Falsterbo Peninsula, there was no design dune volume assigned to the current dune system. Future studies in this area should therefore aim to define the appropriate design of dune volume, to ensure a certain level of coastal safety for the entire area situated behind the dune.

The dune volume varies along the dune system in the Falsterbo Peninsula. The lowest dune volume is found in the transect situated at the far-right end of the dune system when facing north. The predicted dune erosion due to the 1872 storm by the morphological models shows that this specific transect is the critical point for potential dune breaches. For better preparedness, it is

recommended that further studies should focus on assessing the potential consequences of dune breaches within the study area. The insights can aid in developing comprehensive strategies to mitigate and respond to such breaches.

Long-term Monitoring of Dune System

The crucial recommendation is to establish a long-term monitoring program for the dune system within the study area. The program should include the regular measurement of the dune's profile, specifically focusing on pre- and post-storm profiles. The collected data can be used in fine-tuning morphological models to enhance the accuracy and reliability of the model results. Additionally, it can aid in the understanding of dune dynamics. Trends and patterns in dune erosion and recovery, obtained from the data, can be utilized in formulating effective measures to protect the hinterland and infrastructure adjacent to the coastline.

Bibliography

Adell, A., Almström, B., Kroon, A., Larson, M., Uvo, C. B., and Hallin, C. (2023). Spatial and temporal wave climate variability along the south coast of sweden during 1959–2021. *Regional Studies in Marine Science*, 63:103011.

Andrews, B., Gares, P. A., and Colby, J. D. (2002). Techniques for gis modeling of coastal dunes. *Geomorphology*, 48(1-3):289–308.

Andrews, D. and McIntyre, M. (1978). An exact theory of nonlinear waves on a lagrangian-mean flow. *Journal of fluid Mechanics*, 89(4):609–646.

Baensch, J. (1875). Die sturmfluth vom 12./13. november 1872 an den ostseeküsten des preußischen staates. *Zeitschrift für Bauwesen*, 25:156–220.

Battjes, J. A. and Janssen, J. (1978). Energy loss and set-up due to breaking of random waves. *Coastal Engineering Proceedings*, (16):32–32.

Birkemeier, W. A. and Savage, R. J. (1988). A collection of storm erosion field data.

Blomgren, S. and Hanson, H. (2000). Coastal geomorphology at the falsterbo peninsula, southern sweden. *Journal of coastal research*, pages 15–25.

Blomgren, S., Larson, M., and Hanson, H. (2001). Numerical modeling of the wave climate in the southern baltic sea. *Journal of coastal research*, pages 342–352.

Bochev-Van der Burgh, L., Wijnberg, K. M., and Hulscher, S. J. (2011). Decadal-scale morphologic variability of managed coastal dunes. *Coastal engineering*, 58(9):927–936.

Bontje, L. E., Fredriksson, C., Wang, Z., and Slinger, J. H. (2016). Coastal erosion and beach nourishment in scania as issues in swedish coastal policy. *VATTEN J. Water Manag. Res*, 72:103–115.

Booij, N., Ris, R. C., and Holthuijsen, L. H. (1999). A third-generation wave model for coastal regions: 1. model description and validation. *Journal of geophysical research: Oceans*, 104(C4):7649–7666.

Bosboom, J. and Stive, M. J. (2021). Coastal dynamics.

Callaghan, D., Nielsen, P., Short, A., and Ranasinghe, R. (2008). Statistical simulation of wave climate and extreme beach erosion. *Coastal Engineering*, 55(5):375–390.

Carter, R. and Stone, G. W. (1989). Mechanisms associated with the erosion of sand dune cliffs, magilligan, northern ireland. *Earth Surface Processes and Landforms*, 14(1):1–10.

Cavaleri, L. and Rizzoli, P. M. (1981). Wind wave prediction in shallow water: Theory and applications. *Journal of Geophysical Research: Oceans*, 86(C11):10961–10973.

Chen, Y., Li, J., Pan, S., Gan, M., Pan, Y., Xie, D., and Clee, S. (2019). Joint probability analysis of extreme wave heights and surges along china's coasts. *Ocean Engineering*, 177:97–107.

Colding, A. (1881). Nogle undersøgelser over stormen over nord-og mellem europa af 12-14 november 1872 of over den served fremkaldte vandflod i Østersøen. *Avec un résumé en français. Videnshkabernes Seldkabs Skrifter, 6. Raekke, naturwiderskabelig of mathematisk Afdeling 1,4, Kopenhagen, 1881.*

Collins, J. I. (1972). Prediction of shallow-water spectra. *Journal of Geophysical Research*, 77(15):2693–2707.

Delft, T. (2022). Swan user manual cycle iii version 41.41. *Delft, Nederlands: Delft University of Technology Faculty of Civil Engineering and Geosciences Environmental Fluid Mechanics Section*.

Duo, E., Sanuy, M., Jiménez, J. A., and Ciavola, P. (2020). How good are symmetric triangular synthetic storms to represent real events for coastal hazard modelling. *Coastal Engineering*, 159:103728.

E, S. (2022). Analysis of waves during the 1872 storm on the south coast of sweden.

Earle, S. (2015). *Physical geology*. BCcampus.

Eldeberky, Y. (1996). Nonlinear transformationations of wave spectra in the nearshore zone. *Unpublished doctoral dissertation, Delft University of Technology, Delft, The Netherlands*.

Fisher, J., Overton, M., and Chisholm, T. (1987). Field measurements of dune erosion. In *Coastal Engineering 1986*, pages 1107–1115.

Fredriksson, C., Tajvidi, N., Hanson, H., and Larson, M. (2016). Statistical analysis of extreme sea water levels at the falsterbo peninsula, south sweden. *Journal of Water Management and Research*, 72:129–142.

Galappatti, R. (1983). A depth integrated model for suspended transport. *Communications on hydraulics, 1983-07*.

Geertsen, K.-S., Knudsen, N. R., and Sorensen, P. (2020). Applying xbeach on 7,300 km coast: Coastal cliff retreat during a storm. *Coastal Engineering Proceedings*, (36v):6–6.

Group, T. W. (1988). The wam model—a third generation ocean wave prediction model. *Journal of Physical Oceanography*, 18(12):1775–1810.

Hallin, C., Alexanderson, H., Larson, M., and Ley, T. J. (2022). Stormfloder-en kunskapsöversikt av metoder för att identifiera och kvantifiera extrema havsvattenstånd.

Hallin, C., Almström, B., Hanson, H., Larson, M., and Persson, O. (2017). Sandbehov för att motverka stranderosion utmed skånes sydkust under perioden 2017–2100.

Hallin, C., Hofstede, J. L., Martinez, G., Jensen, J., Baron, N., Heimann, T., Kroon, A., Arns, A., Almström, B., Sørensen, P., et al. (2021). A comparative study of the effects of the 1872 storm and coastal flood risk management in denmark, germany, and sweden. *Water*, 13(12):1697.

Hallin, C., Tajvidi, N., Almström, B., Larson, M., and Hanson, H. (2019). Extreme value analysis of wave runup and dune erosion at ängelholm beach, south sweden. *Journal of Water Management and Research*.

Hanson, H. and Larson, M. (2008). Implications of extreme waves and water levels in the southern baltic sea. *Journal of Hydraulic Research*, 46(S2):292–302.

Hasselmann, K. (1974). On the spectral dissipation of ocean waves due to white capping. *Boundary-Layer Meteorology*, 6(1):107–127.

Hasselmann, K., Barnett, T. P., Bouws, E., Carlson, H., Cartwright, D. E., Enke, K., Ewing, J., Gienapp, A., Hasselmann, D., Kruseman, P., et al. (1973). Measurements of wind-wave growth and swell decay during the joint north sea wave project (jonswap). *Ergaenzungsheft zur Deutschen Hydrographischen Zeitschrift, Reihe A*.

Hasselmann, K. and Collins, J. (1968). Spectral dissipation of finite-depth gravity waves due to turbulent bottom friction. *Journal of Marine Research*, 26:1–12.

Hasselmann, S., Hasselmann, K., Allender, J., and Barnett, T. (1985). Computations and parameterizations of the nonlinear energy transfer in a gravity-wave specturm. part ii: Parameterizations of the nonlinear energy transfer for application in wave models. *Journal of Physical Oceanography*, 15(11):1378–1391.

Hedges, T. and Mase, H. (2004). Modified hunt's equation incorporating wave setup. *Journal of waterway, port, coastal, and ocean engineering*, 130(3):109–113.

Hesp, P. A. and Smyth, T. A. (2016). Surfzone-beach-dune interactions: Flow and sediment transport across the intertidal beach and backshore. *Journal of Coastal Research*, (75):8–12.

Holman, R. A. and Sallenger Jr, A. (1985). Setup and swash on a natural beach. *Journal of Geophysical Research: Oceans*, 90(C1):945–953.

Holthuijsen, L. H. (2010). *Waves in oceanic and coastal waters*. Cambridge university press.

Hünicke, B., Zorita, E., Soomere, T., Madsen, K. S., Johansson, M., and Suursaar, Ü. (2015). Recent change—sea level and wind waves. *Second assessment of climate change for the Baltic Sea basin*, pages 155–185.

Hunt Jr, I. A. (1959). Design of seawalls and breakwaters. *Journal of the waterways and harbors division*, 85(3):123–152.

Hwang, P. A. (2006). Duration-and fetch-limited growth functions of wind-generated waves parameterized with three different scaling wind velocities. *Journal of Geophysical Research: Oceans*, 111(C2).

Irminger-Street, S. (2018). Bilaga b teknisk beskrivning. bilaga till tillståndsansökan om översvämningsskydd på falsterbonäset. mälmo, sweden.

Jensen, J. and Müller-Navarra, S. H. (2008). Storm surges on the german coast. *Die Küste, 74 ICCE*, (74):92–124.

Kamphuis, J. (1991). Incipient wave breaking. *Coastal Engineering*, 15(3):185–203.

Kantamaneni, K., Rice, L., Du, X., Allali, B., and Yenneti, K. (2022). Are current uk coastal defences good enough for tomorrow? an assessment of vulnerability to coastal erosion. *Coastal Management*, 50(2):142–159.

Kok, S., Vreugdenhil, H., IJff, S., and Sørensen, P. (2020). Scaling up building with nature along the danish coast–the socio-economic rationale. *Interreg North Sea Region/Deltares/Milje og Fødevare Ministeriet*.

Komen, G., Hasselmann, S., and Hasselmann, K. (1984). On the existence of a fully developed wind-sea spectrum. *Journal of physical oceanography*, 14(8):1271–1285.

Lantmäteriet (2023). Our responsibility and mission. Accessed on September 12, 2023.

Larson, M. (2005). *Numerical Modeling*, pages 730–733. Springer Netherlands, Dordrecht.

Larson, M., Erikson, L., and Hanson, H. (2004). An analytical model to predict dune erosion due to wave impact. *Coastal engineering*, 51(8-9):675–696.

Larson, M., Hoan, L. X., and Hanson, H. (2010). Direct formula to compute wave height and angle at incipient breaking. *Journal of waterway, port, coastal, and ocean engineering*, 136(2):119–122.

Leick, A., Rapoport, L., and Tatarnikov, D. (2015). *GPS satellite surveying*. John Wiley & Sons.

Lerma, J. L. (2002). Fotogrametría moderna: analítica y digital. *Universidad politécnica de valencia*, page 449.

Levin, N. and Ben-Dor, E. (2004). Monitoring sand dune stabilization along the coastal dunes of ashdod-nizanim, israel, 1945–1999. *Journal of arid Environments*, 58(3):335–355.

Longo, S. (2012). Wind-generated water waves in a wind tunnel: Free surface statistics, wind friction and mean air flow properties. *Coastal Engineering*, 61:27–41.

Longuet-Higgins, M. S. and Stewart, R. (1964). Radiation stresses in water waves; a physical discussion, with applications. In *Deep sea research and oceanographic abstracts*, volume 11, pages 529–562. Elsevier.

Luo, W. and Monbaliu, J. (1994). Effects of the bottom friction formulation on the energy balance for gravity waves in shallow water. *Journal of Geophysical Research: Oceans*, 99(C9):18501–18511.

MacDonald, C. (2019). Modelling seafloor activity for change detection optimization. `https://cradpdf.drdc-rddc.gc.ca/PDFS/unc335/p809858_A1b.pdf`.

Madsen, O. S., Poon, Y.-K., and Graber, H. C. (1988). Spectral wave attenuation by bottom friction: Theory. *Coastal Engineering Proceedings*, (21):34–34.

McCarthy, J. J., Canziani, O. F., Leary, N. A., Dokken, D. J., White, K. S., et al. (2001). *Climate change 2001: impacts, adaptation, and vulnerability: contribution of Working Group II to the third assessment report of the Intergovernmental Panel on Climate Change*, volume 2. Cambridge University Press.

Mehrtens, B., Lojek, O., Kosmalla, V., Bölker, T., and Goseberg, N. (2023). Foredune growth and storm surge protection potential at the eiderstedt peninsula, germany. *Frontiers in Marine Science*, 9:1020351.

Miche, M. (1944). Mouvements ondulatoires de la mer en profondeur constante ou décroissante. *Annales de Ponts et Chaussées, 1944, pp (1) 26-78,(2) 270-292,(3) 369-406*.

Miles, J. W. (1957). On the generation of surface waves by shear flows. *Journal of Fluid Mechanics*, 3(2):185–204.

Mirza, M. M. Q. (2003). Climate change and extreme weather events: can developing countries adapt? *Climate policy*, 3(3):233–248.

Municipality, V. (2023). Skydd mot höga havsnivåer.

Nielsen, H. S., Hansen, J. A., and Juhl, M. B. (2015). Udredning om tilpasning til havvandsstigninger [study of sea level rise adaptation]. Rambøll, Realdania.

on Climate, S. C. and Vulnerability (2007). Sweden facing climate change–threats and opportunities.

Oo, Y. H., Da Silva, G. V., Zhang, H., Strauss, D., and Tomlinson, R. (2022). Estimation of beach erosion using joint probability analysis with a morphological model. *Ocean Engineering*, 264:112560.

Overton, M., Fisher, J., and Fenaish, T. (1987). Numerical analysis of swash forces on dunes. In *Coastal Sediments*, pages 632–641. ASCE.

Phillips, O. M. (1957). On the generation of waves by turbulent wind. *Journal of fluid mechanics*, 2(5):417–445.

Phillips, O. M. (1958). The equilibrium range in the spectrum of wind-generated waves. *Journal of Fluid Mechanics*, 4(4):426–434.

Pierson Jr, W. J. and Moskowitz, L. (1964). A proposed spectral form for fully developed wind seas based on the similarity theory of sa kitaigorodskii. *Journal of geophysical research*, 69(24):5181–5190.

Pörtner, H.-O., Roberts, D. C., Poloczanska, E. S., Mintenbeck, K., Tignor, M., Alegría, A., Craig, M., Langsdorf, S., Löschke, S., Möller, V., et al. (2022). Ipcc, 2022: Summary for policymakers.

Roelvink, D., Reniers, A., Van Dongeren, A., De Vries, J. V. T., McCall, R., and Lescinski, J. (2009). Modelling storm impacts on beaches, dunes and barrier islands. *Coastal engineering*, 56(11-12):1133–1152.

Roelvink, D., Reniers, A., Van Dongeren, A., Van Thiel de Vries, J., Lescinski, J., and McCall, R. (2010). Xbeach model description and manual. *Unesco-IHE Institute for Water Education, Deltares and Delft University of Tecnhology. Report June*, 21:2010.

Roelvink, J. (1993). Dissipation in random wave groups incident on a beach. *Coastal Engineering*, 19(1-2):127–150.

Rosenhagen, G. and Bork, I. (2009). Rekonstruktion der sturmwetterlage vom 13. november 1872. *Die Küste, 75 MUSTOK*, (75):51–70.

Ruggiero, P., Komar, P. D., McDougal, W. G., Marra, J. J., and Beach, R. A. (2001). Wave runup, extreme water levels and the erosion of properties backing beaches. *Journal of coastal research*, pages 407–419.

Rutgersson, A., Kjellström, E., Haapala, J., Stendel, M., Danilovich, I., Drews, M., Jylhä, K., Kujala, P., Larsén, X. G., Halsnæs, K., et al. (2022). Natural hazards and extreme events in the baltic sea region. *Earth System Dynamics*, 13(1):251–301.

Sallenger Jr, A. H. (2000). Storm impact scale for barrier islands. *Journal of coastal research*, pages 890–895.

Sanjaume, E. and Pardo, J. (1991). Dune regeneration on a previously destroyed dune field, devesa del saler, valencia, spain. *Zeitschrift für Gepmorfologie*, 81:125–134.

Serafin, K. A. and Ruggiero, P. (2014). Simulating extreme total water levels using a time-dependent, extreme value approach. *Journal of Geophysical Research: Oceans*, 119(9):6305–6329.

Skaggs, L. L. and McDonald, F. L. (1991). *National Economic Development Procedures Manual: Coastal Storm Damage and Erosion*. US Army Corps of Engineers, Water Resources Support Center, Institute for ….

Smith, A., Houser, C., Lehner, J., George, E., and Lunardi, B. (2020). Crowd-sourced identification of the beach-dune interface. *Geomorphology*, 367:107321.

Soomere, T. (2023). Numerical simulations of wave climate in the baltic sea: A review. *Oceanologia*, 65(1):117–140.

Soulsby, R. (1997). Dynamics of marine sands thomas telford publications. *London, UK*.

Splinter, K. D., Kearney, E. T., and Turner, I. L. (2018). Drivers of alongshore variable dune erosion during a storm event: Observations and modelling. *Coastal Engineering*, 131:31–41.

Stelling, G. S. and Duinmeijer, S. A. (2003). A staggered conservative scheme for every froude number in rapidly varied shallow water flows. *International journal for numerical methods in fluids*, 43(12):1329–1354.

Stockdon, H. F., Holman, R. A., Howd, P. A., and Sallenger Jr, A. H. (2006). Empirical parameterization of setup, swash, and runup. *Coastal engineering*, 53(7):573–588.

Strypsteen, G., Dan, S., Verwaest, T., Roest, B., De Wulf, A., Bonte, D., and Rauwoens, P. (2023). Dune toe dynamics along the urbanised macro-tidal coast of belgium. *Earth Surface Processes and Landforms*, 48(13):2433–2445.

USACE (2008). Coastal engineering manual (cem), volume 1100.

Van Dongeren, A. and Svendsen, I. A. (1996). An absorbing-generating boundary condition for shallow water models. Technical report, DELAWARE UNIV NEWARK CENTER FOR APPLIED COASTAL RESEARCH.

Van Gent, M., de Vries, J. v. T., Coeveld, E., De Vroeg, J., and Van de Graaff, J. (2008). Large-scale dune erosion tests to study the influence of wave periods. *Coastal Engineering*, 55(12):1041–1051.

van IJzendoorn, C. O., de Vries, S., Hallin, C., and Hesp, P. A. (2021). Sea level rise outpaced by vertical dune toe translation on prograding coasts. *Scientific reports*, 11(1):12792.

Van Koningsveld, M., Otten, C., and Mulder, J. (2007). Dunes: the netherlands soft but secure sea defences. In *Proceedings 18th World dredging congress, Florida USA, WODA*.

van Wiechen, P., de Vries, S., Reniers, A., and Aarninkhof, S. (2023). Dune erosion during storm surges: A review of the observations, physics and modelling of the collision regime. *Coastal Engineering*, page 104383.

Wahl, T., Plant, N. G., and Long, J. W. (2016). Probabilistic assessment of erosion and flooding risk in the northern gulf of mexico. *Journal of Geophysical Research: Oceans*, 121(5):3029–3043.

Walker, R. A. and Basco, D. R. (2011). Application of coastal storm impulse (cosi) parameter to predict coastal erosion. *Coastal Engineering Proceedings*, (32):23–23.

Walstra, D., Roelvink, J., and Groeneweg, J. (2001). Calculation of wave-driven currents in a 3d mean flow model. In *Coastal Engineering 2000*, pages 1050–1063.

Weber, S. (1991). Eddy-viscosity and drag-law models for random ocean wave dissipation. *Journal of Fluid Mechanics*, 232:73–98.

Wernette, P., Thompson, S., Eyler, R., Taylor, H., Taube, C., Medlin, A., Decuir, C., and Houser, C. (2018). Defining dunes: Evaluating how dune feature definitions affect dune interpretations from remote sensing. *Journal of Coastal Research*, 34(6):1460–1470.

Wolski, T. and Wiśniewski, B. (2021). Characteristics and long-term variability of occurrences of storm surges in the baltic sea. *Atmosphere*, 12(12):1679.

Woolard, J. W. and Colby, J. D. (2002). Spatial characterization, resolution, and volumetric change of coastal dunes using airborne lidar: Cape hatteras, north carolina. *Geomorphology*, 48(1-3):269–287.

Wu, S.-Y., Yarnal, B., and Fisher, A. (2002). Vulnerability of coastal communities to sea-level rise: a case study of cape may county, new jersey, usa. *Climate research*, 22(3):255–270.

A. Elevation Of Hinterland

The elevation of the hinterland was determined in 23 transects, in Figure A.1, within the dune system. The cross-shore profile of the transects was taken from the topography data. The elevation was defined as the height of the land situated just behind the dune system. The average elevation from the 23 transects was calculated to be 1.97 m. Figure A.2 shows the elevation of the hinterland in the transects has similar value, this indicate that the area behind the dune system is homogeneous.

Figure A.1: *Location of different transects within the dune system.*

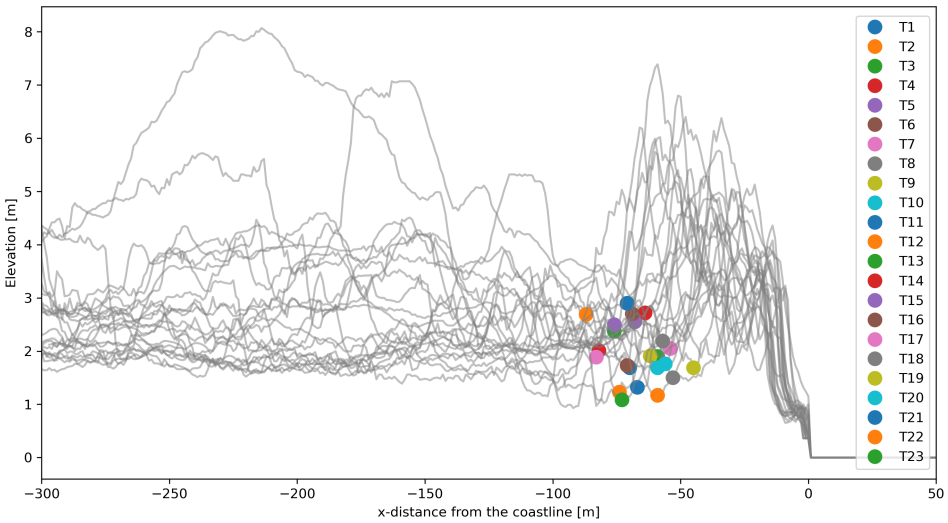

Figure A.2: *Cross-shore profile of the different transects within the dune system. The scatter points indicate the height of the hinterland in each transect.*

B. Measured Dune Profile

The measured profile of the various transects, indicated in Figure B.1, are presented in this appendix. The red line in Figure B.2 B.3, B.4 and B.5 indicates the measured data during the fieldwork in November 2023. The dashed grey line represents the dune profile obtained from the topography data and the solid grey line is the bathymetry profile.

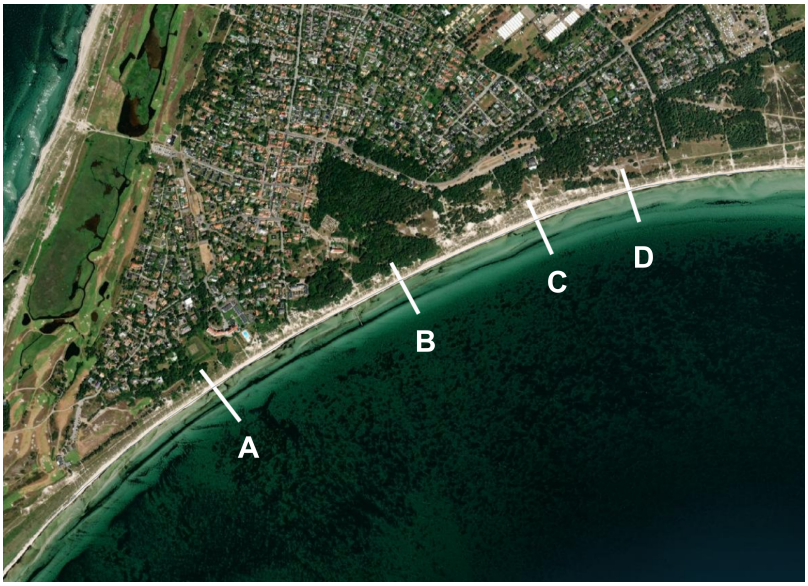

Figure B.1: *Location of transect A, B, C and D in the dune system.*

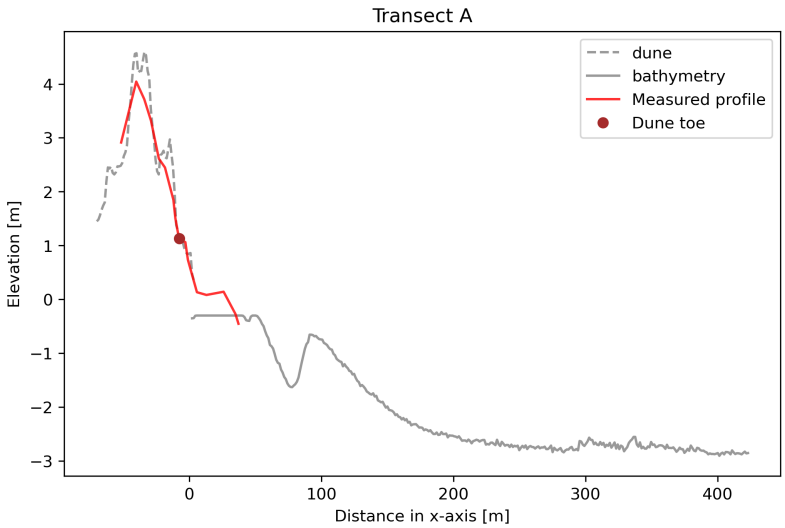

Figure B.2: *The cross-shore profile of Transect A.*

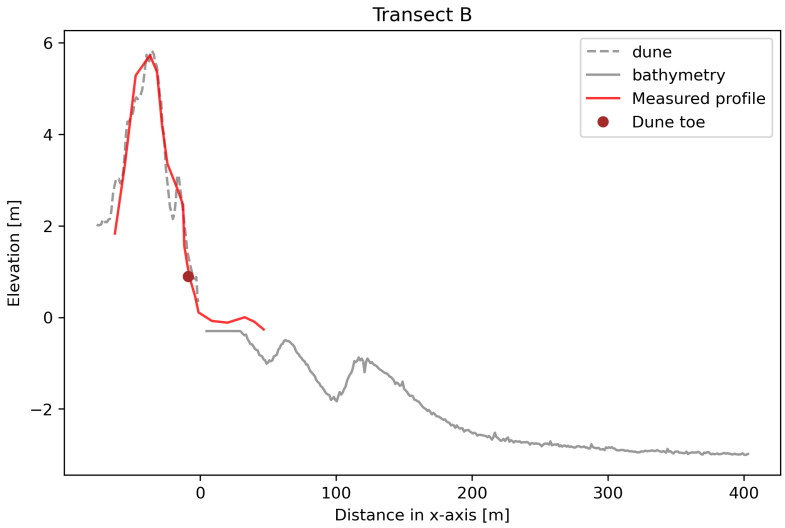

Figure B.3: *The cross-shore profile of Transect B.*

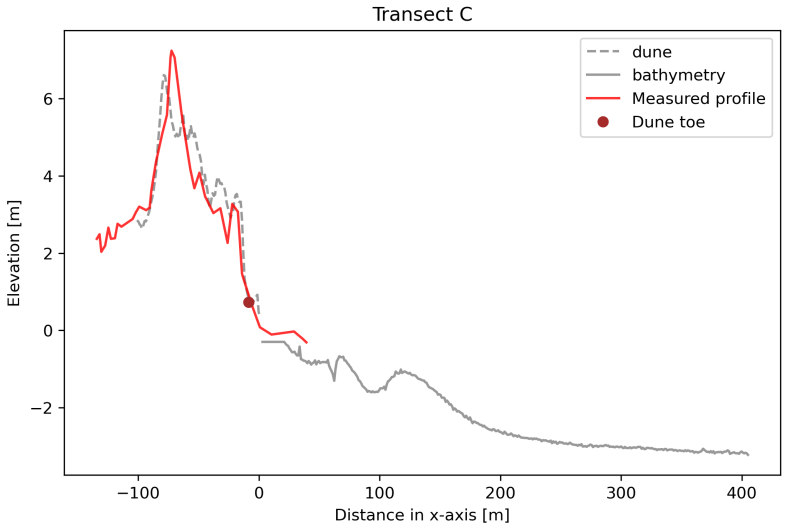

Figure B.4: *The cross-shore profile of Transect C.*

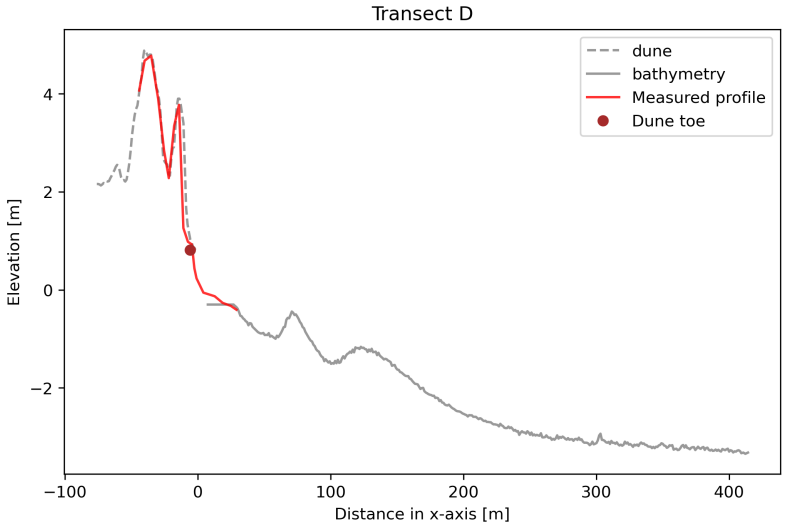

Figure B.5: *The cross-shore profile of Transect D.*

C. SWAN Model

The SWAN model was run using the SWAN script in Figure C.1. Detailed description of the script can be found in the SWAN manual (Delft, 2022). The calibration parameters used in this study was obtained in the study of Adell et al. (2023). The three-hourly wave data in this study was validated in different locations along the Swedish coast, shown in Figure C.2. The correlation value (R^2) for H_s found in the south coast of Sweden ranges from 0.83 to 0.90. For the parameter T_p and wave direction, a lower correlation value were found.

C.1. SWAN Script

```
$************************HEADING************************
$
PROJ 'SWAN_9697' '001'
$
$
$*********************MODEL INPUT*************************
SET MAXERR 2 cdcap=2.5e-3
COORD SPHERICAL

$*** Grid and Bottom
$CGRID UNSTRUC CIRCLE [mdc] [flow] [fhigh] [msc]
CGRID UNSTRUC CIRCLE 36 0.03 1
READGRID UNSTRUC ADC

$*** Wind
$INP WI REG [xpinp] [ypinp] [alpinp] [mxinp] [myinp] [dxinp] [dyinp]
INPGRID WIND REG 2.5 53 0 118 36 0.25 0.25 NONSTAT 19960620.000000 1 HR
READ WIND 1 'swan_wind_9697.dat' 1 1 1 1 FREE

$*** Constant 10 m/s South wind (cartesian angles by default)
$WIND 25 90

$****************BOUNDARY CONDITIONS*********************
$**********************PHYSICS***************************
$*** Third generation mode
GEN3 KOMEN AGROW
WCAP KOMEN cds2=1.1e-5
$*** Activates dissipation by depth-induced wave breaking
BREAKING
$*** Activates dissipation by bottom friction
FRICTION
$*** Activates three wave-wave interactions
TRIADS6
$**********************NUMERICS**************************
$**********************OUTPUT****************************
$POINTS 'points' FILE 'SMHI.txt'
$TABLE 'points' HEAD 'SWAN_SMHI.tab' TIME XP YP DEP WIND HS TPS DIR OUT 19690620.0000 1 HR

POINTS 'WD' FILE 'WaveDroid.txt'
TABLE 'WD' HEAD 'SWAN_WD_test.tab' TIME XP YP DEP WIND HS TPS DIR OUT 19960620.000000 1 HR

$TEST 100

BLOCK 'COMPGRID' NOHEAD 'SWAN_9697.nc' LAY 1 XP YP BOTLEV WIND HS TPS PDIR DIR OUT 19960620.000000 1 HR

COMPUTE NONST 19960620.000000 10 MIN 19970701.000000

STOP
```

Figure C.1: *SWAN script used in this thesis.*

C.2. SWAN Validation

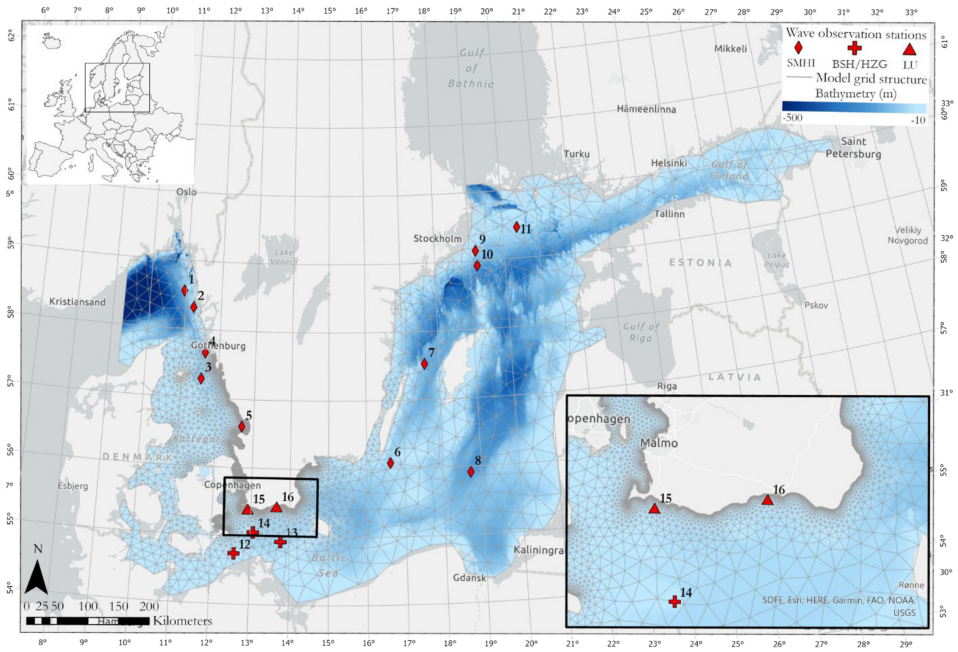

Figure C.2: *The map showing the locations of wave stations in Sweden. Figure by Adell et al. (2023).*

Nr.	Station name	Validation period	Operator	Parameter	R^2	RMSE
1	Väderöarna WR	July 2009–Dec 2021	SMHI	H_s (m)	0.83	0.36
2	Brofjorden WR	Feb 2017–Dec 2021	SMHI	H_s (m)	0.83	0.33
3	Läsö-Ost	May 2001–Feb 2009	SMHI	H_s (m)	0.75	0.25
4	Trubaduren	Oct 1978–Oct 2003	SMHI	H_s (m)	0.71	0.29
5	Laholmsbukten	Mar 1984–Oct 1985	SMHI	H_s (m)	0.88	0.17
6	Ölands S grund	Oct 1978–Mar 2004	SMHI	H_s (m)	0.83	0.29
7	Knolls grund	Nov 2011–Dec 2021	SMHI	H_s (m)	0.84	0.26
8	Södra Östersjön	July 2009–Apr 2011	SMHI	H_s (m)	0.93	0.24
9	Almagrundet	Oct 1978–Sept 2003	SMHI	H_s (m)	0.58	0.49
10	Huvudskär Ost	May 2001–June 2005 July 2009–Dec 2021	SMHI	H_s (m)	0.87	0.23
11	Svenska Björn	Nov 1982–Nov 1986	SMHI	H_s (m)	0.85	0.30
12	Darsser Sill	Feb 1991–June 2005 July 2009–May 2020	HZG	H_s (m)	0.83	0.20
13	Arkona	June 2013–Dec 2021	BSH	H_s (m)	0.89	0.21
14	FINO2 platform	May 2011–Sept 2020	BSH	H_s (m)	0.88	0.21
15	Kämpinge	Nov 2020–Apr 2021	LU	H_s (m)	0.86	0.18
				T_p (s)	0.48	0.93
				θ (deg.) 0.74	26.7	
16	Ystad	Nov 2020–May 2021	LU	H_s(m)	0.90	0.16
				T_p (s)	0.57	0.93
				θ (deg.)	0.61	25.0

Figure C.3: *Wave observation used for the SWAN model validation, in various stations in Sweden. Location of each station are indicated by numbers in Figure C.2. Figure by Adell et al. (2023).*

D. Xbeach Model Script

The XBeach model was employed in this study using the Holland default and the Danish calibration parameters. The model script with the Holland default parameters can be found in Figure D.1, while Figure D.2 represents the script for the Danish calibration.

```
%%%%%%%%%%%%%%%%%%%%%%%%%%%%%%%%%%%%%%%%%%%%%%%%%%%%%%%%%%%%%%%%%%%%%%%%%%%%%%%%
%%% XBeach parameter settings input file                                     %%%
%%%                                                                          %%%
%%% date:     11-May-2023 11:23:30                                           %%%
%%% function: xb_write_params                                                %%%
%%%%%%%%%%%%%%%%%%%%%%%%%%%%%%%%%%%%%%%%%%%%%%%%%%%%%%%%%%%%%%%%%%%%%%%%%%%%%%%%

%%% Bed composition parameters %%%%%%%%%%%%%%%%%%%%%%%%%%%%%%%%%%%%%%%%%%%%%%%%%

D50 = 0.00013

%%% Grid parameters %%%%%%%%%%%%%%%%%%%%%%%%%%%%%%%%%%%%%%%%%%%%%%%%%%%%%%%%%%%%

depfile      = bed.dep
posdwn       = -1
nx           = 2025
ny           = 0
alfa         = 0
vardx        = 1
thetamin     = 90
thetamax     =-90
dtheta       = 20
thetanaut    = 1
xfile       = x.grd
yfile        = y.grd
xori         = 0
yori         = 0

%%% Model time %%%%%%%%%%%%%%%%%%%%%%%%%%%%%%%%%%%%%%%%%%%%%%%%%%%%%%%%%%%%%%%%%

tstop        = 165600


%%% Tide boundary conditions %%%%%%%%%%%%%%%%%%%%%%%%%%%%%%%%%%%%%%%%%%%%%%%%%%%

zs0file      = tide.txt
tideloc      = 1

%%% Wave boundary condition parameters %%%%%%%%%%%%%%%%%%%%%%%%%%%%%%%%%%%%%%%%%

instat       = jons_table


%%% Wave-spectrum boundary condition parameters %%%%%%%%%%%%%%%%%%%%%%%%%%%%%%%%

bcfile        = jonswap_table.txt

%%% Wind input %%%%%%%%%%%%%%%%%%%%%%%%%%%%%%%%%%%%%%%%%%%%%%%%%%%%%%%%%%%%%%%%%%%%%%%

windfile         = wind.txt

%%% Output variables %%%%%%%%%%%%%%%%%%%%%%%%%%%%%%%%%%%%%%%%%%%%%%%%%%%%%%%%%%%

outputformat = netcdf
tintg        = 3600
tstart       = 0

nglobalvar   = 4
zb
zs
H
Hrunup
```

Figure D.1: *XBeach script with the Holland default parameters.*

```
%%%%%%%%%%%%%%%%%%%%%%%%%%%%%%%%%%%%%%%%%%%%%%%%%%%%%%%%%%%%%%%%%%%%%%%%%%%%%%%%
%%% XBeach parameter settings input file                                        %%%
%%%                                                                             %%%
%%% date:     11-May-2023 11:23:30                                              %%%
%%% function: xb_write_params                                                   %%%
%%%%%%%%%%%%%%%%%%%%%%%%%%%%%%%%%%%%%%%%%%%%%%%%%%%%%%%%%%%%%%%%%%%%%%%%%%%%%%%%

%%% Bed composition parameters %%%%%%%%%%%%%%%%%%%%%%%%%%%%%%%%%%%%%%%%%%%%%%%%%%

D50 = 0.00013

%%% Grid parameters %%%%%%%%%%%%%%%%%%%%%%%%%%%%%%%%%%%%%%%%%%%%%%%%%%%%%%%%%%%%
depfile      = bed.dep
posdwn       = -1
nx           = 2025
ny           = 0
alfa         = 0
vardx        = 1
thetamin     = 180
thetamax     = 360
dtheta       = 20
thetanaut    = 1
xfile       = x.grd
yfile        = y.grd
xori         = 0
yori         = 0

%%% Model time %%%%%%%%%%%%%%%%%%%%%%%%%%%%%%%%%%%%%%%%%%%%%%%%%%%%%%%%%%%%%%%%%

tstop        = 165600
maxdtfac     = 200

%%% Morphology parameters %%%%%%%%%%%%%%%%%%%%%%%%%%%%%%%%%%%%%%%%%%%%%%%%%%%%%%

morfac       = 5
morstart     = 100
dryslp       = 0.800000

%%% Sediment transport parameters %%%%%%%%%%%%%%%%%%%%%%%%%%%%%%%%%%%%%%%%%%%%%%

facua        = 0.300000

%%% Tide boundary conditions %%%%%%%%%%%%%%%%%%%%%%%%%%%%%%%%%%%%%%%%%%%%%%%%%%%

zs0file      = tide.txt
tideloc      = 1

%%% Wave boundary condition parameters %%%%%%%%%%%%%%%%%%%%%%%%%%%%%%%%%%%%%%%%%%

instat       = jons_table

%%% Wave breaking parameters %%%%%%%%%%%%%%%%%%%%%%%%%%%%%%%%%%%%%%%%%%%%%%%%%%%

gamma         = 0.550000

%%% Wave-spectrum boundary condition parameters %%%%%%%%%%%%%%%%%%%%%%%%%%%%%%%%%

bcfile        = jonswap_table.txt

%%% Wind input %%%%%%%%%%%%%%%%%%%%%%%%%%%%%%%%%%%%%%%%%%%%%%%%%%%%%%%%%%%%%%%%%

windfile         = wind.txt

%%% Output variables %%%%%%%%%%%%%%%%%%%%%%%%%%%%%%%%%%%%%%%%%%%%%%%%%%%%%%%%%%%

outputformat = netcdf
tintg        = 3600
tstart       = 0

nglobalvar   = 4
zb
zs
H
Hrunup
```

Figure D.2: *Xbeach script with the Danish calibration parameters.*

E. Total Water Level

The total water level represents the combined effect of the waves and water levels and can be calculated according to Equation E.1. The effect of waves is add up to the water level (WL) through the runup height ($R2\%$). The time series of TWL was constructed using the simulated time series of the H_S to calculate $R2\%$, consequently adding to the time series of WL. The time series of TWL in various transects together with the time series of $R2\%$ and WL are shown in the figures below.

$$TWL = WL + R_{2\%} \tag{E.1}$$

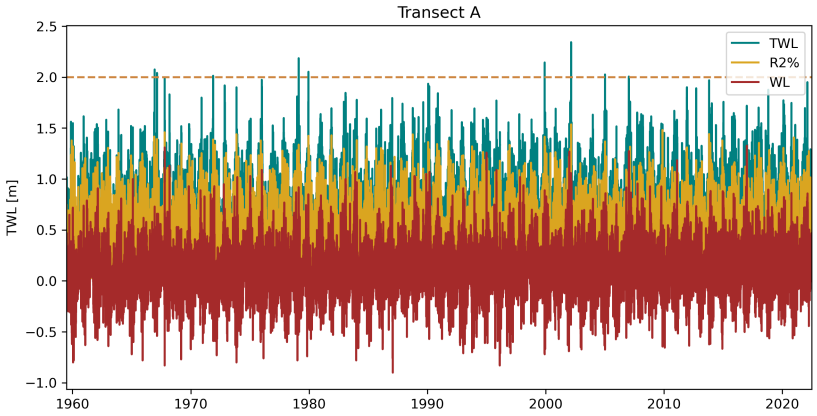

Figure E.1: *Time series of TWL, $R2\%$ and WL in Transect A.*

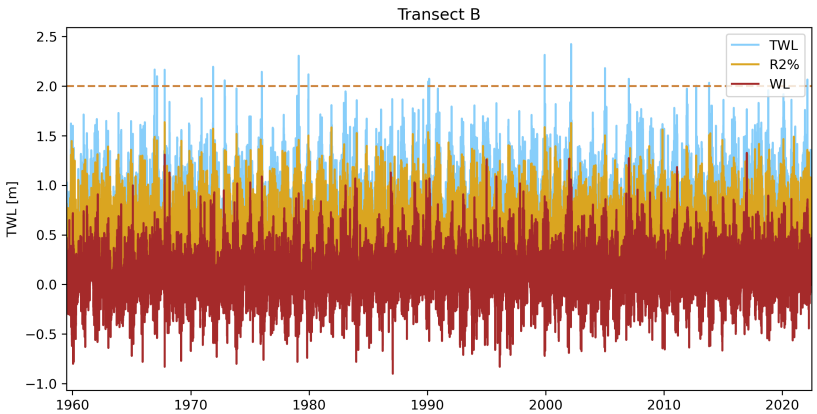

Figure E.2: *Time series of TWL, $R2\%$ and WL in Transect B.*

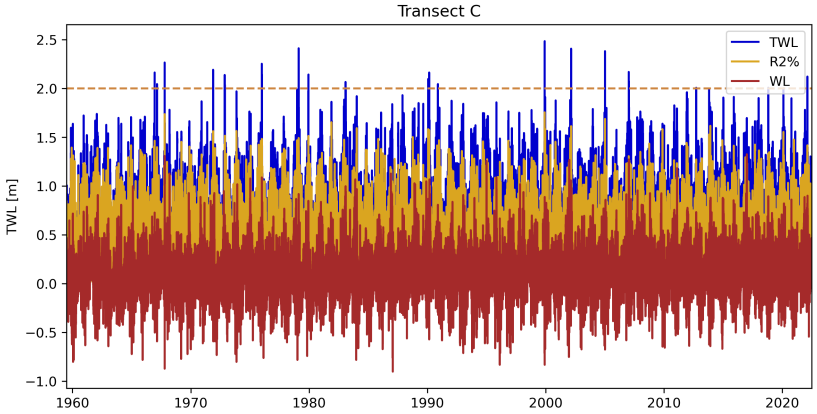

Figure E.3: *Time series of TWL, $R2\%$ and WL in Transect C.*

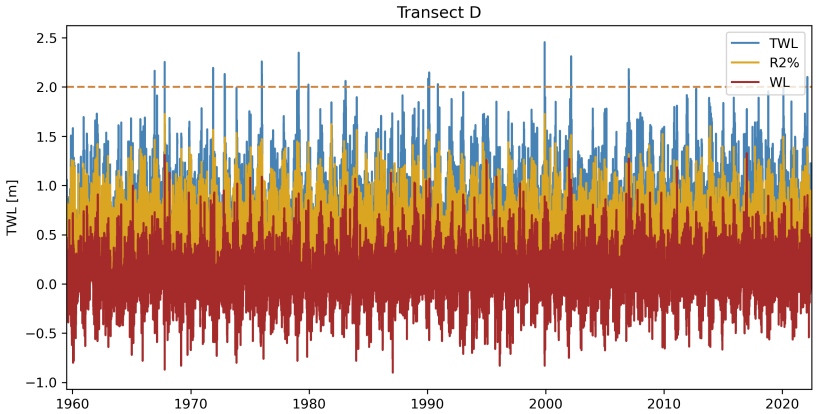

Figure E.4: *Time series of TWL, $R2\%$ and WL in Transect D.*

F. Extreme Event Parameters

Extreme conditions were defined based on the time series of TWL in each transects. For each conditions, storm parameters with the same timestamp as the peak of the TWL were extracted from the time series. The obtained results are shown in the figures below. Highest number of extreme conditions were identified in Transect C, while the smallest number of conditions were obtained in Transect A.

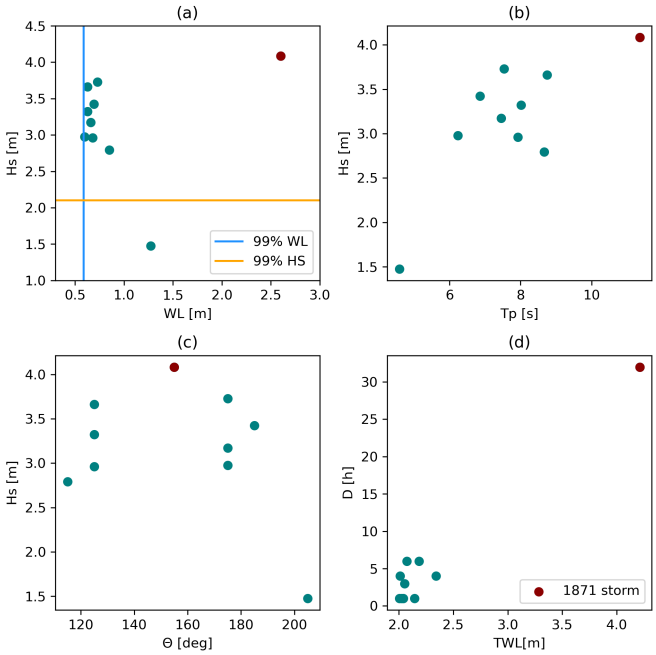

Figure F.1: *Parameters corresponding to extreme events in Transect A.*

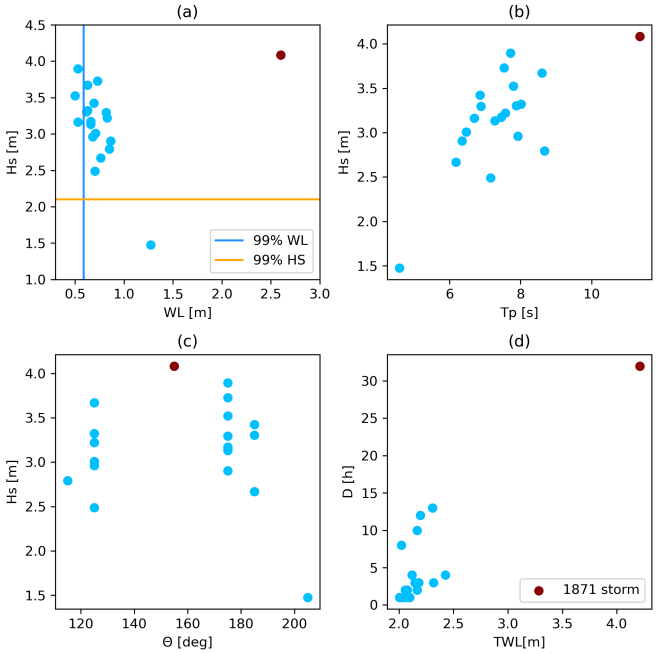

Figure F.2: *Parameters corresponding to extreme events in Transect B.*

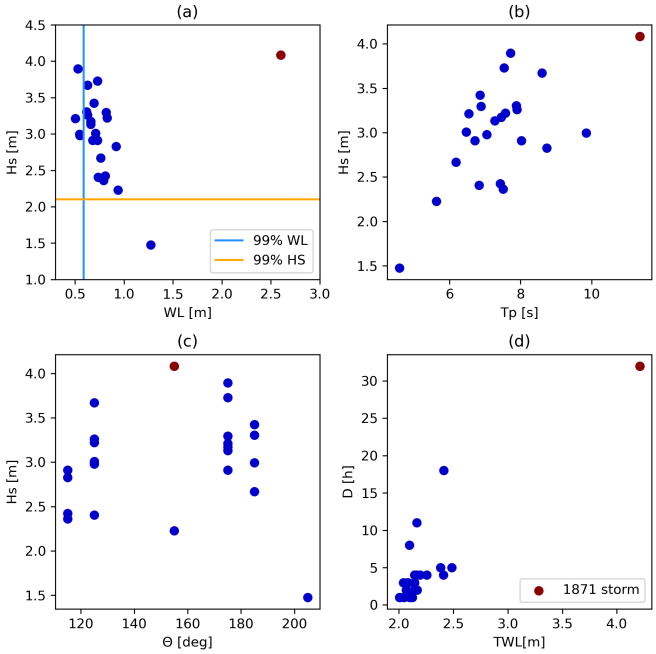

Figure F.3: *Parameters corresponding to extreme events in Transect C.*

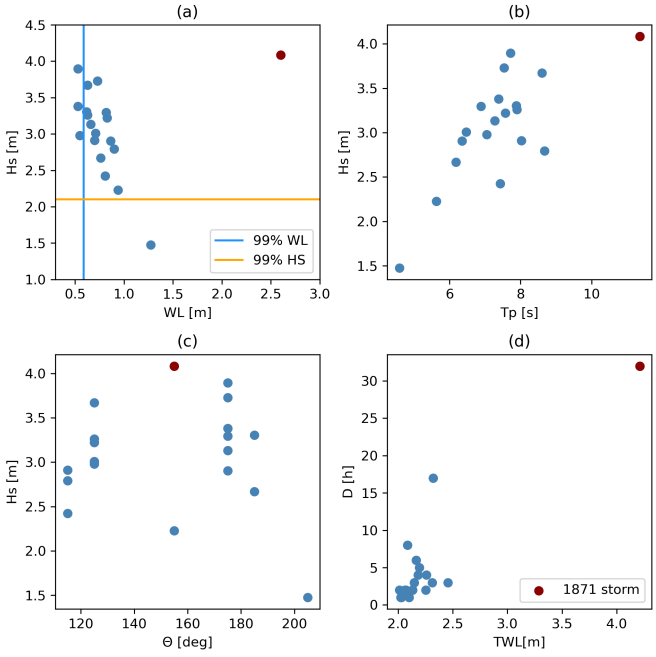

Figure F.4: *Parameters corresponding to extreme events in Transect D.*

G. 1872 Storm Dune Erosion

The 1872 storm is simulated in the XBeach model. The bed level change was determined using the Danish calibration and the Holland default parameters. The bed level change in various transects are shown in the figures below. More erosion was observed in the model result simulated by the Holland default parameters.

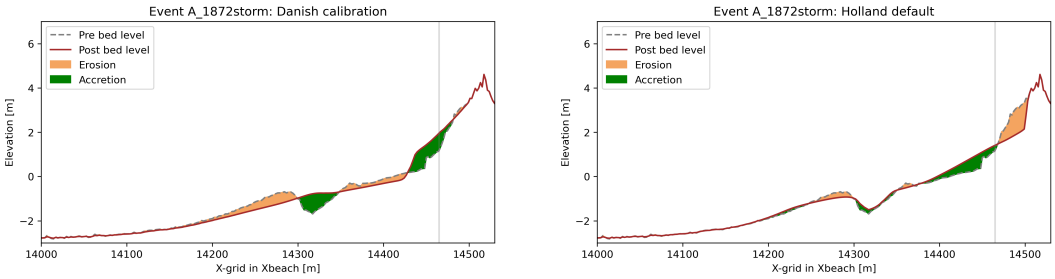

(a) *Danish calibration* **(b)** *Holland default*

Figure G.1: *Bed level change by the XBeach model due to the Danish calibration and Holland default in Transect A.*

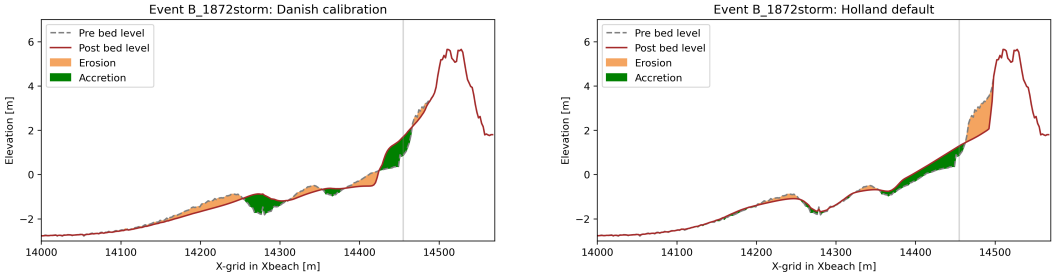

(a) *Danish calibration* **(b)** *Holland default*

Figure G.2: *Bed level change by the XBeach model due to the Danish calibration and Holland default in Transect B.*

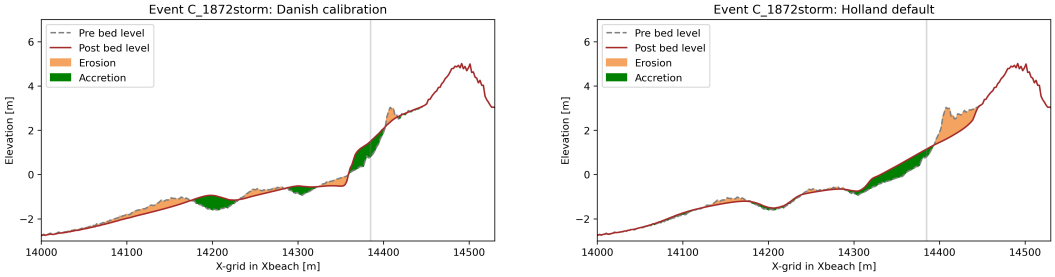

(a) *Danish calibration* **(b)** *Holland default*

Figure G.3: *Bed level change by the XBeach model due to the Danish calibration and Holland default in Transect C.*

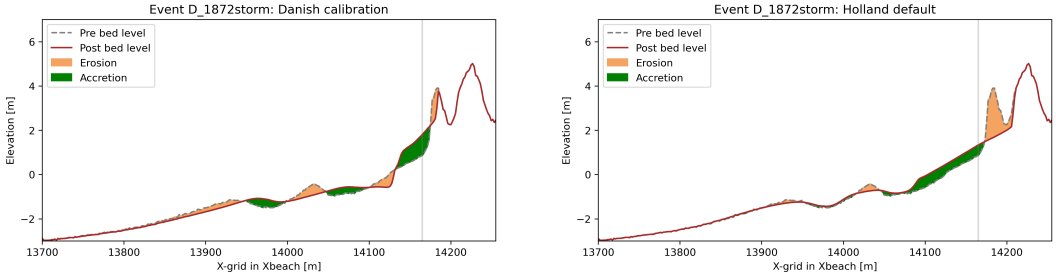

(a) *Danish calibration* **(b)** *Holland default*

Figure G.4: *Bed level change by the XBeach model due to the Danish calibration and Holland default in Transect D.*

H. Morphological Model Results

The model results obtained by the morphological models under extreme conditions during the period of 1959 to 2022 are shown for each transects. Figure H.5, shows the dune erosion in all four transects under the 1872 storm.

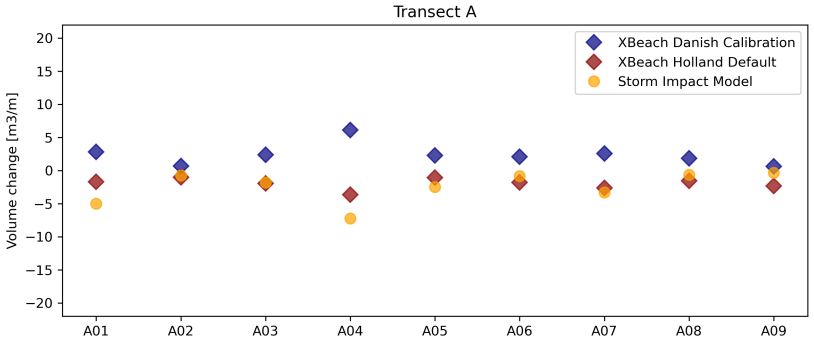

Figure H.1: *Estimated dune erosion under extreme conditions by various models in Transect A.*

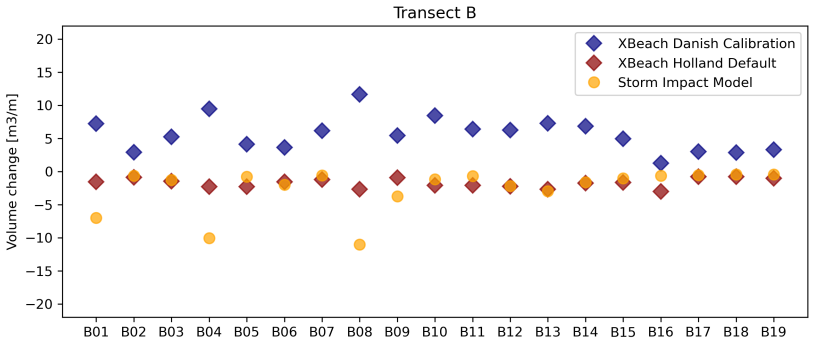

Figure H.2: *Estimated dune erosion under extreme conditions by various models in Transect B.*

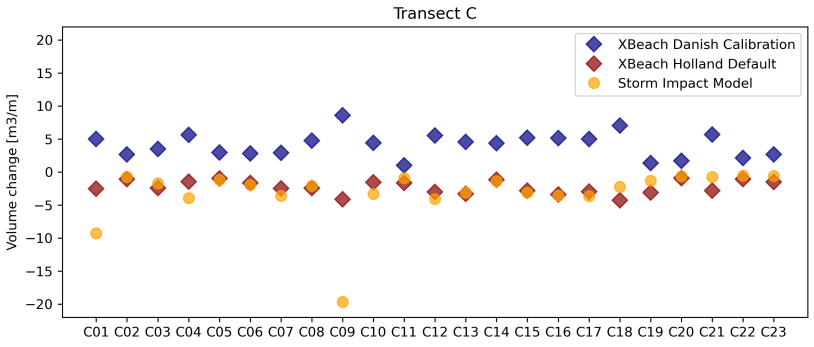

Figure H.3: *Estimated dune erosion under extreme conditions by various models in Transect C.*

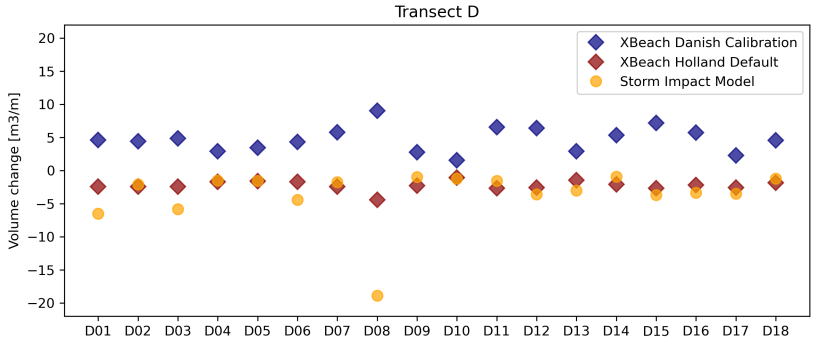

Figure H.4: *Estimated dune erosion under extreme conditions by various models in Transect D.*

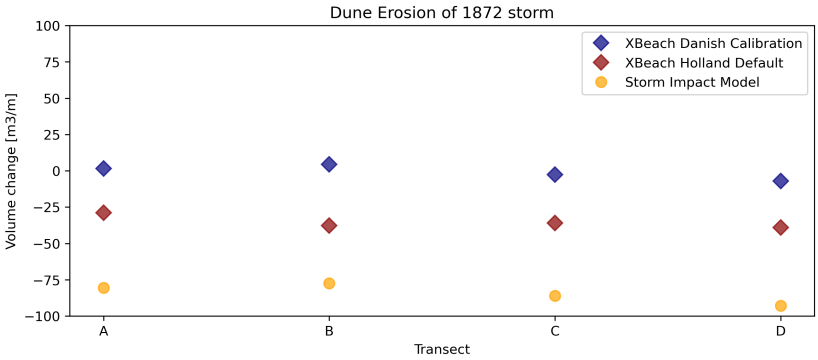

Figure H.5: *Estimated dune erosion under the 1872 storm by various models in all four transects.*